EXOCYST DYSFUNCTION LEADS TO DEFECTS IN UROTHELIAL DIFFERENTION IN A NOVEL MOUSE MODEL OF CONGENITAL URETER OBSTRUCTIONS

A DISSERTIATION SUBMITTED IN PARTIAL FULFILLMENT OF THE REQUIREMENTS FOR THE DEGREE OF

DOCTOR OF PHILOSOPHY IN

CELL AND MOLECULAR BIOLOGY

University of Hawaii John A. Burns School of Medicine

Spring 2017

Submitted by

Amanda Lee

Committee Members:

Ben Fogelgren, Ph.D (Advisor)
Scott Lozanoff, Ph.D
Takashi Matsui, MD, Ph.D
Marla Berry, Ph.D
Pratibha Nerurkar, Ph.D

Key words: exocyst, mouse model, urothelial differentiation

ACKNOWLEDGEMENTS:

I would like to thank my committee members (Dr. Ben Fogelgren, Dr. Scott Lozanoff, Dr. Takashi Matsui, Dr. Marla Berry, and Dr. Pratibha Nerurkar) and the Fogelgren lab (Dr. Noemi Polgar, Vanessa Lui, Jo Andrea Napoli, Kadee-Kalia Tamashiro, and Brent Fujimoto) for their endless support and guidance throughout the years.

I would also like to thank, Tina Carvalho at the University of Hawaii Biological Electron Microscopy Core Facility for TEM and SEM services. Karolina Peplowska and Maarit Tiirikainen at the University of Hawaii Cancer Center Genomics Shared Resource Core Facility for Affymetric microarray services. Miyoko Bellinger and Kristen Ewell at the University of Hawaii RCMI Histology and Imaging core facility for histology services.The European Conditional Mouse Mutagenesis program for generating the conditional Sec10 mouse allele in ES cells. Engineered Models Resource of the HRFDCC and the UAB ES Cell/ Transgenic Core Facility for generating the floxed Sec10 transgenic mice from EUCOMM ES cells.

Funding:

This work was supported in part by grants from the NIH (1K01DK087852 and 1R03DK100738, P20GM103457-06A1-8293 to BF), Hawaii Community Foundation (12ADVC-51347 to BF), March of Dimes (Basil O'Conner #5-FY14-56 to BF), and Hepato/Renal Fibrocystic Diseases Core Center (HRFDCC) at the University of Alabama at Birmingham (5P30DK074038 Pilot and Feasibility Award

ABSTRACT:

The exocyst is an eight protein trafficking complex responsible for polarized exocytosis of a certain subset of vesicles to the plasma membrane. The exocyst is present in a large variety of cell types and is involved in many different cellular processes. The protein, *Sec10,* has been reported to be a central component of the exocyst, and loss of this protein leads to inactivation of the entire complex. Here we show that the exocyst complex is essential for primary cilia formation, epithelial homeostasis, and cell survival in a cell culture model. We also report generation of a conditional knockout mouse for *Sec10*, which is the first conditional allele for any exocyst gene. Inactivation of *Sec10* in ureteric bud derived cells results in severe bilateral hydronephrosis and complete anuria in newborns, with death occurring 6-14 hours after birth. *Sec10* conditional knockout mice develop ureteropelvic junction obstructions between E17.5 and E18.5 due to failure of urothelial progenitor cells to differentiate into superficial cells, which are responsible for producing uroplakin plaques on the luminal surface. These *Sec10* knockout urothelial cells undergo cell death by E17.5 and the urothelial barrier becomes leaky to luminal fluid. Also at E17.5, we measured increased expression of *TGFβ1* and genes associated with myofibroblast activation, with evidence of stromal remodeling. Our findings support the model that a defective urothelial barrier allows urine to induce a fibrotic wound healing mechanism, which may contribute to human prenatal UPJ obstructions.

TABLE OF CONTENTS

LIST OF FIGURES:

Chapter 4:

LIST OF ABBREVIATIONS:

ANOVA	analysis of variance
BMP4	Bone morphogenetic protein
CAKUT	congenital anomalies of the kidney and urinary tract
DMEM	Dulbecco's modified Eagle medium
DMSO	dimethyl sulfoxide
DNA	deoxyribonucleic acid
ECM	extracellular matrix
EMT	Epithelial to mesenchymal transition
ER	endoplasmic reticulum
ESRD	end-stage renal disease
fgf2	Fibroblast growth factor
FITC	Fluorescein isothiocyanate
GDNF	glial-derived growth factor
GLUT4	glucose transporter 4
H&E	hematoxylin and eosin
IFT	intraflagellar transport
KD	knockdown
KSP	kidney specific
MDCK	madin-darby canine kidney
MEM	minimum essential media
mg	Microgram
mL	Milliter
MM	metanephric mesenchyme
mRNA	messenger ribonucleic acid
ND	nephric duct
PARP	Poly ADP ribose polymerase
PBS	phosphate buffered saline
PCP	planar cell polarity
PCR	polymerase chain reaction
PFA	paraformaldehyde
PKD	polycystic kidney disease
PPARϒ	Perioxisome proliferator-activated receptor gamma
qPCR	quantitative polymerase chain reaction
RA	retonic acid
RV	renal vesicles
SEM	Scanning electron microscopy
shh	Sonic hedgehog
shRNA	short hairpin ribonucleic acid
SKI II	sphingosine kinase inhibitor II
SMA	smooth muscle actin
TEM	transmission electron microscopy
TGFβ1	transforming growth factor beta 1
UB	ureteric bud
UPJ	ureteropelvic junction
Upk	uroplakin
UUO	Unilateral ureter obstruction
UV	ultraviolet
μL	Microliters
μM	micromolar

CHAPTER 1: Introduction

1.1) Kidney and ureter development:

The kidney is a complex organ that consists of blood vessels, thousands of nephrons, and a collecting duct system. The basic structure of a nephron consists of glomeruli, proximal tubules, distal tubules, and the loop of Henle. Nephrons are responsible for filtering blood and producing urine. The collecting duct system consists of the collecting ducts, calyces, papilla, and the ureter. The collecting duct system is responsible for transporting urine from the nephrons through the ureter into the bladder[1].

During kidney development the dorsal portion of the intermediate mesoderm gives rise to the nephric duct (ND) and ventral portion gives rise to the metanephric mesenchyme (MM)[2–4]. The ND will eventually develop into the collecting duct system while the MM develops into nephrons. Kidney development occurs in three successive stages that include: the pronephros, mesonephros, and the metanephros. The pronephros and mesonephros are the embryonic kidney precursors which are transient structures that either degenerate or have no function as the embryo continues to develop[1,3]. The pronephros begins development at embryonic day 8.5 (E8.5) when precursors of the ND separate from the intermediate mesoderm and undergo multiple epithelial-to-mesenchymal transitions that form an epithelial tube. As the pronephros begins to regress the mesonephros arises at the caudal end and will eventually give rise to the nephrons.

The metanephros is the structure that develops into the mature mammalian kidney. The metanephros begins to form when the MM secretes several signals to initiate ureteric bud (UB) branching. The glial cell-line derived neurotrophic factor (GDNF)/*Ret* pathway is one of critical regulators that initiate this branching[5–7]. GDNF is secreted from the MM to the *Ret* receptors of the nephric duct and initiates branching of the UB toward the MM[1,4]. The UB undergoes many rounds of branching to form the collecting duct system of the kidney. As the UB continues to branch into the MM, the stalk extends downward to become the mature ureter where it will eventually connect with the embryonic bladder[8]. The MM consists of various progenitor cell types that develop into the different components of the kidney. The cell population closest to the

ureteric bud branching tips, also known as the cap mesenchyme, is positive for *Six2* and *Cited1.* This population undergos epithelial differentiation to form pretubular aggregates that eventually develop into renal vesicles (RV)[4]. RV is the precursor for the main body of the nephron. The second population of cells in the MM, also known as stromal progenitors, positive for *Foxd1,* and gives rise to the interstitial cell types such as podocytes and mesangial cells. The final cell population is the vascular progenitors that form the vascular support of the UB outgrowth.

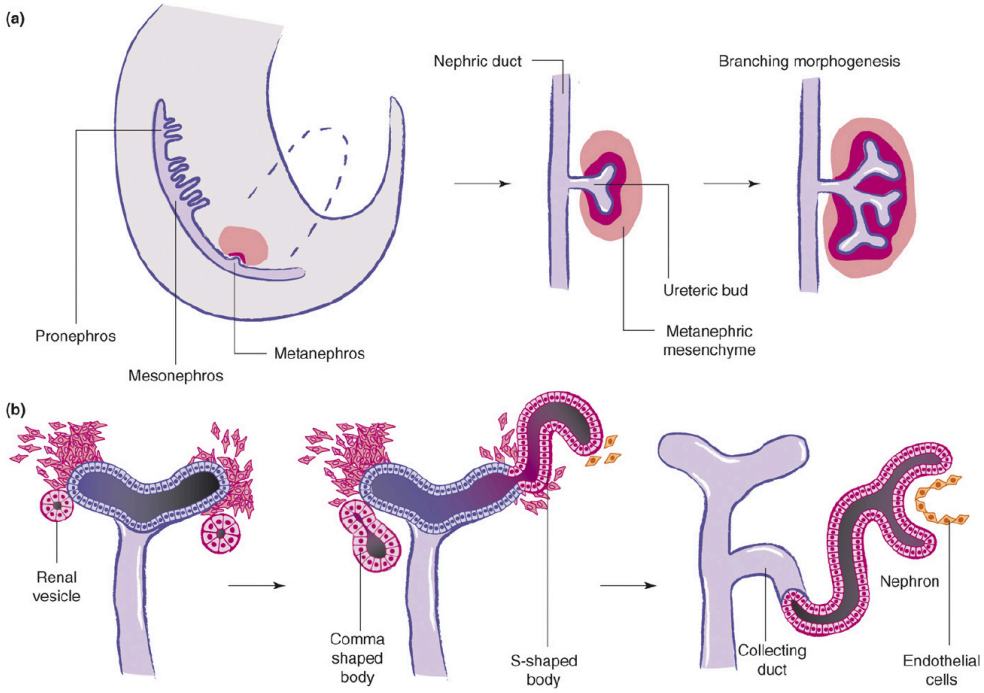

Figure 1: Kidney and ureter development. A) Kidney development begins when the ureteric bud (UB) receives signals from the metanephric mesenchyme (MM) to begin branching from the nephric duct. B) As the ureteric bud branches into the MM it undergoes many rounds of branching morphogenesis toward the MM and the stalk of the UB elongates downward to become the ureter. Figure taken from Uhlenhaut, N.H. and Treier, M. *Trends in Genetics*, 2008[9].

1.2) The Exocyst Complex and *Sec10*:

In this dissertation, we focus on the exocyst, an eight protein trafficking complex previously described in epithelial polarity. The exocyst is responsible for polarized exocytosis of a certain subset of vesicles to the plasma membrane. Drs. Peter Novick and Randy Schekman initially discovered the exocyst in yeast from comprehensive mutagenesis screens for intracellular trafficking genes[10–12]. Based on these discoveries, Dr. Schekman shared the 2013 Nobel Prize in Physiology or Medicine. The exocyst complex is highly conserved from yeast to human, and has been identified with a rapidly increasing number of biological functions in various mammalian cell types. These recently described roles include GLUT4 trafficking in response to insulin signaling in adipocytes[13], neuronal growth and neuromuscular synapse formation[14–16], cellular invasion of bacteria pathogens and toxins[17], tumor invasion and cell migration[18], and cellular autophagy[19]. We have been studying the exocyst's intracellular trafficking to the primary cilia of renal epithelial cells[20,21], and required an *in vivo* model of exocyst disruption during mammalian kidney development. The one previous knockout of an exocyst component targeted *Sec8* in a general mouse knockout, which resulted in arrested embryonic development at E6.5 [22]. Thus, we embarked to generate a novel murine model for conditional inactivation of the Sec10 subunit, which has shown to be central to the exocyst's stability and function because it is required for binding Sec15 on the surface of cargo vesicles to the rest of the exocyst complex on the plasma membrane[21,23,24].

Figure 2: The Exocyst is an eight subunit protein complex responsible for targeting a certain subset of polarized vesicles to the plasma membrane. The protein *Sec10* has been reported as being a central subunit required for the binding of Sec15, on the surface of cargo vesicles, to the rest of the exocyst complex on the plasma membrane.

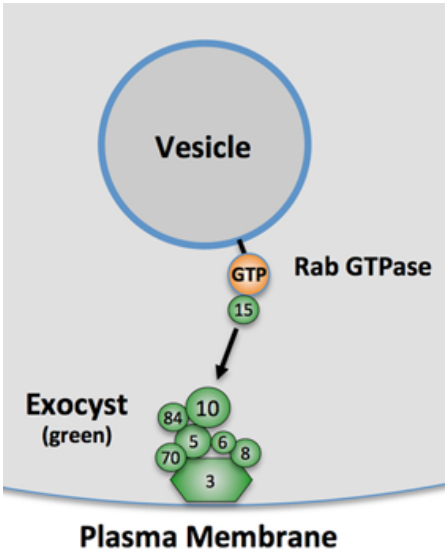

1.3) Congenital Anomalies of the Kidney and Urinary Tract:

Congenital anomalies of the kidney and urinary tract (CAKUT) are a heterogeneous spectrum of disorders that include renal dysplasia, aplasia, ureteral duplication, horseshoe kidney, and obstructions along the urinary tract. Polycystic kidney disease (PKD) falls within CAKUT and occurs in 1 out of every 400 births[25]. In PKD large cyst formation occurs in the kidneys and can lead to chronic kidney disease (CKD) or end-stage renal disease (ERSD), the most severe form of kidney disease. In the past decade, it has been established that most forms of cystic kidney disease have been linked to defects in primary cilia in mouse models as well as clinical human cases. The primary cilium is a microtubule-based cell signaling organelle located on almost all cell types and there is one primary cilium per cell[26,27]. The primary cilium is thought to function as a sensory organelle due to the presence of receptors, ion channels, and signaling molecules that localize only to the primary cilium[27,28]. The structure of the primary cilium includes a basal body located on the plasma membrane connected via transition fibers that hold a transition zone in place. The transition zone is where molecules remain until they are ready to be transported up the primary cilium via a process called intraflagellar transport (IFT). Defects in the structure or function of the primary cilium can lead to disorders termed ciliopathies, and in recent years, increased characterization of the biological roles of primary cilia has led to the reclassification of

many diseases as ciliopathies[29]. Ciliopathies include a wide range of phenotypes that can affect many different organ systems including the renal system. The most prevalent ciliopathy affecting the renal system is PKD[30,31].

We hypothesized that since cell culture experiments suggested that the exocyst complex was important for trafficking important molecules to the primary cilium, a kidney-specific Sec10 knockout would lead to ciliary defects that lead to polycystic kidney disease. In order to test this hypothesis, we created a novel *Sec10* conditional knockout mouse using the Cre-LoxP recombination system (described in Chapter 3).

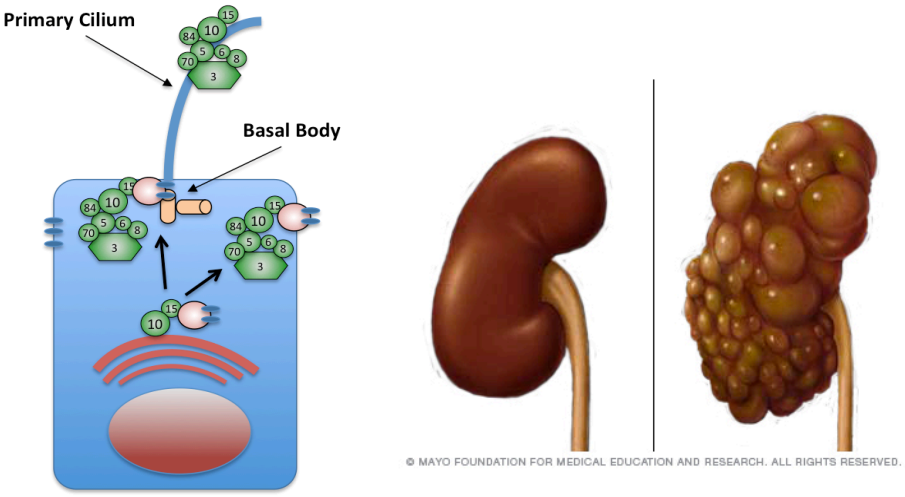

Figure 3: Previous studies in culture cells and zebrafish models suggested that exocyst complex trafficks proteins to the primary cilium. A) The primary cilium is a microtubule-based organelle located on most cell types. Previous studies have shown that members of the exocyst complex not only localizes to the primary cilum but also, trafficks key molecules involved in its formation. B) Defects in primary cilia structure or function may result in diseases termed ciliopathies. Among the ciliopathies is polycystic kidney disease (PKD) that results in large cyst formation and can lead to end-stage renal disease. Photo courtesy of Mayo Clinic (http://www.mayoclinic.org/diseases-conditions/polycystic-kidney-disease/multimedia/normal-and-polycystic-kidneys/img-20006896)

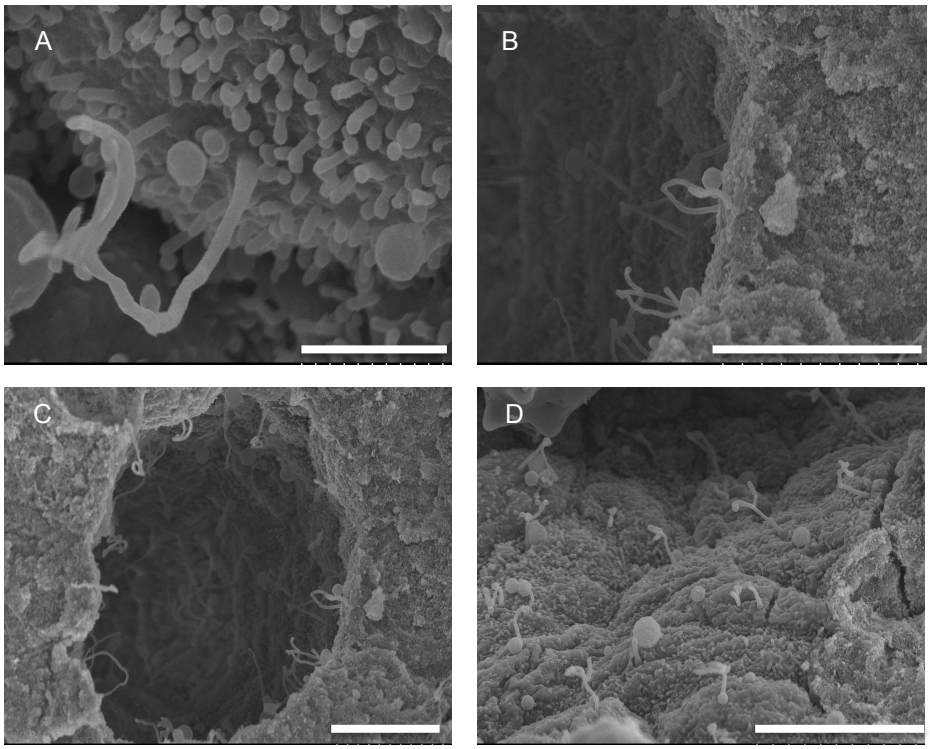

Figure 4: Most forms of polycystic kidney disease have been associated with defects of the primary cilium. A-D) Scanning electron microscopy (SEM) images of a primary cilia in E16.5 embryonic mouse kidney tubules. A) magnification 40,000x; scale bar = 1μm. B) magnification 11,000x; scale bar = 5μm. C) magnification 6,000x; scale bar = 5μm. D) magnification 9,000x; scale bar = 5μm.

Within CAKUT, congenital obstructive nephropathy (CON) is the most common cause of CKD and ESRD for infants and children[32–34]. The obstructed outflow of urine leads to hydronephrosis, which is the enlargement of the kidney due to a build up of urine in the renal pelvis (Fig.5). Detection of CON often occurs during prenatal development, and hydronephrosis is detected by ultrasound in ~1% of pregnancies[35–37]. Although about 70% of prenatal hydronephrosis cases spontaneously resolve, the remaining 30% of cases can worsen and cause lasting renal damage[37]. The severe cases require surgical correction, such as stent placement or a pyeloplasty. The most common site of obstruction in CON is at the ureteropelvic junction (UPJ), which is where

the kidney pelvis transitions into the ureter[35,38,39]. The underlying molecular causes of congenital UPJ obstructions are poorly understood, as are the contributing environmental factors and natural variability. *The gap in knowledge about CON and UPJ obstructions is in part due to the lack of genetic, non-surgical animal models to study these diseases*[38,40].

Figure 5: The most common cause of congential obstructive nephropathy (CON) is an obstruction in the ureteropelvic junction (UPJ). Schematic of kidney with obstruction at the ureteropelvic junction (UPJ). The UPJ is the region where the renal pelvis transitions into the ureter.

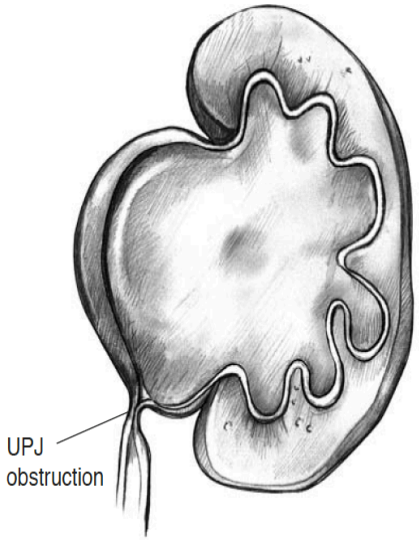

1.4) Urothelium: a Specialized Epithelium Lining the Urinary Tract:

The urothelium, also called the transitional epithelium, is a specialized multi-layered epithelium that lines the renal pelvis, ureters, bladder, and most of the urethra[41]. The main characteristic of the urothelium is that it has the ability to contract and relax upon the passage of urine, while maintaining a strong hydrophobic barrier. One hypothesis for urothelial differentiation is that there is an organized sequence where the keratin-5 expressing basal cells produce intermediate and superficial cells, which form the three layers of the urothelium[42]. Each of the cell types in the different layers expresses proteins that are indicative of the specific layers. The basal layer expresses keratin-5 and p63. The intermediate layer expresses uroplakin genes and p63 but not keratin-5. The superficial layer expresses uroplakins but not p63 or keratin-5. In 2013, it was shown that keratin-5 basal cells rarely produce intermediate and superficial cells and that they arise from a completely separate population of progenitor cells. This study also

showed that retinoic acid (RA) signaling was crucial for the differentiation of superficial and intermediate cell layers[43]. In 2015, another report contradicted the 2013 study and claimed that the superficial cell layer has the ability to regenerate itself by its own progenitor population and basal cells regenerate strictly from their population[44]. In conclusion, there have been fate-mapping and mouse studies to determine the development of a mature bladder. These studies are contradictory, and given the important of a functional urothelium to renal and urinary tract physiology, more studies of urothelial development are important.

The uroplakin family of proteins is critical for urothelial tissue function and maintenance. The expression of uroplakins on the apical surface of superficial cells is indicative of a mature urothelium. These uroplakin plaques cover a majority of the apical plasma membrane and are connected by flexible hinge regions. The four members of the uroplakin family (Upk1a, Upk1b, Upk2, and Upk3) are transmembrane proteins that assemble into heterodimers in the ER (Upk1a-Upk2 and Upk1b-Upk3) before being trafficked through the Golgi and to the apical surface in discoid/fusiform vesicles[45]. A pool of these uroplakin-containing vesicles are maintained under the apical surface of the mature superficial cells, and the dynamic exocytosis and endocytosis allows the

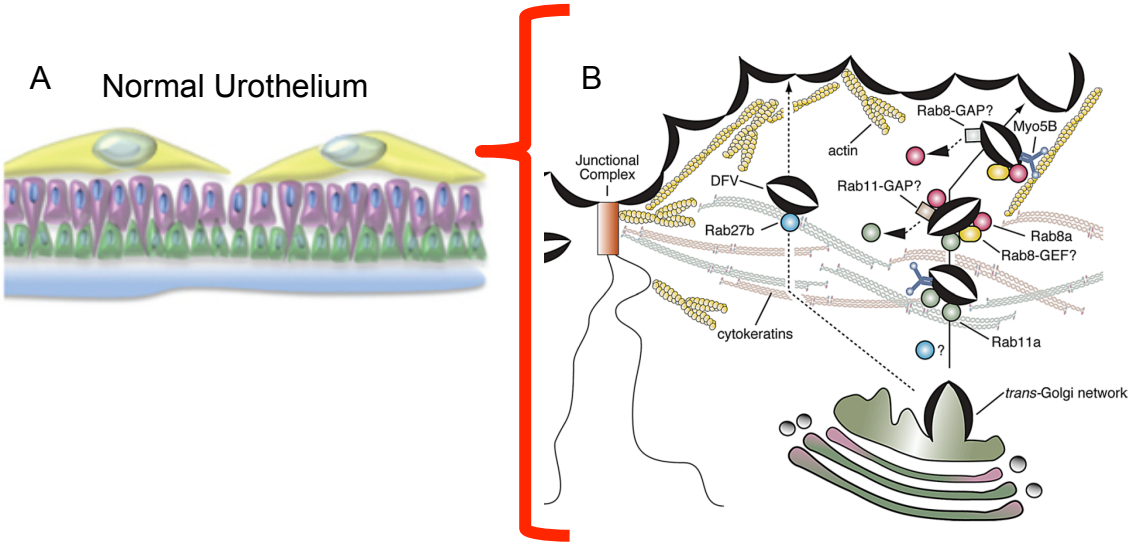

Figure 6: Uroplakins are transmembrane proteins located on the apical surface of superficial urothelial cells that form a water-tight barrier. A) A normal urothelium consists of three cell layers: a basal layer, intermediate layer, and superficial layer. Image taken from Van Batavia et al., Nat Cell Biol, 2014 B) The four main uroplakin proteins trafficked to the plasma membrane where they form a scalloped structure at the apical membrane. Image take from Khaldelwal et al., Mol Biol Cell, 2013.

urothelial surface area to expand and contract in response to mechanical stretch[46]. High expression of the uroplakin family members and formation of these plaques is critical for the development and maintenance of the urothelial barrier.

1.5) SPECIFIC AIMS OF THIS DISSERTATION:

Congenital obstructive nephropathy (CON) is a chronic kidney disease that affects infants and children. The most common cause of CON is an obstruction in the upper ureter at the ureteropelvic junction (UPJ) that leads to prenatal hydronephrosis. Hydronephrosis is the build-up of urine in the kidney detected via ultrasound in 1:100 pregnancies. Understanding the etiology of UPJ obstructions is difficult because the causes are unknown and there are no animal models that recapitulate the disease's development *in utero*.

We have recently created a *Sec10* conditional knockout mouse (*Sec10$^{FL/FL}$;Ksp-Cre*) model using the Cre-Lox technology which knocks out *Sec10* in the epithelial cells lining the ureter and collecting ducts of the kidney. This is the first conditional knockout for any exocyst component. Preliminary analysis of *Sec10$^{FL/FL}$;Ksp-Cre* mice revealed severe bilateral hydronephrosis, complete anuria, and UPJ obstructions that develop late in gestation. Initial analysis of *Sec10$^{FL/FL}$;Ksp-Cre* ureters showed decreased uroplakin 3 expression on the apical surface of the ureter, which can indicate defects in ureter maturation. We also observed cells with a mesenchymal phenotype in the actual obstructed area of the ureter.

The overall goal of this research is to better understand the molecular background of kidney and urinary tract development, and how defects of these mechanisms cause congenital malformations. **The goals of this dissertation** are*:* 1. Determine the role of *Sec10* in epithelial morphogenesis (chapter 2) 2. Characterize *Sec10* conditional knockout in a mouse model (chapter 3) 3. Determine the mechanism behind the phenotype we observed upon *Sec10* knockout (chapter 4).

Our original hypothesis was that the exocyst complex trafficks proteins necessary for the development of the primary cilium, and *Sec10* knockout mice would have a polycystic kidney phenotype. After initial analysis, we concluded that our data did not support our initial hypothesis, *Sec10* knockout in kidney collecting ducts and the ureter resulted in neonatal death due to a physical obstruction in ureteropelvic junction (UPJ), where the kidney transitions into the ureter. *We then hypothesized that Sec10 plays a crucial role in the maintenance urothelial cell differentiation and development of the urothelial barrier.*

Specific Aim 1: Define the role of the exocyst in cyst and lumen formation in Sec10-KD MDCK cells.

Hypothesis: Loss of Sec10 will lead to defects in cyst and lumen formation, which are important characteristics of epithelial morphogenesis.

Approach: In this aim, we will seed Sec10 knockdown (Sec10-KD) and control MDCK cells in type I collagen, where they naturally form cysts. MDCK cyst and tubule formation is a complex process that requires the establishment of apico-basal polarity and the formation of cell-cell junctions making it a useful tool to study epithelial morphogenesis. After seeding Sec10-KD and control MDCK cells we will allow them to develop a lumen and collect them at various time points during development. We will determine a timeline for cyst development without *Sec10* and perform immunohistochemistry of polarity markers, primary cilia, and cell-cell junctions.

Specific Aim 2: Determine the changes in urothelial differentiation upon inactivation of *Sec10*.

Hypothesis: Sec10 and the exocyst complex are necessary for urothelial cell differentiation, and defects in urothelial differentiation lead to a disrupted urothelial barrier formation.

Approach: In this aim, we will analyze the ultrastructure of the superficial, intermediate, and basal urothelial cell layers in E15.5-E17.5 *Sec10$^{FL/FL}$;Ksp-Cre* ureters and controls using transmission electron microscopy (TEM). We will compare the formation of fusiform vesicles, the presence of uroplakin plaques on the apical surface of the urothelium, tight junction formation, and the integrity of the basement membrane. In addition, we have established a ureter explant model that will allow us to determine if the exocyst complex is involved in urothelial differentiation. We will use *Sec10$^{FL/FL}$;Ksp-Cre* and control *Sec10$^{FL/FL}$* ureters *ex vivo* to identify key molecular controllers of urothelial cell differentiation using small molecular inhibitors and growth factors to promote or inhibit differentiation. Finally, we will compare the expression of urothelial differentiation markers in ureters from Sec10$^{FL/FL}$;Ksp-Cre and control animals using qPCR and immunohistochemistry.

Specific Aim 3: Identify pathogenic changes in cell signaling that drive the overgrowth in surrounding mesenchyme in *Sec10$^{FL/FL}$;Ksp-Cre* ureters.

Hypothesis: Weakening of the urothelial barrier allows urinary damage to the underlying mesenchyme and stimulates a fibroproliferative response, associated with an increase in TGFβ1 expression and extracellular matrix deposition.

Approach: We will first use the *ex vivo* ureter explant model that we have established to determine if the obstruction occurs in the absence of urine. Second, we will quantify the degree of cellular death in the urothelium and surrounding mesenchyme by quantifying changes in cell signaling using protein-signaling arrays. Finally, will determine the characteristics of the obstruction to identify the presence of a fibroproliferative response: indicated by activated fibroblasts and ECM deposition. These experiments will be performed using immunohistochemistry, Western blotting, and qPCR analysis at E18.5 and newborn embryonic stages.

The anticipated outcome of this dissertation is to show that the exocyst complex is necessary for the proper development of the mammalian ureter by promoting differentiation. This work will better define a unique genetic model of CON, which has revealed a novel mechanism for the formation of prenatal UPJ obstructions. This *Sec10$^{FL/FL}$;Ksp-Cre* mouse could be used in future studies to test novel surgical and drug therapies, identify predictive biomarkers, and candidate genes for human UPJ obstructions.

CHAPTER 2: *Sec10* and the exocyst complex in epithelial morphogenesis

2.1) INTRODUCTION

The development of epithelial tissue depends on an organized process of cell signaling events that translate into physical cellular responses. This organized process is called epithelial morphogenesis, where epithelia form cohesive sheets. These epithelial sheets serve a barrier separating the internal environment from outside environmental factors that line organs such as the kidneys, lungs, and liver. These organs contain a lumen, which are hollow spaces that allow exchange of nutrients, gases, and hormones[47]. During lumen formation epithelial cells must establish apico-basal polarity (before lumen formation), tight cell-cell contacts (before or during lumen formation), and planar cell polarity (after lumen formation)[48]. In apico-basal polarity, columnar epithelial cells are arranged with one end facing the lumen (apical domain) and the basal domain directly opposite attached to the underlying basement membrane[49]. Epithelial cells establish apico-basal polarity via three main protein complexes, the *Crumbs* complex, the *Par* complex, and the *Scribble* complex[50]. The *Crumbs* and *Par* complex aggregate near the apical membrane, while the *Scribble* complex near the lateral surface of polarized epithelia[50]. The cells require signals from the extracellular matrix in order to establish this polarity and distribute proteins to the proper locales[51]. The formation of tight cell-cell contacts between cells is another important aspect of lumen formation. Since the purpose of lumen formation is to separate physiological compartments, tight and adherens junctions are required to prevent fluid from entering the spaces outside the lumen, and vise versa. Tight junctions seal epithelial cells laterally at the apical surface and control the passage of substances between the apical and basal compartments[51]. Occludins and claudins are the two transmembrane components of tight junctions that associate with the actin cytoskeleton and link junctions together. Adherens junctions have a similar function to tight junctions, where they provide adhesive contacts between cells. Cadherins (such as E-cadherin) and Catenins (such as Beta-Catenin) are examples of an adherens junction that stabilize contacts between cells.

Planar cell polarity (PCP) refers to the cell polarity that runs perpendicular to the apical-basal polarity axis[52] (Fig.7). PCP is important for the development of epithelial

sheets and guides proper orientation of cell division as well as the formation of a luminal structure[52]. The main proteins involved in the maintenance of PCP are considered “core” genes. The core genes include *Frizzled, Dishevelled, Van Gogh, Prickled, Flamingo,* and *Diego*[53]*.* These genes were originally discovered in *Drosophila* and conserved in vertebrates and mammals. These PCP genes have been linked to other developmental pathways and mechanisms such as the *Wnt* signaling pathway and primary cilia signaling. Defects in the establishment of planar cell polarity can result in defects such as neural tube closure and ciliopathies, such as polycystic kidney disease[52,54].

Figure 7: Cell polarity is essential in the formation of epithelial tissues. Epithelial cell polarity is established by the formation of an apical membrane formation with a basal end opposite the apical membrane. Planar cell polarity forms perpendicular to the apical and basal ends of the cell. Figure taken from Piecyznski, *Am J Physiol Renal Physiol,* 2011[50].

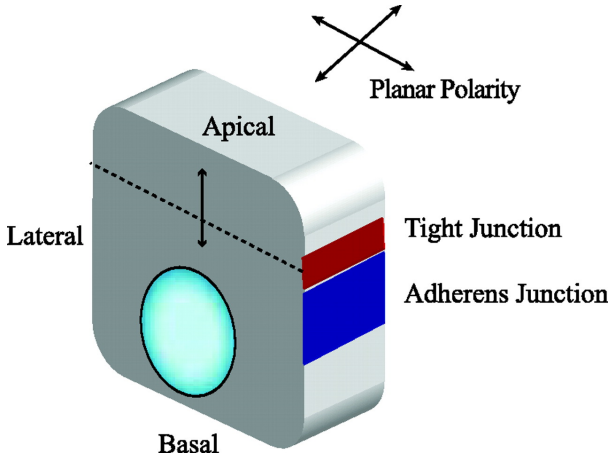

Lumen formation requires targeted delivery of proteins to distinct regions of the plasma membrane in order to establish apical and basolateral polarity[47]. This process is dependent on vesicle trafficking of polarity proteins to the appropriate cell membrane[47] The protein *Sec10* and the exocyst complex has been shown to be enriched at sites of membrane expansion and can be involved in both basolateral and apical protein trafficking in epithelial cells[24,55]. It has also been shown to localize to tight junctions and govern the clustering of E-cadherin at the adherens junctions[56] suggesting the exocyst complex is crucial in the signaling network of epithelial cell polarity and lumen formation.

The Madin-Darby Canine Kidney epithelial cell line (MDCK cells) is derived from the canine renal tubular epithelium and can be used as an *in vitro* model of cyst and tubule formation. When MDCK cells are seeded in a 3-dimensional culture of

extracellular matrix they naturally form hollow cysts with a lumen. These luminal structures must form and maintain apico-basal polarity and cell-cell junctions to survive in culture. There have been two different naturally occurring mechanisms of cyst development that have been described. The cavitation-dependent method involves programmed cell death in the center of a mass of cells to form a lumen. The hollowing-dependent method, is where targeted apical exocytosis and membrane expansion is required to form the lumen[48]. It has been proposed that depending on the rate of apico-basal polarity establishment, the same epithelial cells can shift between the two different processes for cystogenesis. It has been shown that for MDCK cells, the process of cavitation is responsible for generation of the lumen when grown in a Type I collagen matrix[57]. Conversely, we would see hollowing when grown in matrigel and *Sec10* and the exocyst complex have been shown to regulate vesicle trafficking during hollowing[58].

Lipschutz et al 2009[59] knocked down *Sec10* in MDCK cells using short-hairpin RNA (shRNA) that targets and silences specific gene expression. They reported that *Sec10* knockdown in MDCK cells seeded in a collagen matrix did not form a luminal cyst. Instead, they found that *Sec10* knockdown in MDCK cells formed irregular clumps without a lumen. *Sec10* knockdown cysts had decreased primary cilia length and cilia-to-nuclei compared to controls. They also reported that when *Sec10* is overexpressed in MDCK cells, there is an increase in primary cilia length and cilia-to-nuclei ratio[59]. *Here, our specific aim was to further examine the role of Sec10 and the exocyst in primary cilia and cyst formation during cavitation.*

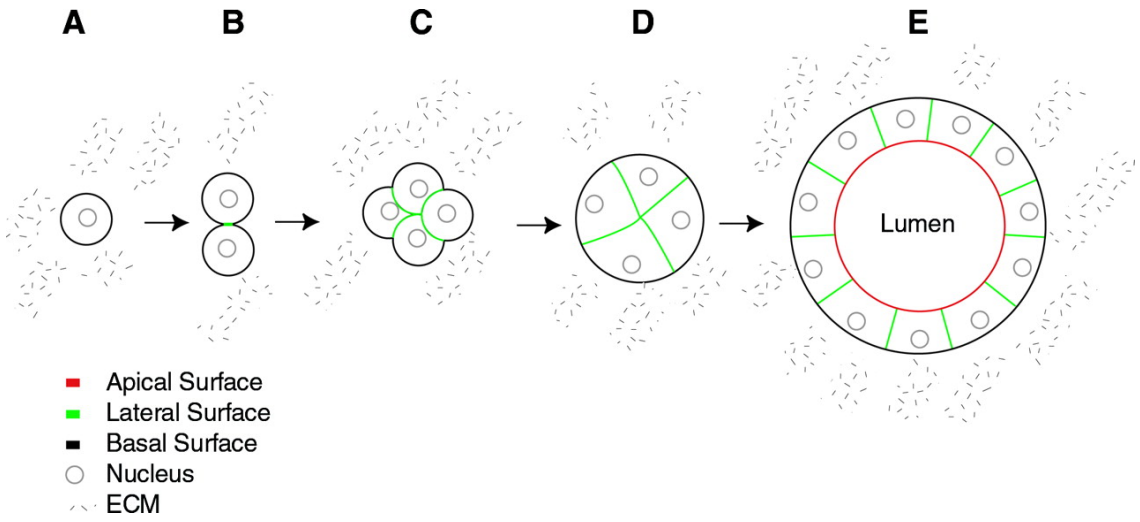

Figure 8: MDCK cells form cysts when cultured in extracellular matrix. A) MDCK cells are seeded as a single cell suspension in a 3-dimensional matrix. B-D) As the MDCK cells divide they begin to establish polarity with the basal side in direct contact with the extracellular matrix and the apical surface directly opposite. E) After approximately 8-10 days in culture, the MDCK cysts have a distinct lumen with a well-established cell polarity. This MDCK cyst model is a useful *in vitro* tool for studying lumen formation and cystogenesis that occur in the development of various organs within the body. Figure taken from Kroschewski, *News Physiol Sci,* 2004.

2.2) RESULTS

2.2.1) *Sec10* knockdown MDCK cysts form lumens but exhibit defects in primary cilia formation and disrupted cyst homeostasis in 3D collagen cultures.

As mentioned previously, Lipschutz et al showed shRNA mediated *Sec10* knockdown in MDCK cells did not produce cysts with a lumen and instead formed a mass of cells when seeded in a collagen matrix[59]. Our results showed that abnormal cyst development does not occur until later in the development with apoptotic cell extrusion from the epithelial monolayer. Sec10-KD cysts initially developed an intact lumen and the cells on the inside of Sec10-KD cysts underwent apoptosis similar to controls, which are consistent with the cavitation dependent method of lumen formation[56]. The cavitation method of cyst formation (cystogenesis) requires alternative mechanisms from hollowing, including apoptosis (programmed cell death) of the interior cells of the cell cluster to form the lumen. Our results suggest that the exocyst complex does not affect the cavitation dependent method of lumen formation. Instead, *Sec10*

knockdown is necessary for lumen formation through hollowing. In a study done on matrigel, knockdown of *Sec10* led to vesicular accumulation and the process of hallowing depends on the exocyst to coordinate exocytosis of membrane-bound vesicles at the apical membrane[58]. We evaluated cystogenesis over a 12-day time span in *Sec10* knockdown (Sec10-KD*)* and control MDCK cells seeded in type I collagen. Although these cell lines have been well validated[59], we confirmed Sec10-KD in MDCK cells after they were allowed to form cysts in type I collagen using Western Blot analysis (Fig. 9A). Sec10-KD MDCK cysts were able to initially form a lumen as indicated by gp135 immunostaining (Fig. 9C). Between days 4 and 12 the cells on the inside of the *Sec10-KD* cysts had a similar phenotype to the controls and had apoptotic cells in the center of the lumen (Fig. 9B).

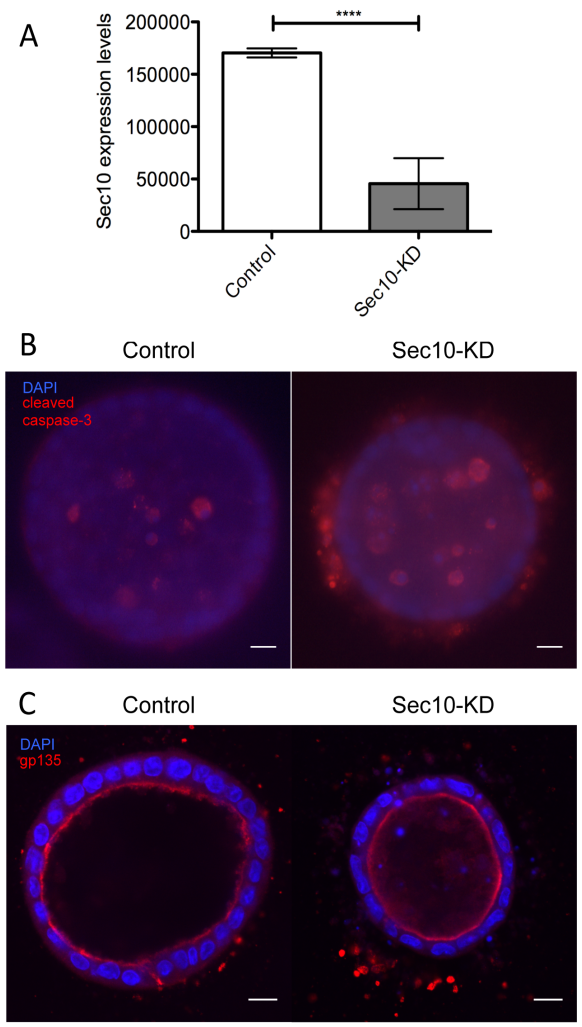

Figure 9: *Sec10*-knockdown (Sec10-KD) cells are capable of forming mature cysts. A) Western blot analysis of control and Sec-KD expression in MDCK cells. B) Immunohistochemistry for apoptotic marker cl-caspase 3 (red) and Dapi (blue) in control and Sec10-KD cysts at day 12 of cystogenesis. Scale bar = 10μm C) Immunohistochemistry of apical marker gp135 (red) and Dapi (blue) in control and Sec10-KD cysts showing lumen formation at day 12 of cystogenesis. Scale bar = 10μm.

This showed that Sec10-KD in 3 dimensional cultures did not hinder the apoptotic process needed for the initial lumen formation through cavitation.

We observed abnormal cysts starting at day 12 of cyst development in Sec10-KD MDCK cultures. There were a greater amount of apoptotic cells on the outside of Sec10-KD cysts that were not observed in control cysts (Fig. 10A). We grouped the apoptotic cells based on the number of cl-caspase 3 positive cells on the outside of the cysts (basal surface). The cyst groupings were 0, 1-3, 4-10, and >10 cells.

We found that there were dramatically more apoptotic cells on the basal surface of the Sec10-KD cysts compared to controls at day 12 (Fig. 10B). There were no changes in the number of apoptotic cells in Sec10-KD cysts at earlier time points day 4, 8, or 10 (data not shown). The basally extruded cells in the Sec10-KD cysts only occurred in collagen matrices maintained for 12 days or longer. *This suggests that the extruded cells in Sec10-KD cysts are a result of defects in epithelial maintenance rather than defects in the cavitation process.*

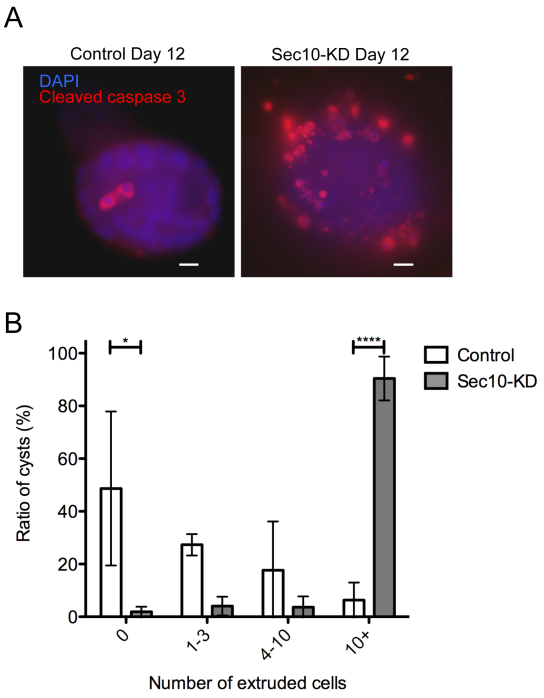

Figure 10: Sec10-KD cysts exhibit a higher rate of basal extrusion of apoptotic cells. A) Immunohistochemistry of control and Sec10-KD cysts showing increased apoptotic cells (red) on the outside of the MDCK cyst at day 12 of cytogenesis. Scale bars = 10μm B) Quantification of the ratio of apoptotic cells on the outside of the cysts compared to the number on the inside in control and Sec10-KD cysts at day 12 of cystogenesis n=100 cysts. * p< 0.05, **** p< 0.001

Cyst development is dependent on the proper formation of apical-basal polarity. In polarized epithelial cells, primary cilia formation is an important marker for the final stage of apico-basal polarization and the establishment of PCP. Previous studies have shown that in 2-dimensional cultures, Sec10-KD cells have decreased primary cilia-to-nuclei ratios and a decrease in cilia length. This suggests a potential role of the exocyst complex in primary cilia trafficking and ciliogenesis, thus epithelial polarity. Here we tested the hypothesis that Sec10-KD MDCK cysts in 3-dimensional cultures will also have defects in primary cilia formation. MDCK cells were seeded in a collagen matrix, fed every other day, and collected at various time points during cystogenesis. Primary cilia were analyzed at day 8, 10, and 12 of cyst development using immunohistochemistry of acetylated alpha-tubulin, a common marker for primary cilia[23,60]. In control cysts, primary cilia appeared on the apical surface starting at Day 8. In contrast, Sec10-KD cysts did not show any primary cilia until Day 10 of cyst development. At Days 10 and 12, Sec10-KD cysts demonstrated a significantly lower cilia-to nuclei ratio (Fig. 11B) and the cilia that were present were significantly shorter than the control cysts (Fig. 11A and C). Primary cilia measurements and quantification were taken using ImageJ software.

These results show that depleting *Sec10* has a similar effect on ciliogenesis in both 2D and 3D MDCK cultures. The onset of the cilia defect in the Sec10-KD cysts suggest that neither *Sec10* nor primary cilia are required for the process of cavitation in cystogenesis, but it raised the possibility that primary cilia are required for epithelial homoeostasis once the lumen has already formed.

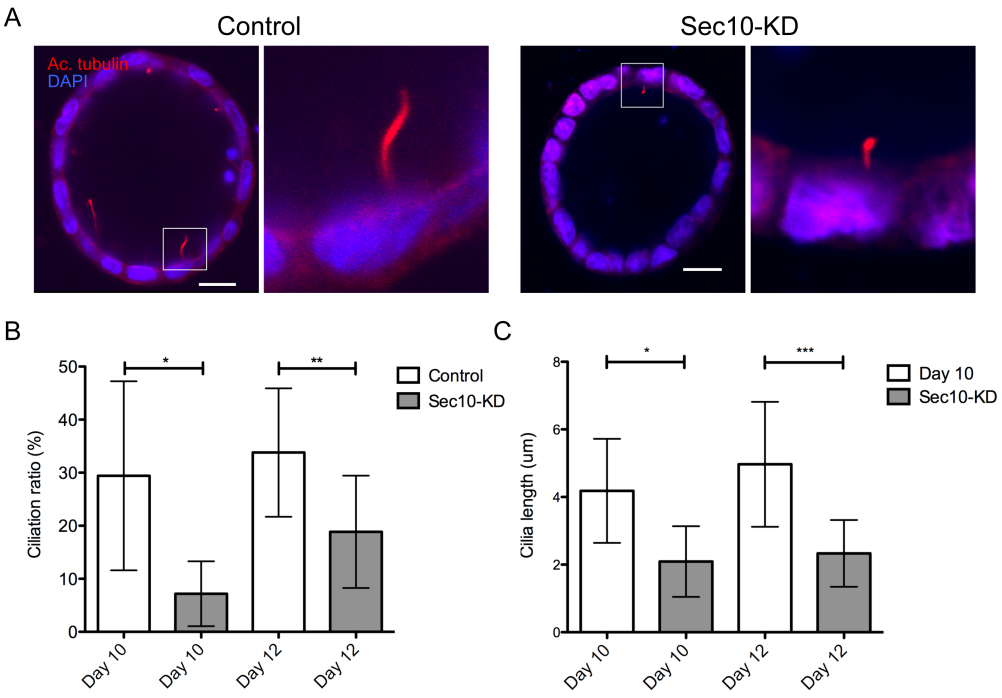

Figure 11: Defective primary cilia assembly in 3D cultures of Sec10-KD MDCK cysts. A) Immunohistochemistry of acetylated tubulin (primary cilia axoneme) in control and Sec10-KD cysts at day 12 of cystogenesis. B) Cilia-to-nuclei ratio at Day 10 and 12 in control and Sec10-KD cysts. C) Primary cilia lengths at Day 10 and 12 of cystogenesis in control and Sec10-KD cysts. * p< 0.05, ** p< 0.01 ***p<0.005

2.2.2) Higher rate of cell extrusion in *Sec10* knockdown cysts is due to increased apoptosis and not proliferation.

Epithelial cell extrusion has been described as a phenomenon that is required in order to maintain epithelial barrier integrity by the elimination of individual cells from the monolayer. Cell extrusion has been thought to occur as a result of two possible triggers: epithelial cell damage/death, or overcrowding due to increased cell proliferation of migration. As previously described, Sec10-KD cells grown in 2D culture have a higher rate of proliferation compared to controls[21]. We measured and compared the proliferation rates of Sec10-KD versus control cysts grown in 3D collagen culture. Sec10-KD and control cysts were collected at days 4,8, and 12 and immunostained for the proliferation marker Ki67, which is a gene expressed only during phases of mitosis.

We counted the cells in cysts positive for Ki67, and normalized this by total cell count of the cyst, to calculate the ratio of proliferating cells. Both Sec10-KD and control cysts had high rates of proliferation at day 4 compared to the later time points, due to the maturation and cyst development. There were also no significant differences in proliferation rates between Sec10-KD and control cysts at later time points (Fig. 12A). We additionally measured the diameter of the Sec10-KD and control cysts at the different time points to determine if there was a difference in the size of cyst development between Sec10-KD versus control cysts. At day 12, Sec10-KD cysts had a decrease in lumen size and were significantly smaller than control cysts. *The timing of the decrease in size of the Sec10-KD cysts is likely due to the increase in cellular extrusion that also appears at Day 12 of cyst development.*

Figure 12: Cell proliferation rates of Sec10-KD cysts do not differ compared to control cysts. A) Cell division using the proliferation marker Ki67 shows similar proliferation rates in Sec10-KD cells compared to controls n> 50. B) Measurements of cyst diameter at 4 different time points during cyst development showing that there is a decrease in the size of Sec10-KD cysts compared to controls. n> 25 in each group. * p< 0.05; *** p<0.005; **** p< 0.001.

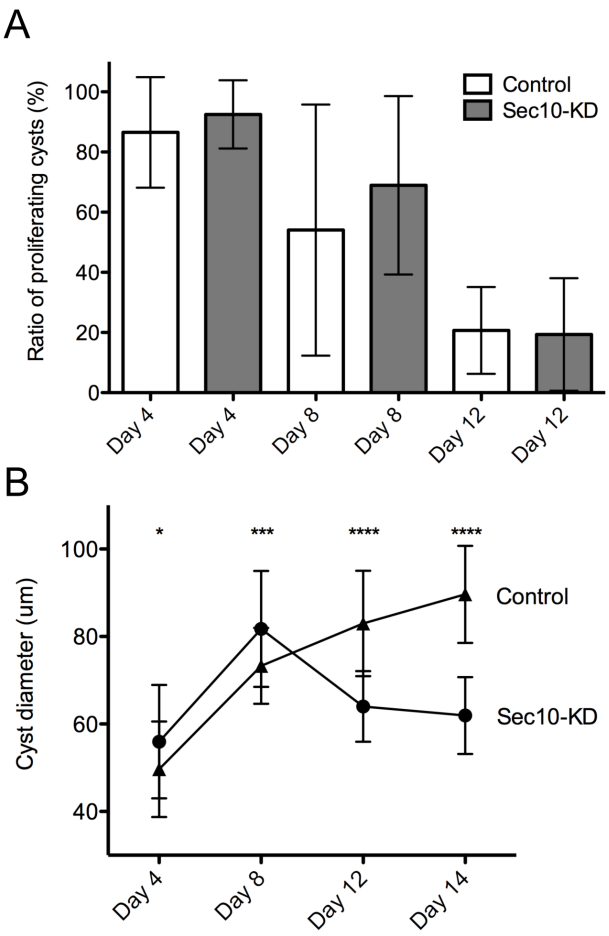

Due to the observation that there were no significant differences in the proliferation rate between Sec10-KD and control cysts, we tested for the activation of the apoptosis-induced cell extrusion pathway. We used different compounds to inhibit both apoptosis (broad spectrum caspase inhibitor Z-VAD-FMK) and apoptosis-induced extrusion signaling (sphingosine-1-phosphate S1P pathway)[61]. Sphingosine-1-phosphate has been shown to coordinate the mechanical process of eliminating cells from the epithelial monolayer. Treatment with the caspase inhibitor Z-VAD-FMK drastically reduced Sec10-KD extrusion to normal levels (Fig. 13A). In addition, S1P pathway inhibitors JTE013 and SKI II also led to almost no cellular extrusion in Sec10-KD cysts (Fig.13B). *This indicates that the cell extrusion observed in Sec10-KD cysts is likely due to an increased rate of apoptosis.*

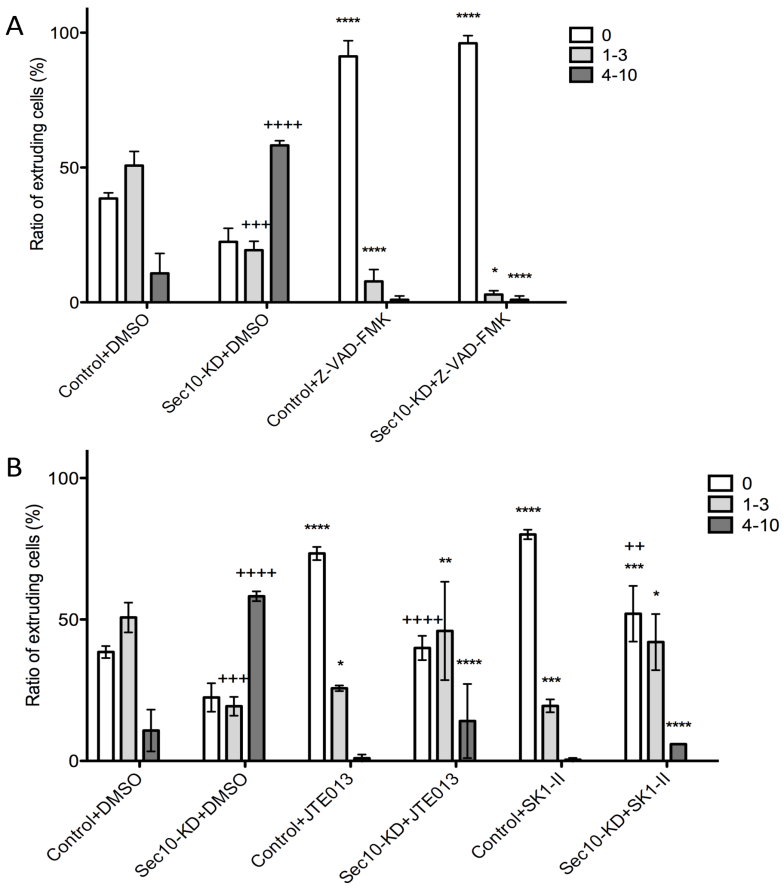

Figure 13: Inhibiting cell extrusion in Sec10-KD cysts restores normal cyst morphology. A) Treatment with Caspase inhibitor Z-VAD-FMK in Sec10-KD cysts with extruded cells to similar levels of the controls treated with the same inhibitor n>90. B) Chemical inhibitors for epithelial extrusion signaling (JTE013) and sphingosine kinase inhibitor II (SKI II) n>75. 1-way ANOVA. *Significance compared with DMSO treatment. + Significance compare with treated control cysts. *p<0.05; ** p<0.01; *** p<0.005; **** p<0.001; ++ p<0.01; +++ p<0.005; ++++ p<0.001.

2.2.3) *Sec10* knockdown cells are more sensitive to apoptotic stimuli

Since Sec10-KD MDCK cells in 3D culture have an increased rate of apoptosis, we analyzed the underlying cause of the higher apoptotic rate using Sec10-KD and control MDCK cells grown in 2D culture on transwell filters. These conditions provide enough time for the cells to establish polarization and high rates of primary cilia formation[21]. MDCK cells were seeded on transwell filters and grown for 7-10 days. We induced apoptosis using etoposide, a drug that forms a DNA complex with topoisomerase II causing breaks in the DNA. Sec10-KD cells had a significant increase in apoptotic cells upon etoposide treatment compared to control cells (Fig. 14A). Additionally, we induced apoptosis via UV irradiation from a HybriLinker UV crosslinker at 60mJ/cm^2 [62]. With just UV irradiation, Sec10-KD cells had a significant increase in apoptosis compared to controls with a $p<0.005$ (Fig.14B). Following induction of apoptosis, we wanted to determine if we could rescue the cells using caspase inhibitor Z-VAD-FMK. After 6 hours of incubation with the apoptosis inhibitor, the ratio of apoptotic cells in both the Sec10-KD and control cells significantly decreased (Fig. 14A). This shows that Sec10-KD MDCK cells are more sensitive to apoptotic stimuli compared to control cells.

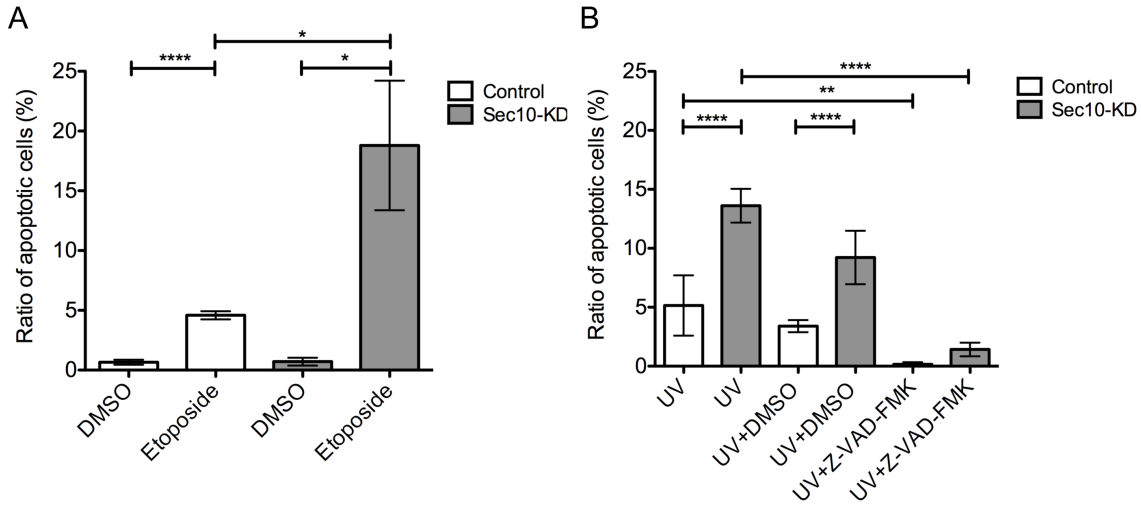

Figure 14: Sec10-KD cells demonstrate an increased sensitivity to apoptotic stimuli. A) Treatment of control and Sec10-KD cells grown on 2D transwells with topoisomerase inhibitor (etoposide) led to an increase in cells positive for activated Caspase 3 even though Sec10-KD cysts have a higher apoptotic ratio. B) UV treated MDCK cells showed that there is an increase in apoptotic sensitivity of the Sec10-KD cell line compared to controls. *p<0.05; ** p<0.01; *** p<0.005; **** p<0.001

2.2.4) *Sec10* knockdown cysts have defects in planar cell polarity

Cellular extrusion in 2D cell culture models has been previously described as being directed towards the apical surface of an epithelial monolayer into the lumen. To determine why Sec10-KD cysts have apoptotic cells extruding from the basal surface, we investigated the effect of Sec10 on apico-basal polarity in the epithelial monolayer. We examined polarity defects at the same time point in cyst development when cellular extrusion occurred. At day 12, collagen grown MDCK cysts were collected and immunostained for a basolateral protein (E-cadherin), apical protein (gp135), and tight junction protein (ZO-1). Sec10-KD cysts did not display abnormal staining patterns in polarity markers compared to control cysts, indicating that there was no gross defects in apico-basal polarity upon loss of Sec10 (Fig. 15A). We also evaluated the orientation of mitotic spindle formation in planar cell polarity in Sec10-KD cysts. Planar cell polarity is important for the development and maintenance of epithelial sheets. In a control MDCK cyst with proper planar cell polarity, the angle of the mitotic spindle is usually within the epithelial sheet, perpendicular to a line drawn from the cell to the center of the lumen. Immunohistochemistry of beta-tubulin allowed us to measure the mitotic spindle angles of dividing cells in collagen-grown Sec10-KD and control cysts. MDCK control cysts had a mean mitotic spindle angle of 62° (n=22) with majority of the mitotic spindles within the plane of the epithelial sheet. In contrast, Sec10-KD cysts had a mean mitotic spindle angle of 44° with a subpopulation oriented less than 20° relative to the center of the cyst (Fig. 15B and C). *This suggests a disruption of planar cell polarity in Sec10-KD cysts, which may contribute to the increased cellular extrusion observed on the basal surface of the epithelial monolayer.*

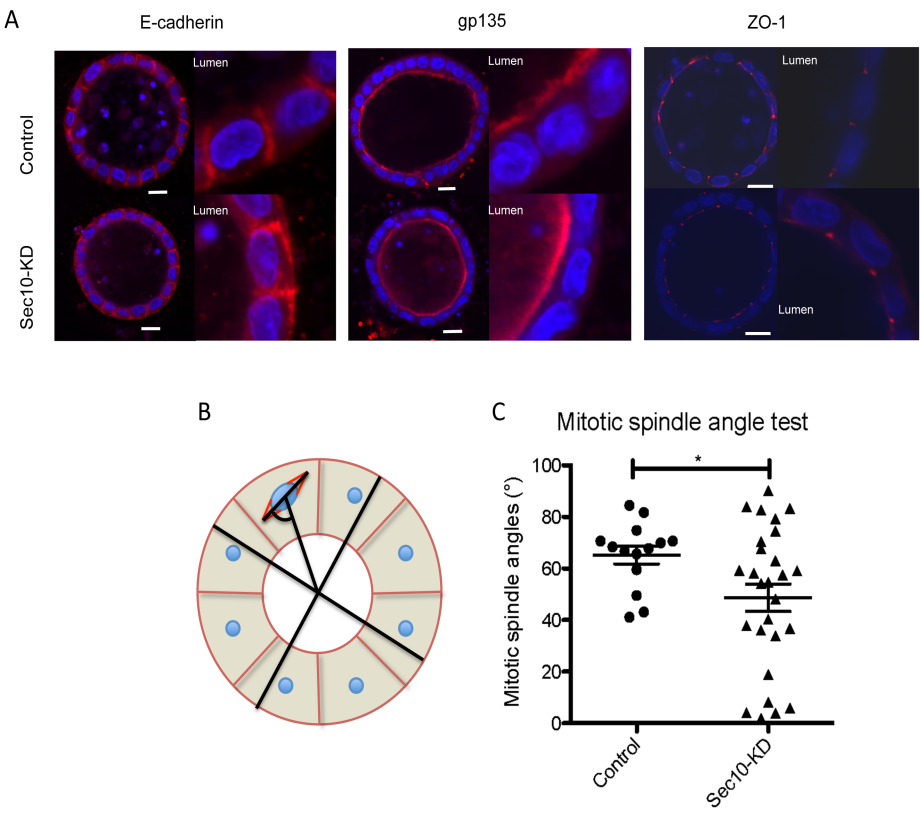

Figure 15: Analyzing apico-basal and planar cell polarity in MDCK cysts. A) Immunohistochemistry of day12 Sec10-KD and control cysts. Ecadherin (basolateral marker in red), gp135 (apical marker in red), and ZO-1 (tight junction marker in red). Dapi (blue. Scale bars = 10μm B) Schematic diagram of mitotic spindle angle calculations. C) Quantification of Sec10-KD and control cysts mitotic spindle angle formation at day 6. Quantification performed using B-tubulin immunohistochemistry. *p<0.05

2.3) DISCUSSION

In this study, we examined the role of *Sec10* and the exocyst complex in primary cilia and cyst formation, as essential mechanisms for epithelial cell morphogenesis and homeostasis. We used a Madin-Darby Canine Kidney Epithelial (MDCK) cell line derived from renal tubular epithelial cells as an *in vitro* tool to observe cyst formation in 3D culture. Cyst formation is a crucial process that involves lumen formation similar to what is observed during development of epithelial tissues, such as the kidney.

Initial reports suggested abnormal cyst formation in Sec10-KD MDCK cells, where there was no lumen present when seeded in type I collagen gel. Type I collagen allows MDCK cysts to form via the cavitation process rather that hollowing. We found in our experiments that *Sec10* depletion does not hinder lumen formation via the cavitation-dependent model during initial stages of cyst formation, but at later time points, they begin to show abnormalities. Our detailed analysis demonstrated that the cells within the lumen of Sec10-KD cysts, similarly to controls, underwent apoptosis, which is necessary for cavitation. Although Sec10-KD cysts did have apoptotic cells in the center of the lumen, they also had a significantly higher number of apoptotic cells on the basal surface of the cysts that was not observed in controls. We used small chemical inhibitors to determine whether the apoptotic cells on the basal surface were undergoing cellular extrusion, a process described by Rosenblatt et al[63] as a mechanism to maintain barrier integrity when cells in the epithelium begin to die. Cell extrusion is required for the regulation of cell density and critical for maintaining epithelial homeostasis[64]. Cellular extrusion can be triggered either by apoptosis of the cells within the epithelial sheet or overcrowding due to increased proliferation.

Using a broad-spectrum caspase inhibitor we were able to inhibit cell extrusion in the Sec10-KD cysts to normal levels, indicating that cell damage or apoptosis were possible triggers of extrusion in the Sec10-KD cysts. We also tested the possibility of overcrowding or over proliferation as a possible trigger of cell extrusion. We used Ki67 as a marker of proliferation, but measured no differences in the proliferation rate of Sec10-KD cysts compared to controls. These data suggested that the Sec10-KD cysts were more sensitive to apoptosis, which caused an increase in cell extrusion that led to a disrupted epithelial sheet. During apoptosis mediated cell extrusion, an epithelial cell

destined to undergo apoptosis triggers an actin and myosin ring formation in the neighboring cells that squeeze out the dying cell and control the direction of the extrusion[63]. This process does not disturb the barrier integrity, epithelial sheet, or any junction proteins[63]. Loss of *Sec10* and the exocyst complex could lead to abnormal epithelial cell extrusion and ultimately have an detrimental effect on the maintenance of epithelial homeostasis.

Due to our observation of an increase in apoptosis mediated cell extrusion, we next looked at the underlying mechanisms responsible for the disruption of epithelial homeostasis in Sec10-KD cysts. We concluded that Sec10-KD cysts have delayed primary cilia formation and the cilia that do develop were much shorter by day 10 of cystogenesis. This defect in primary cilia formation coincides with the timing of the increased cell extrusion. The primary cilium has been linked to the maintenance of epithelial homeostasis, including planar cell polarity[54]. Inversin, the mammalian homolog to one of the planar cell polarity core proteins, is localized to the primary cilium[65]. Many models of defective primary cilia have shown misregulated planar cell polarity in the developing epithelial tissues, such as polycystic kidney disease[66]. The increase in apoptotic sensitivity in Sec10-KD cysts can be linked to an increase in cell death associated with primary cilia defects observed in many *in vitro* and animal models[67,68]. The increase in apoptotic sensitivity we observed also supports the hypothesis that cell stress and injury can lead to primary cilia disassembly or reabsorption[69]. It is hypothesized that primary cilia respond to environmental cues to help cope with cell stress and injury, without it, cells become more sensitive to cell death[31,69]. The exact mechanism of the connection between primary cilia and cell survival is still unknown and further studies are warranted.

To our knowledge, this is the first report linking primary cilia to epithelial cell extrusion. Based on previous work, we had hypothesized that the exocyst complex is involved in maintenance of the barrier integrity of renal tubular epithelia. *Here we provide the first evidence that links the exocyst complex and epithelial cell extrusion.* In this study, we did not detect any differences in apical-basal polarity in Sec10-KD cysts compared to controls. However, there were discrepancies in the angles of the mitotic spindle, suggesting defects in planar cell polarity, which is responsible for the proper

orientation of daughter cells following cell division. This defect in planar cell polarity can be a contributing factor to the basal cell extrusion observed in the Sec10-KD cysts. We hypothesize that if the cells surrounding an apoptotic cell in the Sec10-KD cysts are not situated properly within the plane, proper cell extrusion will be comprised resulting in an increased ratio of basally extruded apoptotic cells.

In this model, MDCK cyst formation allowed us to look at the general maintenance of the epithelial barrier, but does not allow for influence of factors present in physiological settings. Here, we have shown a connection between the exocyst complex, ciliogenesis, cystogenesis, and cellular extrusion. We suggest that the exocyst plays a role in the maintenance of the epithelial barrier and loss of this complex may lead to disease pathologies, such as ciliopathies. In the following chapters, we generate a mouse model with tissue-specific knockout Sec10 to continue our studies of the exocyst in epithelial morphogenesis in an *in vivo* manner.

2.4) MATERIALS and METHODS

Cell Culture

Normal and Sec10-KD MDCK cell lines were a generous gift from Dr. Joshua Lipschutz (Medical University of South Carolina, Charleston, SC). Sec10 depletion in these cell lines was done used shRNA-mediated knockdown, monoclonal selection, and extensive validation[59,70]. MDCK cells were cultured in MEM with 10% fetal bovine serum and penicillin/streptomycin (complete medium). To grow cells as polarized epithelial monolayers, MDCK cells were seeded at a density of 2.5 x 10^5 cells/cm^2 on 12 mm Transwell polycarbonate filters (0.4um pore size; Corning Costar) and grown for 7-14 days with changes of medium every 2 days. To grow cells in 3D collagen gels, a single cell suspension of MDCK cells were added to a type I collagen (4,000U/ml) solution (PureCol Ez, Advanced Biomatrix) at a 5 x 10^4 cells/ml final density [71]. The cells in the collagen suspension were plated onto a 10 mm filter (0.020 - 0.20 mm pore size, Nunc), and collagen was allowed to gel at 37°C before the medium was added, which was then changed every 2 days.

Histological analysis

Immunoflourescent analysis of collagen-embedded MDCK cysts was performed as previously described[71]. Briefly, collagen gels were washed twice with PBS+ (1xPBS with 0.90mM Ca^{2+} and 0.49mM Mg^{2+}) treated with collagenase type VII (Sigma-Aldrich) for 10 minutes at 37°C, fixed with 4% paraformaldehyde at room temperature for 30 minutes, then quenched with 50mM NH_4CL for 10 min, and permeabilized with 0.1% saponin and 0.7% gelatin for 30 minutes. Samples were incubated in primary antibodies at 4°C overnight. To stain the cysts, the following primary antibodies were used: anti-E-cadherin, anti-ZO1, anti-cleaved caspase-3, and anti-Ki67 (Cell Signaling Technology); anti-gp135 (a generous gift from Dr. George K. Ojakian, State University of New York); anti-acetylated alpha-tubulin and anti-beta-tubulin (Sigma). After sufficient washes, cysts were incubated in DyLite 594-conjugated secondary antibody (Vector Laboratories) at a 1:1000 dilution at room temperature for 2h. Following extensive washes, cysts were stained for nuclei with DAPI at RT for 5 minutes. All samples were mounted with Prolong mounting medium (Molecular Probes) and then dried overnight.

Transwell filter-grown 2D cultures were subjected to a similar immunostaining procedure with the exception of collagenase treatment.

Microscopy

For quantification purposes, cells and cysts were viewed with an Olympus BX41 microscope using epifluorescence. For detailed analysis of cell polarity and primary cilia, cysts were imaged using an Olympus Fluoview1000 confocal microscope. All cilia length and cyst diameter measurements were performed using ImageJ software (NIH)[72].

Analyzing cellular extrusion and apoptosis

MDCK control and Sec10-KD cells were grown for one week on Transwell filters for apoptotic induction by UV–irradiation or etoposide treatment. To induce cell death, following the removal of medium, the cells were exposed to UV irradiation (60mJ/cm^2) in a HL-2000 HybriLinker UV crosslinker and left to recover in fresh medium for 6 hours in the presence or absence of caspase inhibitor Z-VAD-FMK (10μM), or DMSO vehicle alone (0.1%), prior to fixation and processing for immunofluorescent staining. For the etoposide treatment, upon removal of the medium, fresh complete medium was supplemented with etoposide (10μM), or DMSO alone (0.1%) as control, and the cells were incubated for 6 hours prior to fixation and processing for immunofluorescent staining with cleaved-caspase-3 antibody (Cell Signaling Technology).

Cell extrusion was inhibited starting at day 8 of cystogenesis, when collagen-grown Sec10-KD and control MDCK cysts were treated with either of the following agents: caspase inhibitor Z-VAD-FMK (10μM), sphingosine 1-phosphate receptor antagonist JTE013 (10μM), sphingosine kinase inhibitor SKI II (10μM), or DMSO (0.1%) as vehicle control until day 12 of cyst formation. Following treatment, the collagen-cultures were fixed and immunostained with cleaved caspase-3 antibody.

To determine the ratio of apoptotic cells in the monolayers, the number of active caspase-3 positive cells and the total nuclei were counted and averaged in 3 non-overlapping images of 60x magnification. These apoptosis induction experiments were repeated in three independent trials.

Cell extrusion was quantified in 3D collagen cultures, where 100 cysts were classified into groups based on the number of apoptotic cells on their outer side. Active caspase-3 positive cells that were outside of the spherical monolayer of the cyst epithelium were considered basally extruded.

Statistics

Graphs show means ± SD. Cilia length comparisons were performed using a nonparametric Kruskal-Wallis test. Cell extrusion rates following inhibitor treatment were analyzed using a one-way ANOVA with Bonferroni's post hoc test. In all other cases, a student t-test was performed to determine *p* values and determine significance.

Measurement of Mitotic Spindle Orientation

MDCK cysts were grown in type I collagen gels for 96 hours as above, and to increase the number of cells undergoing mitosis, a double-thymidine block was introduced based on the previously described method of Mao et al[68]. Briefly, after 96h in collagen culture, the forming MDCK cysts were incubated with 3mM thymidine in complete medium for 18h, released into fresh medium for 6 h, and incubated for a further 18 h with 3mM thymidine before their release from S phase by extensive washes with PBS to remove thymidine. Gels were fixed with 4% PFA and immunostained with anti-beta-tubulin antibody as above. To measure the spindle angles in 3D, z-stack images of meta- and early anaphase cells were taken in the middle region of the cysts and merged so that both poles of a spindle were in the same image. The center of the cyst was defined as the point of intersection between lines representing its longest and shortest diameters. The midpoint of the line connecting the two poles of the mitotic spindle was defined as the spindle center. The mitotic spindle angle was defined as the angle between the spindle axis and the line connecting the center of the cyst and the center of the spindle.

CHAPTER 3: *In vivo Sec10* knockout in urinary tract epithelial cells results in prenatal ureter malformations in mice

3.1) INTRODUCTION

In this chapter, we describe the generation of a novel transgenic mouse strain that for the first time, allows a tissue-specific deletion of the Sec10 gene. In the previous chapter, we reported new discoveries about the exocyst complex and its involvement in the maintenance of planar cell polarity, primary cilia formation, and epithelial cell extrusion. We showed that the exocyst complex plays a role in epithelial homeostasis and can have adverse effects if perturbed. Here, we extend our studies by knocking out the exocyst *Sec10* gene in epithelial cells of the ureteric bud in a mouse model. Previous attempts at an *in vivo* general knockout of exocyst members resulted in early embryonic lethality (mentioned in chapter 1). Therefore, we have established the first conditional allele of any exocyst member. Due to the role of the exocyst complex in other cell types other than epithelial cells, such as GLUT4 trafficking in adipocytes, we can use this conditional *Sec10* mouse to knockout the exocyst complex in other tissues to elaborate various functions of the exocyst complex in a mammalian model.

The Cre/loxp recombination system is one of the main strategies for gene deletion in mice. Cre recombinase is a specific DNA recombinase that recognizes 34 base pair regions called loxp sites[73]. When loxp sites are introduced into a gene flanking specific exons, the Cre-mediated recombination will delete the DNA located between the loxp sites[74]. This deletion inhibits both mRNA and protein expression.

The specificity of the targeted gene deletion in the Cre/loxp system relies on a engineered promoter to drive the Cre recombinase transgene in a specific cell type. Ksp-cadherin is a tissue specific cadherin that is exclusively expressed in the kidney and developing GU tract[75–78]. In the kidney, Ksp-cadherin has highest expression in the collecting ducts, loops of Henle, and the distal tubules. Ksp-Cadherin is a plasma membrane protein that mediates cell-cell interactions, including those important for epithelial differentiation[78]. The Ksp-1.3 Cre transgenic mouse was created in 2002, as reported by Shao et.al[79]. This mouse strain was created via the synthesis of a plasmid that contained 1.3 kb of the Ksp-cadherin 5' flanking region, a beta-globin promoter, and the Cre recombinase gene[75]. The Cre expression in these mice has been well-

established to duplicate native Ksp-cadherin expression, including in the embryonic ureteric bud[77,78]. We received these mice from the Jackson Laboratories, and subsequently crossed it with our floxed-*Sec10* mouse strain (described in Results) to induce knockout of Sec10 in a highly targeted manner.

3.2) RESULTS

3.2.1) Generation and validation of *Sec10* mouse model with targeted inactivation in upper urinary tract epithelium.

In order to study the consequences of *in vivo* disruption of Sec10 and the exocyst, we generated a floxed-*Sec10* (*Sec10^{FL}*) mouse strain that could be conditionally inactivated when crossed to Cre recombinase-expressing mice. To verify our floxed allele with a global knockout of *Sec10*, we crossed *Sec10$^{FL/FL}$* mice with *Sec10$^{FL/+}$;CMV-Cre/+* mice, which expresses *Cre* in all cells, including germ cells[75]. Despite a theoretical 25% Mendelian inheritance, no *Sec10$^{FL/FL}$;CMV-Cre* pups were born alive, and we failed to find any *Sec10$^{FL/FL}$;CMV-Cre/+* embryos even as early as E8.5 (n= 76 embryos from 8 pregnancies). This finding was consistent with results from the Sec8 general knockout mouse, where embryos failed to develop past gastrulation[22].

For specific inactivation of the *Sec10* gene in the kidney and ureter epithelium, we crossed the *Sec10^{FL}* mice to the *Ksp1.3-Cre* strain (*Ksp-Cre*), which express *Cre* in the branching ureteric buds and all the epithelial cells derived from the ureteric buds. This includes the distal nephron tubules and urothelium of the renal pelvis and ureter[73,77,80], but it excludes the proximal nephron and urothelium of the bladder. After crossing the *Sec10^{FL}* and *Ksp-Cre* strains, PCR assays were used to confirm the genotypes (Fig. 16A), with confirmation of the deletion of *Sec10* exons 7-10 due to Cre recombination only in genomic DNA isolated from newborn kidneys and ureters of *Sec10$^{FL/FL}$;Ksp-Cre* mice (Fig. 16A). Measuring Sec10 proteins levels by Western blots showed a clear decrease in *Sec10$^{FL/FL}$;Ksp-Cre* newborn kidneys and ureters compared to *Sec10$^{FL/FL}$;+/+* littermate controls (Fig. 16B and C). As expected, the ureters, comprised of mainly two cell types, the *Cre*-expressing urothelial cells and the non-*Cre* expressing surrounding smooth muscle cells, demonstrated a much larger decrease in Sec10 level than the kidneys, which contained many cell types not expressing *Cre*.

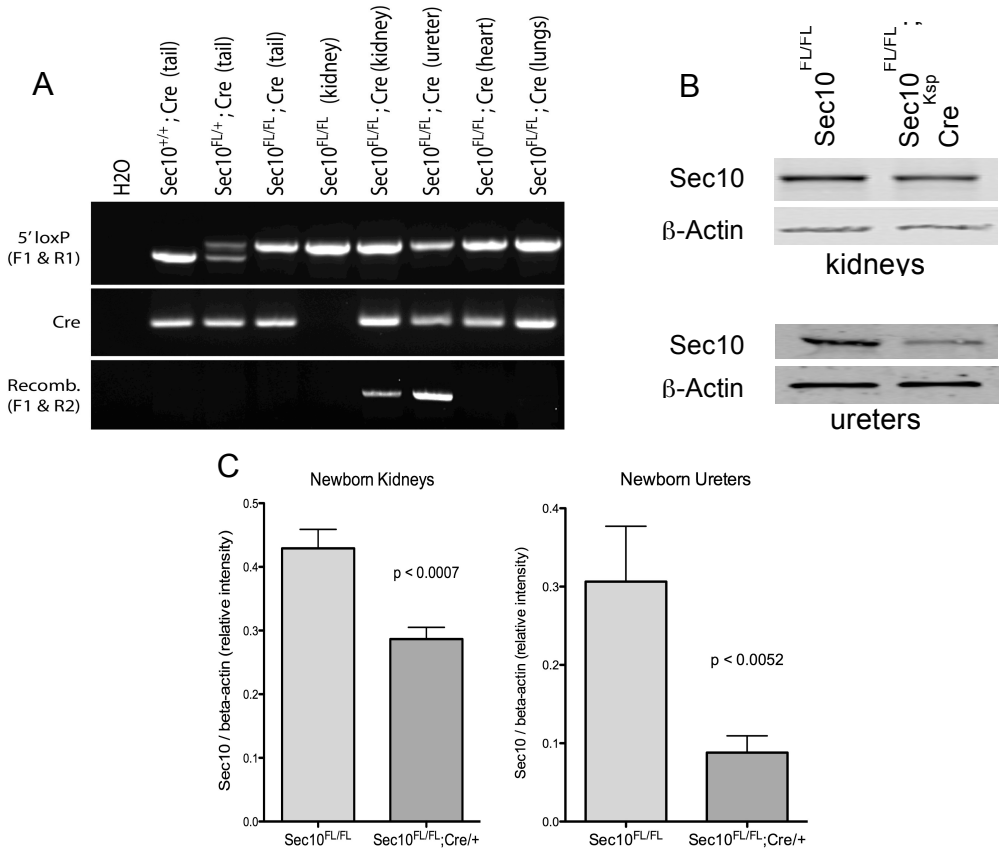

Figure 16: Validation of targeted *Sec10* knockout in *Sec10$^{FL/FL}$;Ksp-Cre* mice. A) PCRs from genomic DNA of various tissues were able to genotype floxed-Sec10 alleles (upper gel), confirm Cre transgene in our strains (middle gel), and detect recombination deleting exons 7-10 specifically in Cre-expressing tissues (lower gel). B) In Sec10$^{FL/FL}$;Ksp-Cre mice, Western blotting showed reduced Sec10 protein in whole kidney lysates and isolated ureters, compared with Sec10$^{FL/FL}$ littermate controls. C) Quantification of newborn kidney and ureter western blots. (n=5).

3.2.2) Newborn *Sec10$^{FL/FL}$;Ksp-Cre* pups have bilateral obstructions in the ureteropelvic junctions leading to complete anuria by birth

We were surprised to observe *Sec10$^{FL/FL}$;Ksp-Cre* pups almost always died as neonates, although a few (<1%) survived past the first day, typically dying the next day. The longest lived *Sec10$^{FL/FL}$;Ksp-Cre* mouse was sacrificed at 6 weeks, and the second oldest mouse survived to 18 days. The *Sec10$^{FL/FL}$;Ksp-Cre* mouse that survived had abnormal kidneys with a cystic phenotype shown in figure 26. In all of the dead newborn *Sec10$^{FL/FL}$;Ksp-Cre* pups, we observed severe bilateral hydronephrosis (Fig.17 B,D,F), which was never detected in any control littermates (Fig. 17 A,C,E).

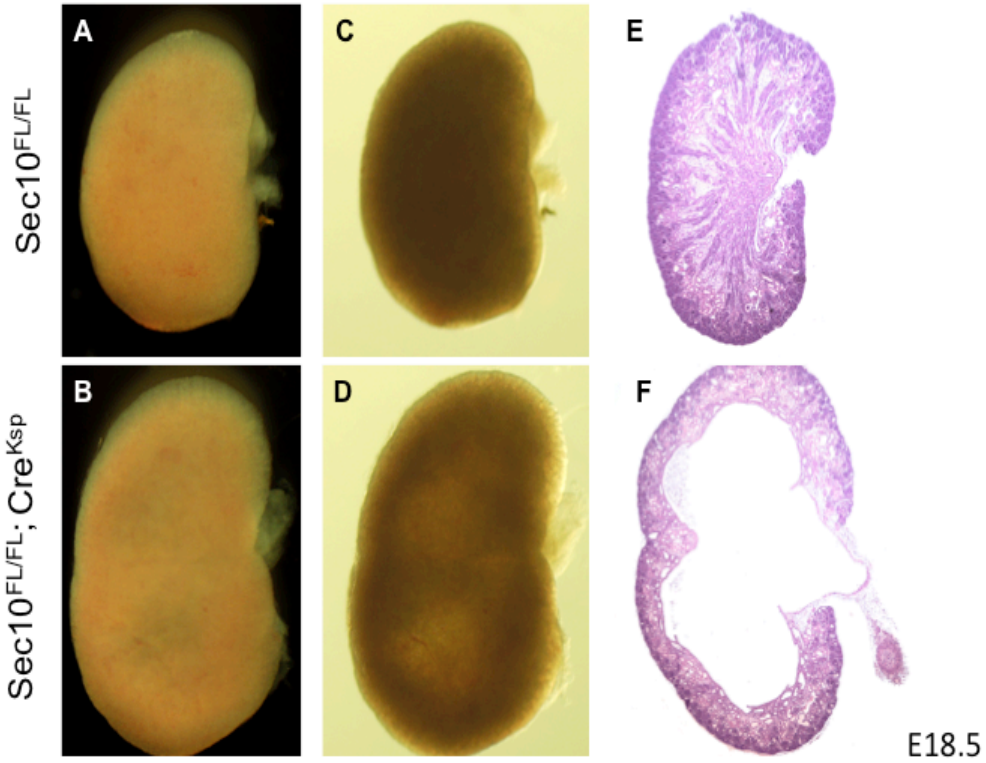

Figure 17: Conditional deletion of *Sec10* resulted in neonatal lethality and severe bilateral hydronephrosis. B,D,F) Dissected kidneys from E18.5 *Sec10$^{FL/FL}$;Ksp-Cre* and A,C,E) *Sec10$^{FL/FL}$* control littermates demonstrated significant enlargement due to hydronephrosis. A-B) Observations from gross dissections. C-D) backlit images of the dissected kidneys. E-F) H&E stained histology sections confirmed the hydronephrosis observed in the *Sec10$^{FL/FL}$;Ksp-Cre* kidneys.

Hydronephrosis can arise due to physical obstruction of the urinary tract, or a loss of smooth muscle strength surrounding ureters or the bladder leading to impaired peristalsis. Physical obstructions of the urinary tract can occur in two main areas; the upper urinary tract and the lower urinary tract. To test for obstructions in newborn and E18.5 *Sec10$^{FL/FL}$;Ksp-Cre* kidneys, we used a pulled-glass micropipette to inject blue dye into the renal pelvic area of dissected kidneys. In control kidneys (*Sec10$^{FL/FL,}$* and *Sec10$^{FL/+}$;Ksp-Cre)* without hydronephrosis (n = 41), we could easily observe the dye traveling down the length of the ureter and accumulating in the bladder (Fig. 18A). In all *Sec10$^{FL/FL}$;Ksp-Cre* kidneys displaying hydronephrosis (n = 14), dye migration would stop at the ureteropelvic junction (UPJ) (Fig. 18B). In some *Sec10$^{FL/FL}$;Ksp-Cre* ureters, microscopic inspection revealed visible deposits of white debris at the UPJ, also suggesting the presence of a physical obstruction (Fig. 18C). We also performed these dye injections in one *Sec10$^{FL/FL}$;Ksp-Cre* kidney without hydronephrosis, and although the dye traveled down to the bladder, the ureter had visibly abnormal lumens with rough irregular edges, compared with normal controls (Fig. 18D and E). Using histological methods, we analyzed the morphology of obstructed ureters from newborn *Sec10$^{FL/FL}$;Ksp-Cre,* as compared with control littermates.

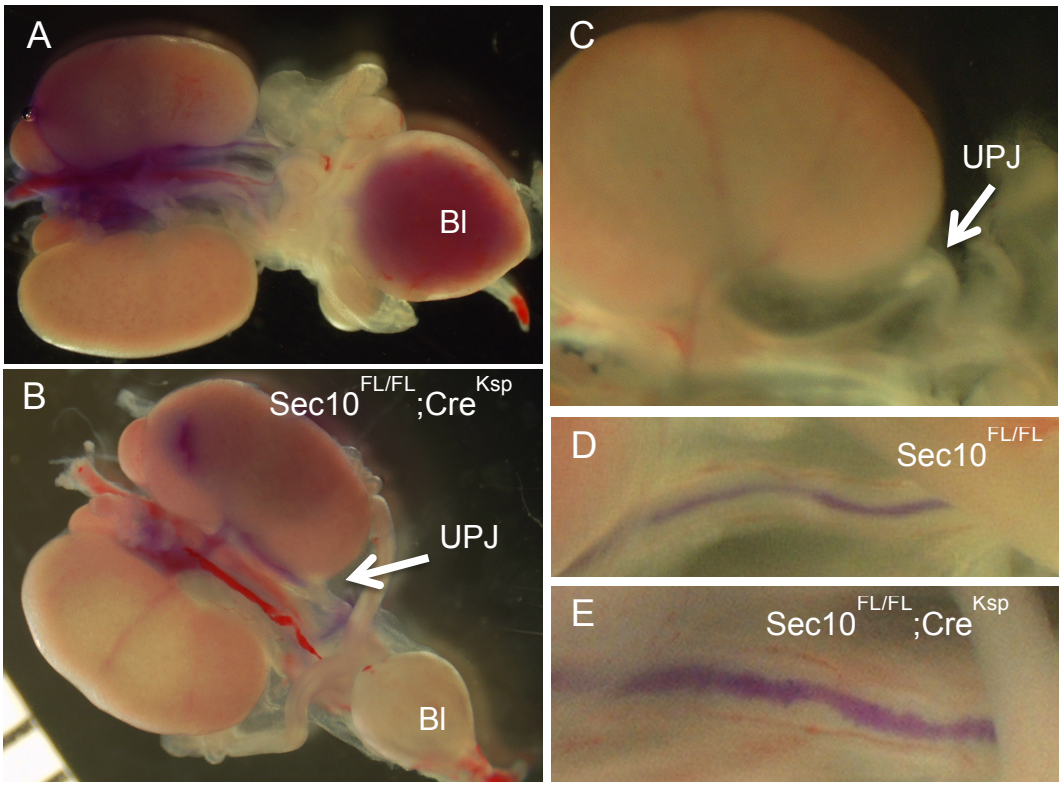

Figure 18: Hydronephrosis in *Sec10$^{FL/FL}$;Ksp-Cre* kidneys is due to functional obstructions in ureters at the UPJ. Urinary tracts, including both kidneys, intact ureters, and bladder were removed from mutant *Sec10$^{FL/FL}$;Ksp-Cre* mice and littermate controls (*Sec10$^{FL/FL}$* and *Sec10$^{Fl/+}$;Ksp-Cre*) at various ages (E17.5, E18.5, and P0). A) Blue dye was injected into the renal pelvis, and in control kidneys with no hydronephrosis, the dye migrated down the ureters and accumulated in the bladder. B) In each hydronephrosed *Sec10$^{FL/FL}$;Ksp-Cre* kidney tested, the dye stopped at the UPJ (indicated by arrow). C) Occasionally in these kidneys, prior to injection, a white mass of debris was visible above the UPJ blockage (indicated by arrow). D-E) In one of the few newborn *Sec10$^{FL/FL}$;Ksp-Cre* kidneys that did not show hydronephrosis, dye injections traveled to the bladder, but revealed a rough urothelial appearance not observed in controls.

H&E-stained sections of the actual UPJ obstructions in newborn *Sec10$^{FL/FL}$;Ksp-Cre* ureters revealed the complete absence of a lumen (Fig. 19B), with loss of urothelial layer (Fig. 19D) compared to control litter mates (Fig. 19A,C). E-cadherin and smooth muscle actin (SMA) immunostaining are markers of the various cell populations within the ureter. Control *Sec10$^{FL/FL}$* mice have a multilayered urothelium indicated by E-cadherin (green) with surrounding smooth muscle layer (red). In contrast, in the obstructed segments of *Sec10$^{FL/FL}$;Ksp-Cre* ureters, few, if any, cells stained positive for

E-cadherin (Fig 19D). *This indicates a loss of the urothelial layer, required for proper function of the urothelium.*

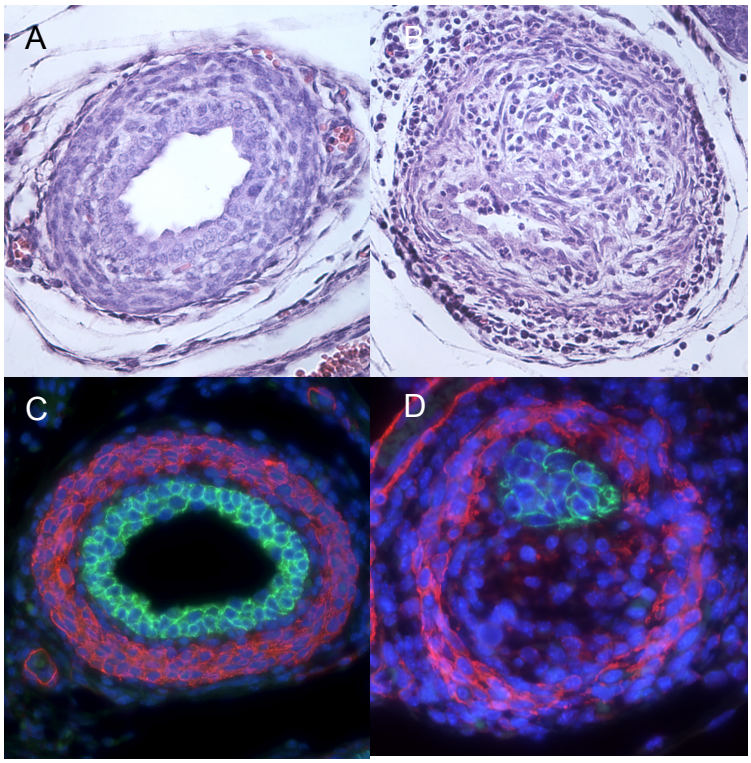

Figure 19: At the UPJ in newborn mice, histological analysis revealed the complete disappearance of the ureter lumen in *Sec10$^{FL/FL}$;Ksp-Cre* ureters due to overgrowth of cells with a mesenchymal morphology. A) H&E staining of control ureter cross-section showing a multilayered urothelium. B) H&E staining of the obstruction in *Sec10$^{FL/FL}$;Ksp-Cre* ureters showing cellular overgrowth C) Immunostaining for E-cadherin (green) and SMA (red), which in control ureters showed a normal cellular organization. D) In *Sec10$^{FL/FL}$;Ksp-Cre* ureters, only at the UPJ obstruction, we found the urothelial cells had greatly reduced in number, the lumens had completely disappeared, and the overgrown cell population was SMA-positive, E-cadherin-negative.

3.2.3) Newborn *Sec10$^{FL/FL}$;Ksp-Cre* mice have complete anuria and likely die of heart failure

In order to attempt to determine the cause of death in the *Sec10$^{FL/FL}$;Ksp-Cre,* we first quantified the amount of urine in newborn bladders. Control and heterozygous mice, had approximately 10-40 μL of urine in their bladders (Fig. 20). In contrast, *Sec10$^{FL/FL}$;Ksp-Cre* pups had no urine in their bladder despite the observation that they were still nursing due to the presence of milk in their stomachs. From this, we hypothesized that the *Sec10$^{FL/FL}$;Ksp-Cre* pups died due to a pressure overload that would lead to cardiac failure.

To test this hypothesis, we performed doppler ultrasound and histological analysis on newborn hearts. Doppler ultrasound has been used as a reliable non-invasive technique for diagnosing relaxation of the left ventricle[81,82]. The early to late filling velocity (E/A ratio) is used to categorize patients as either having diastolic dysfunction or not[81] In healthy individuals the E/A ratio is between 1 and 2, where the E wave of the echocardiography is taller than the A wave. Deviations from this ratio indicate stiffness in the left ventricle. Newborn *Sec10$^{FL/FL}$;Ksp-Cre* mice an E/A ratio of 0.5 compared to control mice that had an E/A ratio of 1.4 (Fig.21A). Histological analysis revealed *Sec10$^{FL/FL}$;Ksp-Cre* also had enlarged hearts compared to control mice. We still do not know the exact cause of death in the *Sec10$^{FL/FL}$;Ksp-Cre* mice, but we hypothesize that the UPJ obstruction inhibits the passage of urine leading to a pressure overload that causes cardiac failure approximately 8-14 hours after birth.

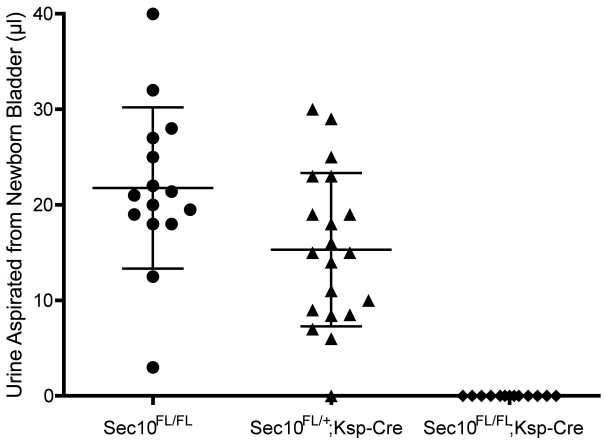

Figure 20: *Sec10$^{FL/FL}$;Ksp-Cre* mice have complete anuria at birth compared to controls. Aspirated urine from bladders of *Sec10$^{FL/FL}$;Ksp-Cre* and control ureters were quantified. Control and heterozygous ureters had between 10-40µL of urine in their bladders, while *Sec10$^{FL/FL}$;Ksp-Cre* mice had no urine.

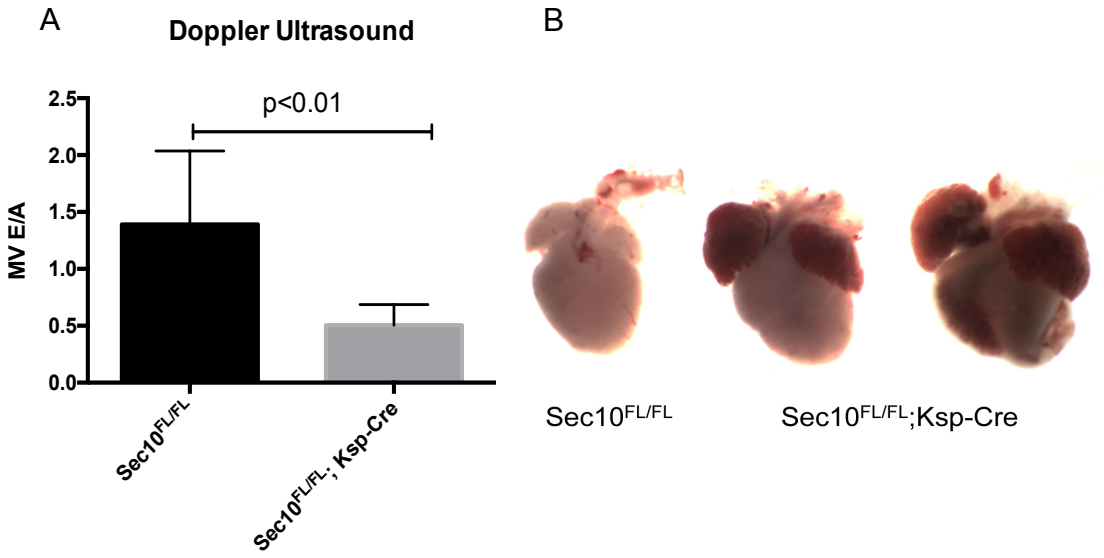

Figure 21: *Sec10$^{FL/FL}$;Ksp-Cre* hearts show enlargement and decreased ventricular relaxation compared to controls. A) Doppler ultrasound of newborns for each genotype. (n=6-9). B) gross heart images of Sec10$^{FL/FL}$;Ksp-Cre and control mice showing distended atria and hemorrhaging.

3.2.4) UPJ obstructions develop prenatally in *Sec10$^{FL/FL}$;Ksp-Cre* embryos between E16.5 and E18.5 and are associated with a disappearance of uroplakins.

We determined that *Sec10$^{FL/FL}$;Ksp-Cre* mice died as neonates due to an obstruction in the UPJ region leading to complete anuria and hydronephrosis. Our next goal was to determine the timeline for the onset of the obstruction and identify the cell population that filled the lumen of the *Sec10$^{FL/FL}$;Ksp-Cre* ureters. Previous immunostaining and H&E staining of ureter cross-sections at newborn and E18.5 showed a physical obstruction already developed (Fig. 19). Therefore, we collected embryos at earlier time points to determine the stage at which the ureter obstruction begins to develop. In control mice, at E16.5 the urothelial layer in the ureter begins to form multiple layers (Fig. 22E). By E17.5, the urothelium is stratified into 2 layers as indicated by E-cadherin (green) (Fig. 22F). In contrast, *Sec10$^{FL/FL}$;Ksp-Cre* ureters appeared relatively normal at E16.5 (Fig. 22G), but by E17.5 the urothelial layer fails to stratify and appears as a severely disrupted monolayer (Fig. 22H). The observation that by E17.5 *Sec10$^{FL/FL}$;Ksp-Cre* ureters begin to lose their urothelial layer, coincides with previous results where the urothelial layer is completely missing by E18.5. This led us to conclude that changes occurring between E16.5 and E18.5 lead to the obstruction prior to birth in *Sec10$^{FL/FL}$;Ksp-Cre* ureters. Uroplakin proteins are commonly used as markers of a stratified urothelium and mark the lumen-facing surface of mature superficial cells. Uroplakin-3 (Upk3) protein is detectable in control ureters beginning at E16.5 and has noticeably increasing expression by E17.5 (Fig. 22 A and B). In *Sec10$^{FL/FL}$;Ksp-Cre* ureters, Upk3 protein was detectable (but patchy) at E16.5, but was severely decreased in amount as the ureter developed to E17.5 (Fig. 22 C and D). This is the first evidence showing that *Sec10* knockout in the urothelial progenitor cells may lead to abnormal urothelial differentiation.

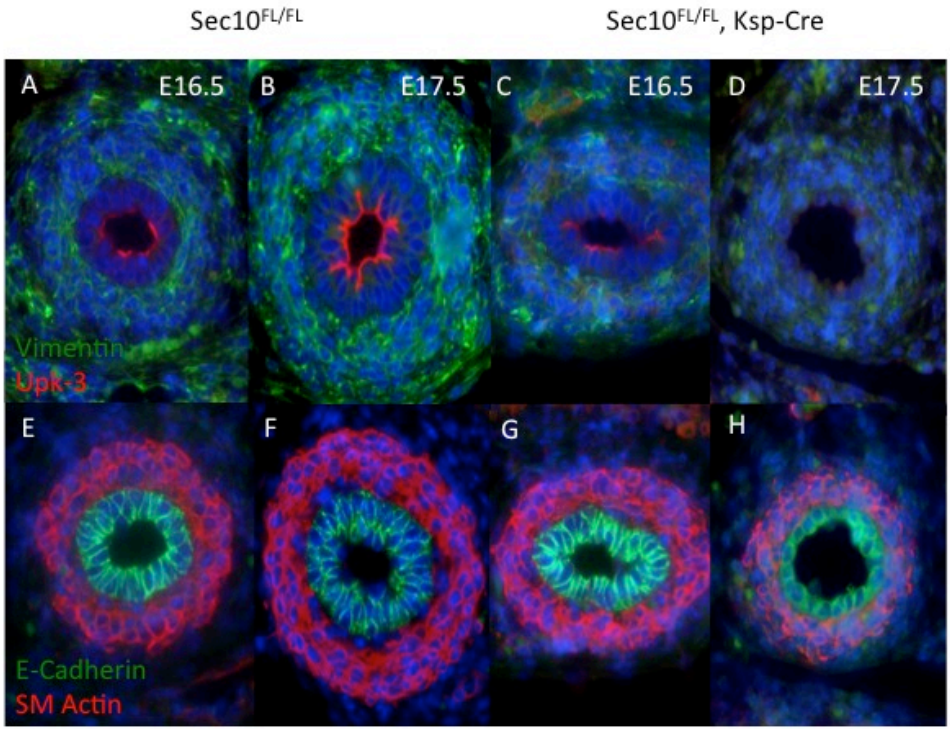

Figure 22: UPJ obstructions in *Sec10$^{FL/FL}$;Ksp-Cre* ureters arise from overgrowth of surrounding mesenchymal cells and disappearance of urothelial cells. A-B) *Sec10$^{FL/FL}$* ureter cross-sections at E16.5 and E17.5 showing an increase in uroplakin 3 expression as the embryo develops. Vimentin (green) Uroplakin-3 (red). C-D) *Sec10$^{FL/FL}$; Ksp-Cre* ureter cross sections showing a decrease in uroplakin expression at the apical surface. E-F) Control *Sec10$^{FL/FL}$* ureters immunostained with E-cadherin (green) and Smooth muscle actin (red) showing a multilayered urothelium with surrounding smooth muscle. G-H) *Sec10$^{FL/FL}$; Ksp-Cre* ureters showing a multilayered urothelium at E16.5 with subsequent loss of E-cadherin cells at E17.5

Above the UPJ blockage, the urothelium of *Sec10$^{FL/FL}$;Ksp-Cre* mice had completely lost the normal multilayered formation and was comprised of a single layer of unusually rounded epithelial cells (Fig. 23 A and B). This was accompanied by a thinning smooth muscle cell layer, which appeared abnormally stretched. This urothelial cell phenotype above the blockage has been noted in other models of UPJ obstruction, including surgical models[40], and so it may be that this change is secondary to the increased pressure and distension of the renal pelvis and hydroureter. Upon further analysis, we found a complete absence of uroplakin-3 in upper ureters and renal pelvis of newborn *Sec10$^{FL/FL}$;Ksp-Cre* embryos, but normal localization in *Sec10$^{FL/FL}$* and *Sec10$^{FL/+}$;Ksp-Cre* litter, (Fig. 23 C and D). As basal urothelial cells express cytokeratin-5 and

superficial urothelial cells do not, immunostaining with cytokeratin-5 suggested there were some superficial *Sec10*$^{FL/FL}$*;Ksp-Cre* urothelial cells remaining in the pelvis, but these superficial cells did not have any measurable uroplakin-3 (Fig. 23 C and D). In sections of the ureter immediately below the obstruction in newborn *Sec10*$^{FL/FL}$*;Ksp-Cre* mice, a complete absence of uroplakin-3 was observed (Fig 23. E and F). However, uroplakin-3 was detected in *Sec10*$^{FL/FL}$*;Ksp-Cre* bladders and lower ureters (Fig. 23, G and H), confirming that the absence of uroplakin-3 was limited to urothelium in the upper ureters and renal pelvis, where Cre was expressed.

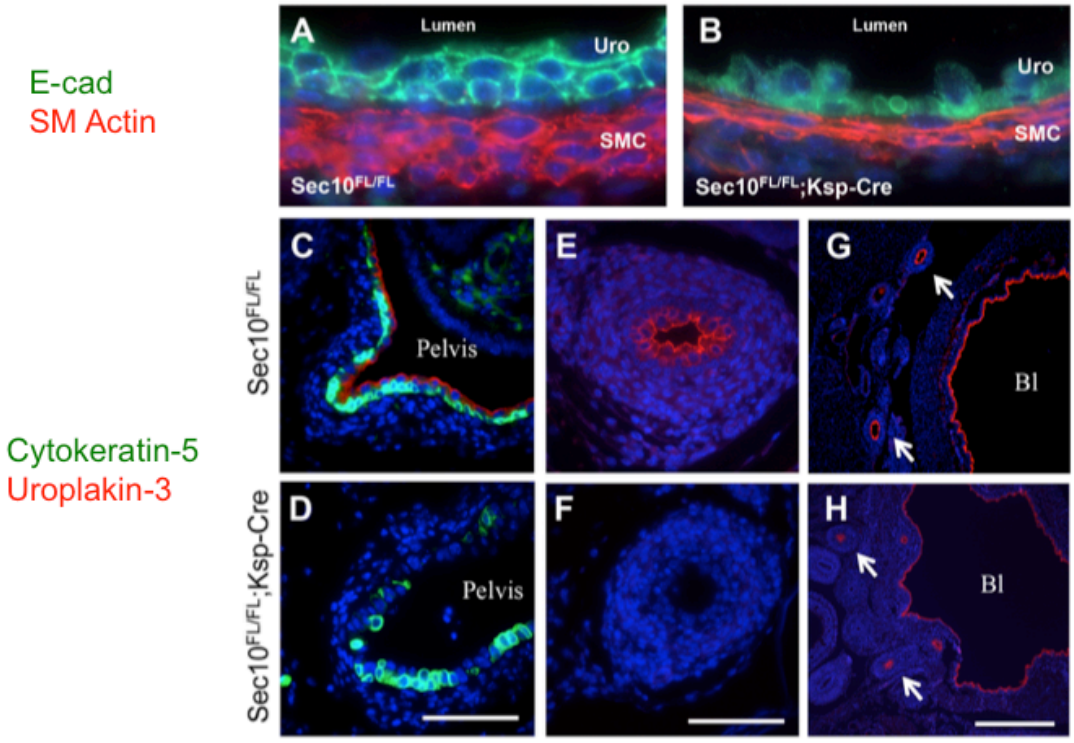

Figure 23: Urothelial cells with *Sec10* inactivation displayed an absence of uroplakin-3 at the luminal surface. A-B) Immunostaining for E-cadherin (green) and SMA (red) in *Sec10*$^{FL/FL}$*;Ksp-Cre* newborn ureters immediately above the blockage revealed urothelial cells that were no longer multilayered, with smaller size and poor cell-cell contact, compared with littermate controls. C-D) Immunostaining for uroplakin-3 (red) and cytokeratin-5 (green) revealed that urothelial cells in the renal pelvis of *Sec10*$^{FL/FL}$*;Ksp-Cre* mice completely lacked uroplakin-3 protein. E-F) Immediately caudal to the UPJ obstruction in newborn *Sec10*$^{FL/FL}$*;Ksp-Cre* ureters confirmed the absence of uroplakin-3 (red) in *Sec10*$^{FL/FL}$*;Ksp-Cre* samples (F), but not in controls (E). G-H) There was no change in uroplakin-3 (red) in the most distal segments of the ureters (arrows) or in the bladder (Bl) of *Sec10*$^{FL/FL}$*;Ksp-Cre* mice. Scale: bar = 0.1mm (B - F); bar = 0.5mm (G and H). Nuclei were counterstained with DAPI.

The presence of a physical obstruction in the ureters by E18.5 also raised the question as to whether or not the cells blocking the lumen of the *Sec10$^{FL/FL}$;Ksp-Cre* ureters were actively proliferating. Ki67 is a protein that is expressed only during mitosis[83], allowing us to visualize cells with immunostaining that are actively dividing. By co-staining ureter sections with Ki67 (green) with smooth muscle actin (SMA, red) at E16.5 and E17.5, we determined the proliferation rate of the non-epithelial cells that filled the lumen of the ureter. There were no significant difference in the proliferation of SMA+ cells at E16.5, but at E17.5 *Sec10$^{FL/FL}$;Ksp-Cre* ureters had an increase in SMA+ cell proliferation (Fig. 24). Since both smooth muscle and myofibroblasts (activated fibroblasts) would be expected to be positive for SMA staining, we could not necessarily conclude which cell type was proliferating into the lumen. However, we hypothesized that this increase of SMA+ cell proliferation could be due to a fibroproliferative response.

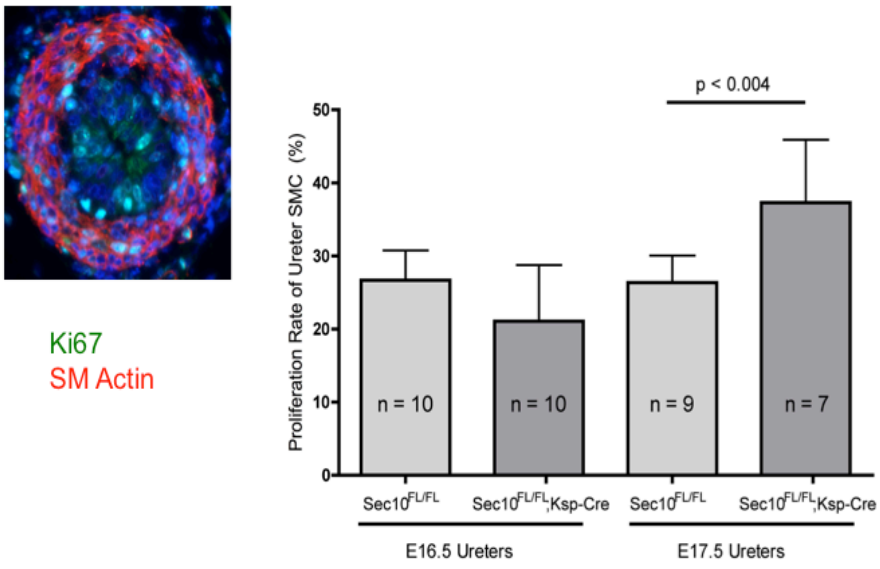

Figure 24: Increased proliferation of smooth muscle actin positive cells at E17.5. Ureter cross sections were stained with Ki67 and SM Actin. The Ki67 positive and SM Actin positive cells were quantified. At E16.5 there is no difference in cell proliferation in the smooth muscle actin positive cells. However at E17.5, there is a significant increase in proliferation in the *Sec10$^{FL/FL}$;Ksp-Cre* ureters compared to controls.

3.2.5) Renal tubules of non-obstructed *Sec10* conditional knockout mice also show primary cilia defects and epithelial cell extrusion similar to the *in vitro* *Sec10* knockdown cells

In our *Sec10*$^{FL/FL}$*;Ksp-Cre* mouse model, ~5% of knockout mice survived passed weaning age into adulthood (Fig. 25). These mice did not display an obstructed ureter phenotype with hydronephrosis.

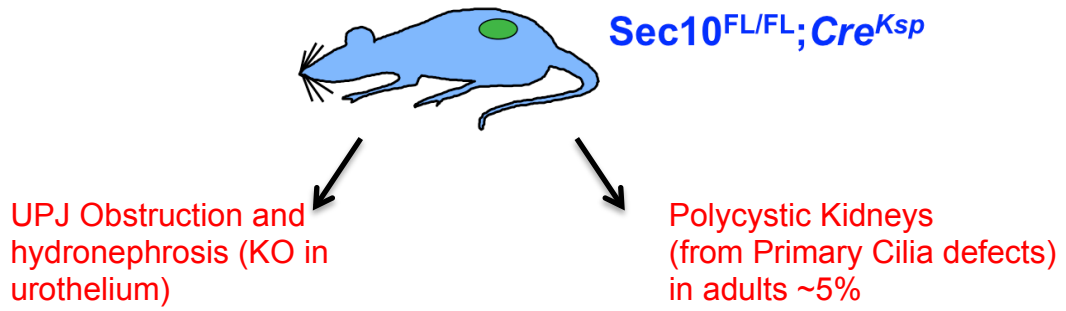

Figure 25: Approximately 5% of *Sec10*$^{FL/FL}$*;Ksp-Cre* mice survive to adulthood. Majority of the *Sec10*$^{FL/FL}$*;Ksp-Cre* mice die within 6-12 hours of birth due to UPJ obstructions and hydronephrosis, but some of the mice survive to adulthood but have primary cilia defects and a polycystic kidney phenotype.

Instead, they exhibited a cystic kidney phenotype with dilated kidney tubules. We analyzed these adult mice and observed similar results to what was seen in our *in vitro* MDCK cyst model. H & E stained kidneys from a 20-day-old adult show the non-obstructed phenotype with dilated tubules (Fig. 26A and B) compared to controls. This phenotype is similar to what we would have expected if there were defects in primary cilia leading to polycystic kidney disease. Therefore, we quantified the number of cilia-to-nuclei in targeted kidney tubules to determine the rate of primary cilia formation and used Image J software to measure the lengths of the primary cilia. *Sec10*$^{FL/FL}$*;Ksp-Cre* mice had a significantly decreased cilia-to-nuclei ratio, as well as, shorter cilia compared to *Sec10*$^{FL/FL}$ mice (Fig. 26C and D).

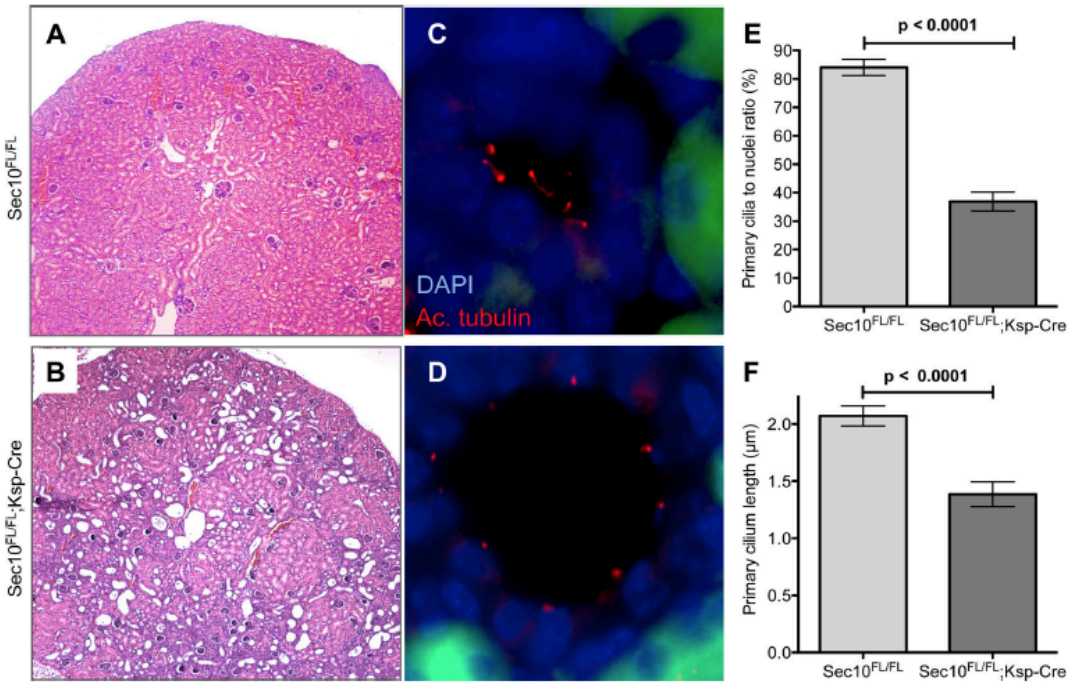

Figure 26: Cystic kidney phenotype and primary cilia defects observed in *Sec10$^{FL/FL}$;Ksp-Cre* mice. A-B) Kidneys from 20 day old control and non-obstructed *Sec10$^{FL/FL}$;Ksp-Cre* mice. *Sec10$^{FL/FL}$;Ksp-Cre* mice revealed a cystic phenotype compared to the controls. C-D) Immunohistochemistry of Acetylated Tubulin in *Sec10$^{FL/FL}$;Ksp-Cre* and control distal kidney tubules. E-F) Quantification of primary cilia immunohistochemistry show that *Sec10$^{FL/FL}$;Ksp-Cre* mice have a decrease in primary cilia formation and cilium length.

Additionally, *Sec10$^{FL/FL}$;Ksp-Cre* renal tubules showed evidence of apoptosis and cellular extrusion from the apical surface of the epithelial lumen (Fig.27). This is in contrast to the basal cellular extrusion observed in the MDCK cysts, but it may be explained due to the architecture of the kidney tissue that prevents basal epithelial extrusion. This data shows that *Sec10* is required for primary cilia formation epithelial monolayer maintenance *in vivo* and the mouse model can also be used to study primary cilia related diseases, such as polycystic kidney disease.

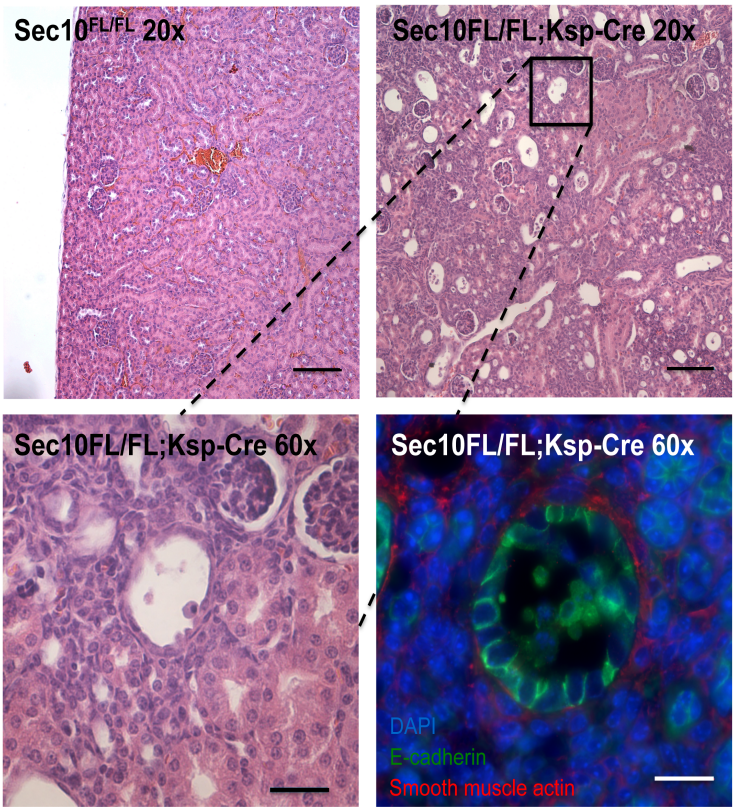

Figure 27: Kidney specific *Sec10* knockout in mice leads to abnormal epithelial cell extrusion. Kidneys from 20 day old mice show extruded apoptotic cells of epithelial origin inside kidney tubules of *Sec10$^{FL/FL}$;Ksp-Cre* mice. Scale bars = 100um in x20 magnification (top), 20um in x60 magnification (bottom).

3.3) DISCUSSION

We report generation of a conditional murine knockout for the *Sec10* gene, a central subunit of the exocyst complex. This is the first such conditional allele reported for any exocyst gene and can be valuable for studying the exocyst's role in a large variety of tissues and diseases. Our *Sec10* conditional knockout mouse is the first non-surgical mouse model of CON with targeted deletion of *Sec10* the ureter. This knockout leads to an obstruction in the ureteropelvic junction, which is a common phenotype observed in clinical cases of CON. We determined a timeline of the progression of the UPJ obstruction, and have concluded that the obstruction begins at E17.5 where we see decreased uroplakin expression on the apical surface of ureter urothelial cells. Uroplakin expression is a marker of differentiated superficial urothelial cells and decreased expression can be indicative of defects in cell differentiation.

The progression of kidney disease arising from CON has been studied for decades, but despite this, we still know very little about the genetic and cellular basis of human UPJ obstructions. The unilateral ureter obstruction (UUO) animal model, which requires surgery to ligate one ureter, has been the most widely studied model of CON. This model has greatly advanced the current understanding of the stages of renal pathology after the ureter obstruction and after correction of the obstruction. The obstructed kidney develops parenchymal loss and interstitial fibrosis that leads to loss of renal function, a pathology common to many renal diseases. However, surgical models like the UUO are labor intensive with some degree of technical variability, and also limited in that they cannot be used to investigate the natural causes of human UPJ obstructions. Additionally, with the exception of large animals models like sheep[42], they cannot be used to study ureter obstructions that occur *in utero*.

Despite many rodent genetic models with adult onset hydronephrosis, few have presented with prenatal development of congenital obstructive nephropathy[38,84,85]. One of these models is the well-characterized *megabladder* mouse that displays hydronephrosis of variable severity and accompanying renal insufficiency[86–88]. The male megabladder mice live up to 4-6 weeks, and the females live up to 1 year[86], which allows study of renal deterioration. However, this mutant mouse strain has an obstruction in the lower urinary tract with an enormous bladder expansion, while our

Sec10$^{FL/FL}$*;Ksp-Cre* mice consistently display *in utero* UPJ obstructions that more commonly present in humans. Likewise, few genetic models of CON have been identified and characterized. These models have arisen from targeted deletion of genes necessary for growth or differentiation of ureter smooth muscle cells or pacemaker cells[44,45]. However, these models are non-obstructive, with a failure of ureter muscle tension that leads to hydroureter and hydronephrosis. The models that display UPJ obstructions typically involve inducing over proliferation of the surrounding smooth muscle, but without urothelial degeneration or fibrotic infiltration of the lumen[46,47]. None of these mouse models of CON are neonatal lethal and they typically have wide-ranging variability and penetrance. Uroepithelium-specific knockout of sonic hedgehog did result in hydroureter and secondary hydronephrosis; however, this was non-obstructive in nature and was a result of reduced smooth muscle cell proliferation[89]. Supporting this finding, inhibiting sonic hedgehog signaling components in the mouse ureter mesenchyme led to non-obstructive prenatal hydroureter and hydronephrosis, with variable early lethality[89,90]. Conversely, targeted knockout of members of the *TGF-β1/BMP4* signaling pathway in ureter mesenchyme, such as Smad4 and Id2, caused UPJ obstructions likely due to changes in smooth muscle proliferation rates[91,92]. In comparison, this *Sec10*$^{FL/FL}$*;Ksp-Cre* model is the most consistently severe, with ~95% of the embryos developing lumen-obliterating bilateral UPJ obstructions with neonatal anuria and death[18].

Several conditional alleles of other ciliary proteins have been inactivated with the same *Ksp-Cre* mouse strain used here, with reports of classic polycystic kidneys developing in the first months of life[75–78]. However, no other conditional knockouts using the *Ksp-Cre* strain to our knowledge has reported a neonatal lethal hydronephrosis or UPJ obstructions. This led us to conclude the phenotype of the *Sec10*$^{FL/FL}$*;Ksp-Cre* embryos is not due to *Sec10*'s role in primary cilia assembly, and indeed, the mouse urothelium was reported to not be a highly ciliated tissue[93]. Given that the exocyst is a major regulatory complex for polarized exocytosis of intracellular vesicles, we can hypothesize trafficking of uroplakin proteins to the apical membrane of superficial cells, which is the very essence of the hydrophobic barrier of the urothelium, involves the exocyst proteins. There are no previous reports in the literature that have examined the

exocyst's role in urothelial biology. However, Rab8 and Rab11 GTPases, which are known to bind exocyst subunits for targeted secretory vesicle trafficking, have been shown to be important for apical trafficking and "stretch-induced exocytosis" in urothelial superficial cells[45,94].

There were a few mice (approximately 5%) that survived to weaning age. It is unknown why these mice were able to escape ureter obstructions, but those that did survive had abnormal kidneys. These kidneys had defects in primary cilia formation and a cystic phenotype. The limitation to this study was the low number of surviving mice with a polycystic phenotype. For future studies, we have a Cre-Ert tamoxifen inducible Ksp-Cre-ERT2 mouse strain where we can knockout *Sec10* in adult mice renal epithelium. We hypothesize that these mice would develop a polycystic phenotype and we can then better analyze the exocyst's role in primary cilia trafficking. We can also narrow down the role of *Sec10* and the exocyst complex in the formation of the primary cilia.

In our *Sec10$^{FL/FL}$;Ksp-Cre* model of prenatal UPJ obstructions, *our working hypothesis is that conditional Sec10 knockout in the urothelial cells of the ureter leads to a failure in the urothelial barrier*. This results in damage to the surrounding mesenchymal and smooth muscle cells, and perhaps analogous to arterial restenosis upon damage to the endothelium, this causes over proliferation of these surrounding cell populations. The small diameter of the developing ureter, and relative high hydrostatic pressure at the UPJ through a "bottleneck" effect, results in rapid lumen closure specifically at the UPJ between E17.5 and E18.5. This has been previously proposed as a mechanism for human UPJ obstructions, as damage to the urothelium and overproliferation of mesenchymal cells has been noted by histological analysis of human ureters[95]. Further study of this novel mouse model should allow us to identify new causes of human UPJ obstructions, characterize the progression of congenital obstructive nephropathy disease at a prenatal stage, and perhaps lead to identification of predictive biomarkers for human disease progression and severity.

3.4) MATERIALS and METHODS

Sec10 conditional knockout mice

C57Bl/6J ES clones containing a conditional allele for the *Sec10* (*i.e. Exoc5*) gene were generated by the trans-NIH Knock-Out Mouse Project (KOMP) and obtained from the KOMP Repository (www.komp.org)[96]. The clone # DEPD00521_3 contains the *Exoc5*$^{tm1a(KOMP)Mbp}$ allele, which was validated by KOMP as having undergone homologous recombination with targeting vector PRPGS00174_A_D07, which contains loxP sites flanking *Sec10* exons 7-10 and *lacZ* and *Neomycin* cassettes flanked by *FRT* recombination sites between exon 6 and 7. Although this vector is designed to cause a general *Sec10* gene knockout, exposure to FLPe recombinase excises the large *lacZ/Neo* cassette and produces a conditional allele. The ES clone was injected into blastocysts (albino C57Bl/6J) by the Engineering Models Resource Core of the HepatoRenal Fibrocystic Diseases Core Center at the University of Alabama at Birmingham, led by Drs. Robert Kesterson and Bradley Yoder, which generated several chimeras with subsequent germline transmission. Genotyping was confirmed using Southern Blotting with probes from both 5' and 3' regions after *XbaI* digestion, as well as with genomic DNA PCR. After germline transmission was achieved, heterozygous mice were mated with the *FLPe* recombinase *B6.129S4-Gt(ROSA)26Sor*$^{tm1(FLP1)Dym}$*/RainJ* mouse strain[97], obtained from Jackson Laboratories, to remove the *lacZ/Neo* cassette, which was confirmed by PCR and sequencing. We designated the final mouse strain the *floxed-Sec10* line (*Sec10*^{FL}). Deletion of *Sec10* exons 7-10 in epithelia derived from the ureteric bud was achieved by mating *Sec10*^{FL} mice with *Ksp1.3-Cre* mice[75–78]. The *Sec10* null allele (*Sec10*$^{-}$) was generated by mating the *Sec10*^{FL} mice with *CMV-Cre*[98]. Husbandry and experiments with all mice were approved in advance either by the University of Hawaii or the University of Alabama at Birmingham IACUC, in accordance the American Association of Accreditation of Laboratory Animal Care.

Histological Analyses

Tissues were dissected, fixed with 4% formaldehyde, and embedded in paraffin and cut into 10 µm sections. To calculate the cystic index, the largest sagittal section of the

kidney containing the cortex, medulla and papilla was stained with H&E, and the cumulative area of cysts and the total area of the kidney section were measured using the ImageJ software (NIH)[72]. Cystic index was then calculated as the percentage of the cumulative cystic area relative to the total area of the kidney section. For immunostaining, tissue sections were deparaffinized, rehydrated in an ethanol gradient, and placed in a pressure cooker for antigen retrieval with citric acid based antigen-unmasking solution (Vector Laboratories H-3300). Sections were blocked with 5% serum, permeabilized with 0.1% Triton X-100, and left in primary antibody overnight at 4˚C. Primary antibodies used were anti-SMA (Sigma), anti-E-cadherin, anti-vimentin, and anti-cleaved caspase-3 (Cell Signalling), Cytokeratin-5 (Abcam), Cytokeratin-20 (Proteintech Group), and anti-uroplakin III (American Research Products, Inc.). Tissue sections were washed and incubated with DyLight secondary antibodies (Vector Laboratories) for 1 hour at room temperature. Nuclei were stained with DAPI. H&E stained and immunostained sections were analyzed using a fluorescent Olympus BX41 microscope.

Dye injections to trace urinary tracts

Using timed matings and Theiler staging criteria, litters of E17.5, E18.5, and newborn mice were collected, and their intact urinary tracts removed, including both kidneys, ureters, and attached bladder. Bromophenol blue (1 mg/ml in PBS) was injected into the renal pelvis from a lateral direction using a pulled glass capillary needle connected via catheter tubing to a 1-ml syringe. Dye was injected at a rate of 100 µl/min until it entered the bladder through the ureter, or until the UPJ obstruction became visible. Following injection, imaging was performed using an Olympus SZ-CTV dissecting microscope with an Olympus DP12-2 camera. Tissue was collected from each dissected mouse for genomic DNA isolation and genotyping.

Western blotting and real time quantitative PCR

Proteins were isolated from homogenized newborn kidneys and ureters using RIPA buffer with protease inhibitors (Sigma #P8340) and phosphatase inhibitors (Sigma #P5726). Protein lysates were loaded at equal amounts and electrophoresed and

blotted using standard methods. Primary antibodies used were anti-Sec10 (Proteintech Group), anti-E-cadherin and anti-Beta-actin (Cell Signaling). Fluorescent secondary antibodies (IRDye) and the LI-COR Odyssey Imager (LI-COR Biosciences) were used for fluorescent detection of proteins, with band intensities quantified using the Licor Image Studio Lite software. RNA was isolated from mouse kidneys and upper ureters using the RNeasy Micro kit (Qiagen), and cDNA was generated with the iScript cDNA Synthesis kit (Bio-rad). Real time quantitative PCR (qPCR) was performed with SYBR Green as previously described[99] using primers against Sec10 and beta-actin (primer sequence available upon request). Amplification and real time measurement of PCR products were performed with CFX96 Real-Time PCR Detection System (Bio-rad).

CHAPTER 4: Defects in urothelial cell differentiation lead to a fibroproliferative response causing congenital obstructive nephropathy in the Sec10-CKO mouse

4.1) INTRODUCTION

Ureter development in mice begins at embryonic day 10.5 (E10.5), as the tip of the ureteric bud grows from the nephric duct and branches into the metanephric mesenchyme to become the kidney, the base migrates down the nephric duct and eventually connects directly with the bladder[8]. Although the stalk of the ureteric bud starts as a single monolayer of epithelial cells, it induces development of an outer smooth muscle layer from recruited mesenchymal cells and then differentiates into a multilayered transitional epithelium called the urothelium[8]. Sonic hedgehog (shh) and fibroblast growth factor 2 (fgf2) are secreted from the urothelial layer to initiate smooth muscle recruitment, proliferation, and differentiation[89,90,100]. Similarly, bone morphogenic protein 4 (BMP4) and retinoic acid (RA) are secreted from the mesenchyme to initiate differentiation of the urothelial layers[90,92]. The bladder also differentiates urothelial lining, but these cells are not derived from the ureteric bud, and it is unclear if the signaling that controls differentiation is the same.

Here, we investigate the pathogenesis of prenatal UPJ obstructions in our novel *Sec10$^{FL/FL}$;Ksp-Cre* transgenic mouse model (described and characterized in the previous chapter). As previously described, we crossed the floxed *Sec10* mice with the *Ksp-Cre* mouse strain[75], where Cre recombinase expression is driven by a 1.3 kb promoter fragment of kidney-specific cadherin (Ksp-cadherin; cadherin 16). During nephrogenesis, Ksp-cadherin is expressed in the ureteric bud and the epithelial cells derived from the ureteric bud, allowing us to investigate the role of Sec10 in these cells during urinary tract development. As described in Chapter 3, we discovered that 95% of the *Sec10* knockout pups (*Sec10$^{FL/FL}$;Ksp-Cre*) died hours after birth with severe bilateral hydronephrosis and complete anuria.

Our goal here was to identify the cellular mechanism that causes the *in utero* UPJ obstructions after the conditional inactivation of *Sec10* in epithelial cells of the ureteric bud. Our specific aims were to: 1. Determine the changes in urothelial differentiation upon inactivation of *Sec10* and 2. Identify the pathogenic changes in cell signaling that drive the overgrowth in surrounding mesenchyme. *Our hypothesis was*

that Sec10 and the exocyst complex are necessary for urothelial cell differentiation and defects in differentiation will lead to a disrupted urothelial barrier that stimulates a fibroproliferative response.

4.2) RESULTS

4.2.1) Prenatal UPJ obstructions in *Sec10$^{FL/FL}$;Ksp-Cre* mice are preceded by a loss of ureter urothelium

Sec10$^{FL/FL}$;Ksp-Cre mice developed bilateral *in utero* UPJ obstructions, severe hydronephrosis (Fig. 30A and B), with neonatal anuria and death, with a 95% penetrance[101]. We observed that the ureter lumen became obstructed at the UPJ region between E17.5 and E18.5, but the underlying basis of the blockage was unclear. By immunostaining for E-cadherin, we saw that epithelial cells had largely disappeared from the obstructed UPJ by E18.5. Representative cross sections of E18.5 ureters stained with Alcian blue show a normal multilayered ureter with a patent lumen (Fig. 28C), but *Sec10$^{FL/FL}$;Ksp-Cre* ureters were completely obstructed by E18.5 (Fig. 28D). Histological analysis showed the *Sec10$^{FL/FL}$;Ksp-Cre* ureters had completely lost the urothelial cell layer by E18.5, and filled with what looked like granulation tissue in the lumen. We utilized a *tdTomato* reporter mouse strain to confirm Cre activity and track *Sec10* knockout cells in the urothelium. We previously showed that Cre is activated in the Ksp-Cre ureteric bud cells prior to E13.5[101], confirming an early deletion of the *Sec10* gene during nephrogenesis. As expected, newborn control mice with both *Ksp-Cre* and *tdTomato* alleles exhibited strong red fluorescence in the urothelium of the pelvis and throughout the entire length of the ureter (Fig. 28E). However, in newborn *Sec10$^{FL/FL}$;Ksp-Cre* mice, red fluorescent cells were visible only in the upper-most ureter (Fig. 28F). As the renal pelvis transitions into the ureter at the UPJ, tdTomato labeling of the urothelial cells revealed an abrupt disappearance of these cells in *Sec10$^{FL/FL}$;Ksp-Cre* ureters (Fig. 28F). Whole mount images of younger tdTomato-labeled ureters (E16.5 - E18.5) also showed that the number of urothelial cells in *Sec10$^{FL/FL}$;Ksp-Cre;To* ureters was significantly decreased at E17.5, and by E18.5 there were very few urothelial cells remaining (Fig. 28G-J). This shows that the loss of *Sec10* in urothelial cells leads to degeneration of the urothelial layer prior to the formation of the UPJ

obstruction. Also, these data showed that epithelial-mesenchymal transition (EMT) does not contribute to the obstruction in this mouse model, since we did not detect any tdTomato-labeled mesenchymal cells among the tissue filling the ureter lumens.

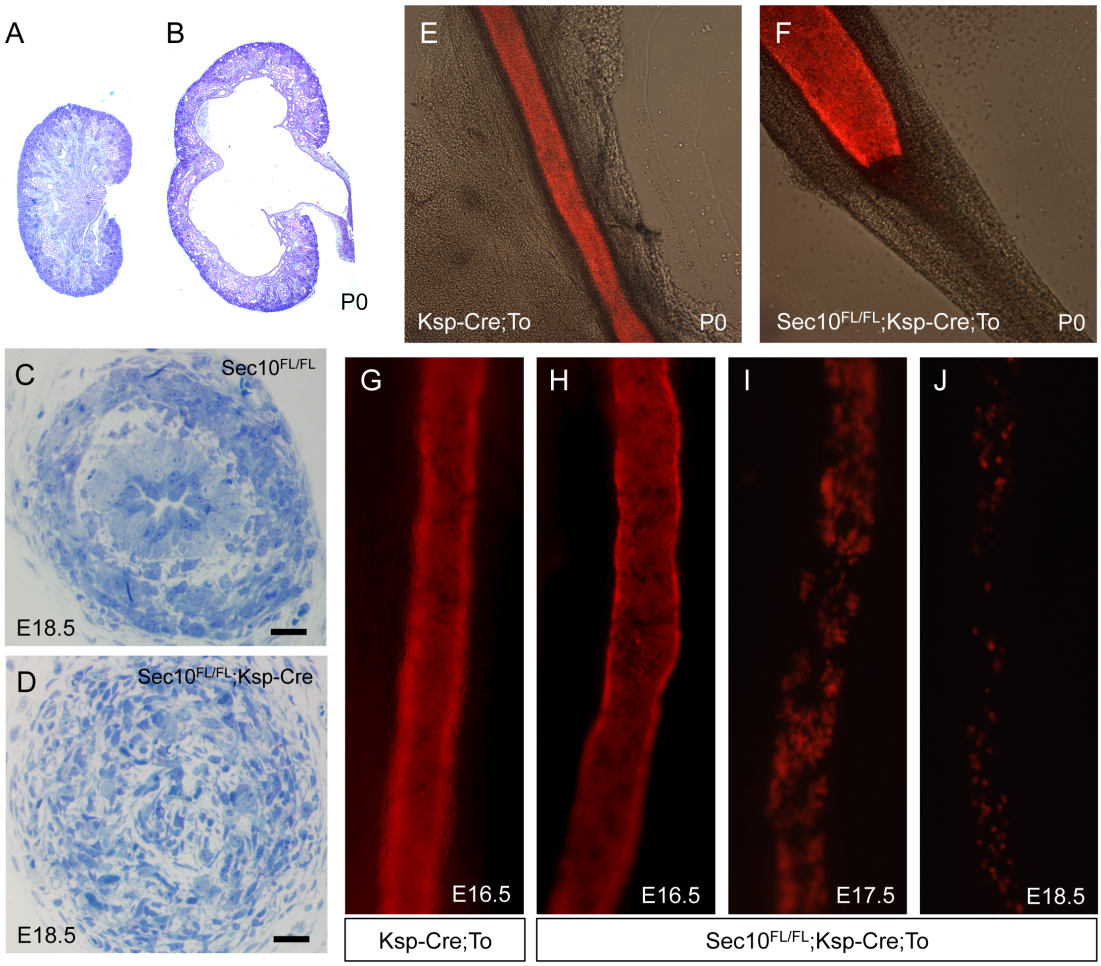

Figure 28: *Sec10$^{FL/FL}$;Ksp-Cre* ureters form complete UPJ obstructions by E18.5 with loss of urothelial cells starting at E17.5. A-B) Representative H&E-stained histological sections demonstrate substantial hydronephrosis in *Sec10$^{FL/FL}$;Ksp-Cre* newborn kidneys (right, B), not present in *Sec10$^{FL/FL}$* control littermates (A). C-D) Alcian blue staining of cross-sections from representative *Sec10$^{FL/FL}$* and *Sec10$^{FL/FL}$;Ksp-Cre* ureters at the UPJ region. Bar = 20 μm. E-F) Fluorescence imaging merged with differential interference contrast (DIC) microscopy of representative P0 *Ksp-Cre;To* control and *Sec10$^{FL/FL}$;Ksp-Cre;To* mutant ureters. Loss of tdTomato-labeled urothelial cells is evident at and below the UPJ obstruction in *Sec10$^{FL/FL}$;Ksp-Cre;To* ureters. G-J) Fluorescence microscopy of whole mount E16.5 *Ksp-Cre;To* control ureters, and of E16.5-E18.5 *Sec10$^{FL/FL}$;Ksp-Cre;To* mutant ureters, showing progressive loss of tdTomato-labeled urothelial cells starting after E16.5.

4.2.2) Sec10 is necessary for normal differentiation of the superficial urothelial cells in the developing ureter

Urothelial cell differentiation and stratification during ureter development is critical for the formation of the mature urothelial barrier against urine. The urothelial progenitor epithelial cells, derived from the stalk of the ureteric bud, are initially present as a monolayer, but as they respond to morphogens from surrounding mesenchymal tissue they stratify into three urothelial cell types: basal cells, intermediate cells, and superficial cells[11,28]. We used transmission electron microscopy (TEM) to compare the ultrastructure of the ureter's urothelium in E16.5 and E17.5 *Sec10*$^{FL/FL}$ and *Sec10*$^{FL/FL}$*;Ksp-Cre* embryos. At E16.5, control ureters had a single urothelial layer with microvilli extending into the lumen of the ureter (Fig. 29A), which looked similar in *Sec10*$^{FL/FL}$*;Ksp-Cre* ureters except for a distinct reduction in apical microvilli (Fig. 29B). In both E16.5 *Sec10*$^{FL/FL}$*;Ksp-Cre* and control ureters, projections were visible between the urothelial cells, an early sign of epithelial stratification. At E17.5, control ureter cross sections revealed a two-layered urothelium with a characteristic scalloped structure with hinge regions on the luminal membrane of the superficial cells (Fig. 29C). However, E17.5 *Sec10*$^{FL/FL}$*;Ksp-Cre* ureters showed a highly abnormal single urothelial layer, with gaps in the epithelium and cells pulling away from the basement membrane toward the center of the lumen (Fig. 29D). These *Sec10*-knockout urothelial cells had lost large amounts of cytoplasm, and showed irregular disrupted plasma membranes and unusual distributions of electron-dense material in the nuclei. From immunostaining E-cadherin and SMA in E16.5 and E17.5 ureter cross sections, we measured the widths of both urothelial and smooth muscle layers in *Sec10*$^{FL/FL}$*;Ksp-Cre* and *Sec10*$^{FL/FL}$ ureters. We confirmed that at E16.5, *Sec10*$^{FL/FL}$*;Ksp-Cre* ureters had no significant difference in the average width of the urothelial layer compared to *Sec10*$^{FL/FL}$ ureters, but by E17.5, the *Sec10*-knockout urothelial layer was about half the width of control urothelium (Fig. 29E). No significant changes in the width of the smooth muscle layer at either E16.5 or E17.5 were measured (Fig. 29F).

Confocal imaging of E16.5 ureter cross sections after immunohistochemistry revealed that members of the exocyst complex, *Sec10* and *Sec3*, localize at the apical

(luminal) plasma membrane in *Sec10*$^{FL/FL}$ urothelial cells (Fig. 30A,C). As expected, in *Sec10*$^{FL/FL}$*;Ksp-Cre* mutant ureters, *Sec10* was completely absent, but also *Sec3* levels were significantly decreased (Fig. 30B,D). Degradation of other exocyst subunits was previously measured in Sec10-knockdown MDCK cells[29], but this is the first *in vivo* evidence that the *Sec10* protein may be required for the expression or stability of the other exocyst subunits. These data also showed that the localization of the exocyst in monolayered urothelial cells at E16.5 differs from previous reports of the exocyst in other monolayered epithelial cells, where it localized to sites of cell-cell contact and had been associated with basolateral membrane delivery[24,70].

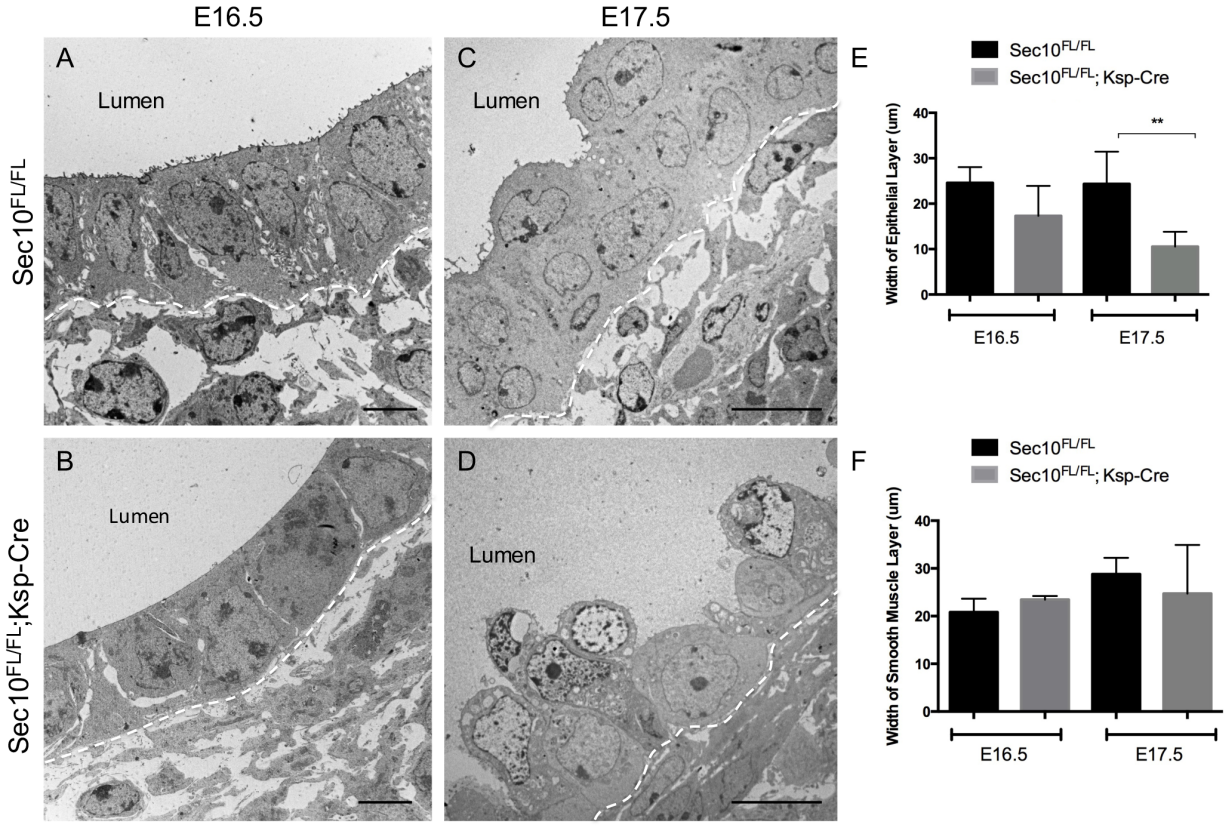

Figure 29: Ultrastructural analysis reveals failure of *Sec10*$^{FL/FL}$*;Ksp-Cre;To* urothelial cells to stratify between E16.5 and E17.5. A-B) Transmission electron microscopy (TEM) of the urothelial layer of E16.5 ureters of *Sec10*$^{FL/FL}$*;Ksp-Cre* and *Sec10*$^{FL/FL}$ control littermates. Dashed line marks the basement membrane. Bar = 4 μm. C-D) TEM of the urothelial layer of E17.5 ureters of *Sec10*$^{FL/FL}$*;Ksp-Cre* and *Sec10*$^{FL/FL}$ control littermates. Scale Bar = 10 μm. E) Measurements of urothelial layer thickness in *Sec10*$^{FL/FL}$*;Ksp-Cre* versus *Sec10*$^{FL/FL}$ ureters at E16.5 and E17.5 (** p<0.01). F) Measurements of smooth muscle layer thickness in E16.5 and E17.5 ureters based on E-cadherin and smooth muscle actin immunostaining. No significant changes were detected in thicknesses of smooth muscle layers.

The decrease in exocyst protein at the apical plasma membrane in E16.5 *Sec10*$^{FL/FL}$*;Ksp-Cre* urothelial cells coincided with highly decreased number of microvilli on the apical surface (Fig. 30E and F). The transcription factor *p63* is highly expressed in the progenitor ureteric bud and has been shown to be important in the growth and differentiation of epithelial tissues[43,102]. In the mature urothelium, it is highly expressed in the basal urothelial cells and is critical for the maintenance the basal layer[42]. Immunohistochemistry of *Sec10*$^{FL/FL}$ and *Sec10*$^{FL/FL}$*;Ksp-Cre* ureters showed similar *p63* levels and localization at E16.5 (Fig. 30G and H).

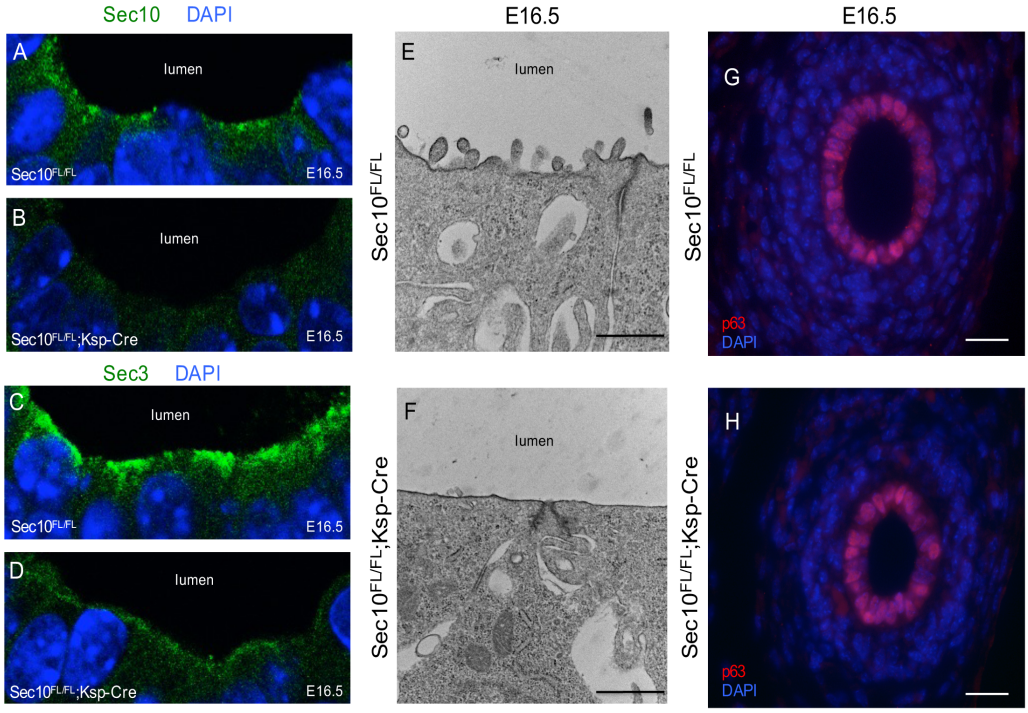

Figure 30: Loss of *Sec10* in urothelial cells results in defective urothelial cell differentiation and stratification. A-D) Immunostaining and confocal microscopy of exocyst members Sec10 and Sec3 in E16.5 ureters revealed exocyst was localized at the apical/luminal plasma membrane. The Sec10 protein was absent in E16.5 *Sec10*$^{FL/FL}$*;Ksp-Cre* urothelial cells compared to *Sec10*$^{FL/FL}$ ureters (A,B), and Sec3 was also significantly decreased in *Sec10*$^{FL/FL}$*;Ksp-Cre* ureters. E-F) TEM of the apical plasma membrane of E16.5 *Sec10*$^{FL/FL}$*;Ksp-Cre* and *Sec10*$^{FL/FL}$ urothelial cells at 6000x. Scale Bar = 500nm. G-H) Immunohistochemistry of p63 (red) in E16.5 *Sec10*$^{FL/FL}$*;Ksp-Cre* and *Sec10*$^{FL/FL}$ ureters showed no detectable differences.

4.2.3) *Sec10*-knockout urothelial cells fail to produce uroplakin plaques on the luminal surface

Differentiation of superficial urothelial cells has been shown, in the bladder, to be an early event in urothelial maturation[103]. Normal mature superficial cells are characterized by the presence of numerous intracellular vesicles carrying uroplakins at the luminal plasma membrane, which establishes and maintains the watertight barrier against urine. Previously, we detected an absence of Upk3 protein in the *Sec10$^{FL/FL}$;Ksp-Cre* urothelium at E17.5 via immunohistochemistry (Fig.22)[101]. Here we investigated production of uroplakins in *Sec10$^{FL/FL}$;Ksp-Cre* urothelium in more detail. TEM of control ureters at E17.5 showed numerous intracellular vesicles that clustered towards the apical membrane of the superficial urothelial cells (arrows, Fig. 31A). However, in the E17.5 *Sec10$^{FL/FL}$;Ksp-Cre* urothelial cells, there was a complete absence of these apical vesicles (Fig. 31B), correlating with the absent uroplakin mRNA gene expression that we measured by qPCR (Fig. 32A-D). Using scanning electron microscopy (SEM) of E17.5 ureter lumens, we could clearly visualize the hexagonal uroplakin plaques on the luminal membrane surface of *Sec10$^{FL/FL}$* control ureters and tight cell-cell contacts (Fig. 31C). SEM also confirmed that uroplakin plaques were completely missing on the luminal surface of E17.5 *Sec10$^{FL/FL}$;Ksp-Cre* ureters (Fig. 31D). We also noted that the *Sec10$^{FL/FL}$;Ksp-Cre* urothelial cells did not show tight cell-cell contacts at E17.5, which confirms findings with TEM that many of these cells are damaged and are becoming detached from the ureter wall.

PPARγ is a nuclear receptor that is a critical activator of uroplakin gene expression and has been reported to be necessary for the differentiation of superficial urothelial cells[42,104,105]. With qPCR, we measured a large decrease in *PPARγ* gene expression in *Sec10$^{FL/FL}$;Ksp-Cre* ureters compared to *Sec10$^{FL/FL}$* ureters from E16.5 to E18.5 (Fig. 32E). That *PPARγ* was 80% decreased in *Sec10$^{FL/FL}$;Ksp-Cre* ureters as early at E16.5, prior to gross morphological changes, supports the hypothesis that *Sec10* is required for the differentiation of superficial urothelial cells in embryonic ureters.

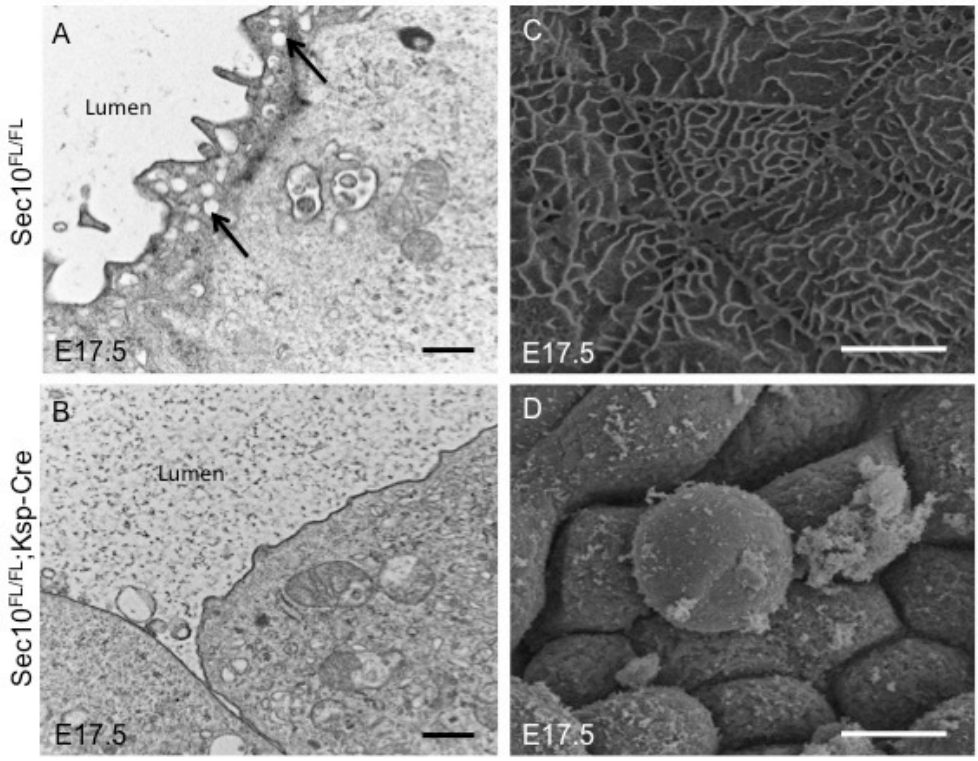

Figure 31: Electron microscopy of E17.5 *Sec10$^{FL/FL}$;Ksp-Cre* ureters showed an absence of uroplakin plaques on the luminal surface of urothelial cells. A-B) TEM of E17.5 *Sec10$^{FL/FL}$* control ureters detected scallop-shaped uroplakin plaques on the apical plasma membrane (arrow heads) and fusiform vesicles being trafficked to the apical surface (arrows), both characteristic of superficial cells. In *Sec10$^{FL/FL}$;Ksp-Cre* ureters, no uroplakin plaques or vesicles were detected. Scale Bar = 0.5 μm. C-D) Scanning electron microscopy (SEM) of the luminal surfaces of E17.5 *Sec10$^{FL/FL}$* control ureters showed hallmark hexagonal uroplakin plaques covered the surface (indicated by arrows), with well-established tight cell-cell junctions (indicated by arrow heads). SEM of the luminal surface of E17.5 *Sec10$^{FL/FL}$;Ksp-Cre* ureters showed a complete absence of uroplakin plaques and damaged cells pulling away from the urothelial layer along with poor cell-cell junctions. Scale Bar = 5 μm.

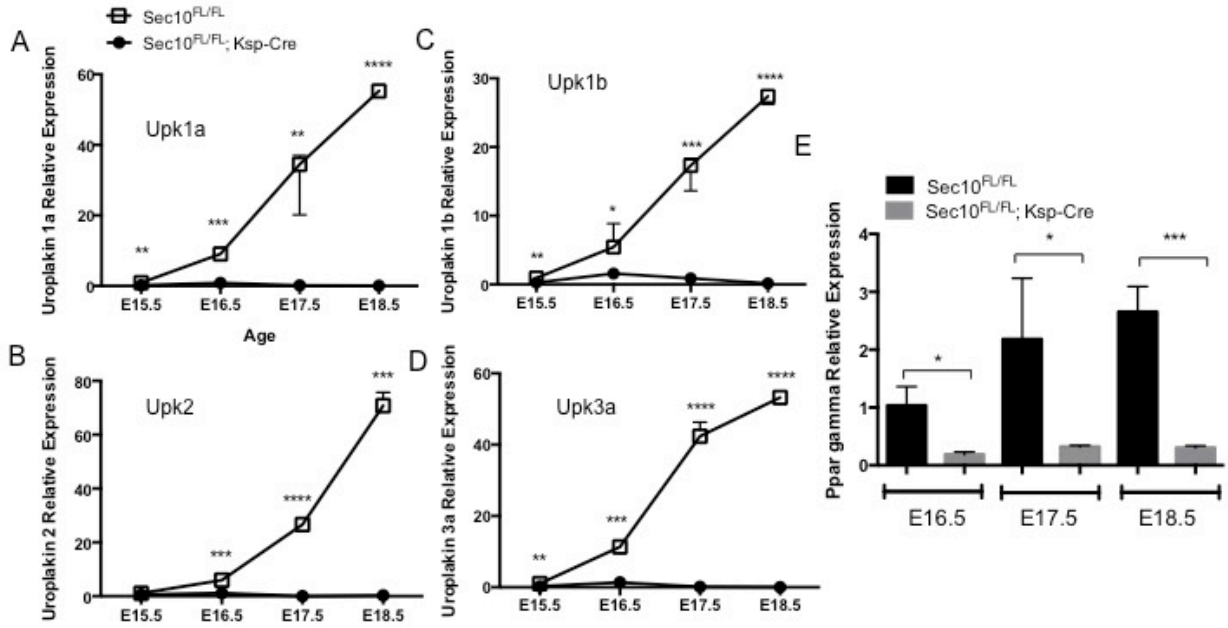

Figure 32: Decrease in uroplakin mRNA expression confirms absence of a mature urothelium A-D) Real time qPCR measurement of *Upk1a*, *Upk1b*, *Upk2*, and *Upk3a* gene expression in *Sec10$^{FL/FL}$;Ksp-Cre* and *Sec10$^{FL/FL}$* ureters collected from E15.5 - E18.5 embryos (* p<0.05, ** p<0.01, *** p<0.001, ****p<0.0001). C_t values for each gene were normalized against beta actin. E) Real time qPCR measurement of *PPARγ* gene expression in E16.5 - E18.5 *Sec10$^{FL/FL}$;Ksp-Cre* and *Sec10$^{FL/FL}$* ureters (* p<0.05; *** p<0.001). C_t values for each gene were normalized against *beta actin*.

4.2.4) Necrosis of urothelial cells contributes to the loss of barrier integrity in *Sec10$^{FL/FL}$;Ksp-Cre* ureters

Analysis of E17.5 *Sec10$^{FL/FL}$;Ksp-Cre* TEM images revealed that the damaged cells pulling away from the basement membrane had morphological characteristics similar to necrosis rather than apoptosis (Fig. 33A and B). Apoptotic cells via TEM exhibit membrane blebbing and nuclear fragmentation, but necrotic cells showed a darkening of the nucleus, uncontrolled swelling of the cell, rough irregular plasma membranes, and an absence of blebbing. Immunohistochemistry of E17.5 ureter cross-sections confirmed that very few urothelial cells were positive for cleaved caspase 3 (Fig. 33C and D), a marker for apoptotic activation. Protein analysis of *Sec10$^{FL/FL}$;Ksp-Cre* and *Sec10$^{FL/FL}$* ureters also confirmed no significant differences between the levels of cleaved caspase-3 or cleaved PARP, another marker of apoptosis (Fig. 33E). The

absence of apoptotic characteristics, and the cell morphology observed via TEM, indicated that *Sec10-KO* urothelial cells in the developing ureter were dying largely due to necrosis.

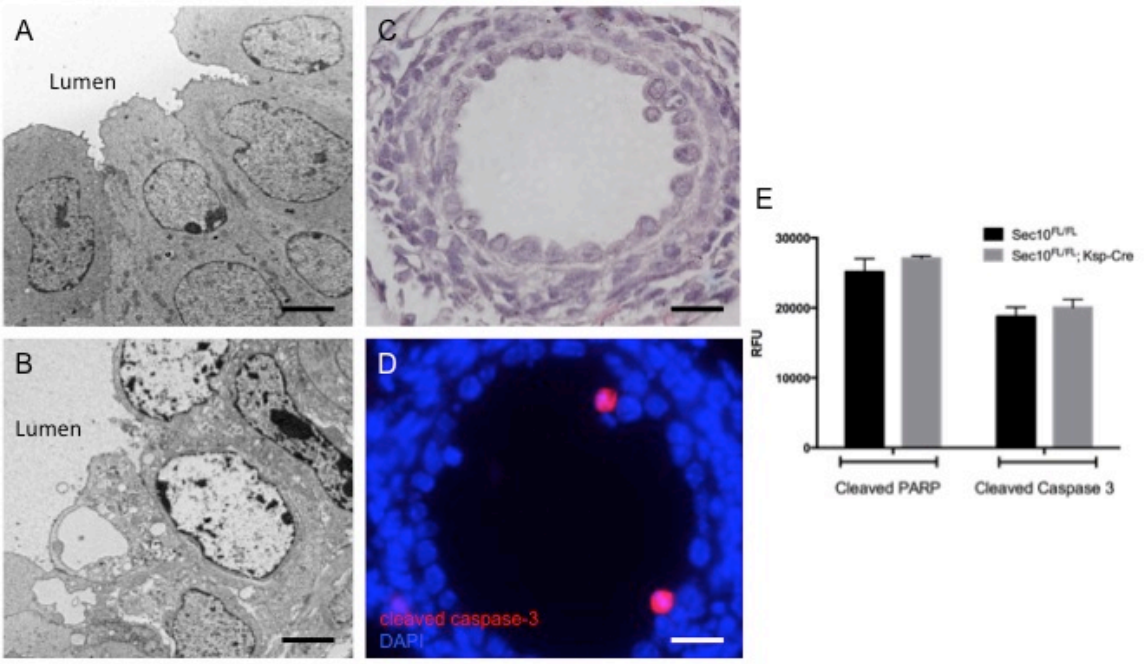

Figure 33: Loss of urothelial cells at E17.5 is primarily due to necrosis and not apoptosis. A-B) Representative TEM of the urothelial layer of E17.5 *Sec10$^{FL/FL}$* and *Sec10$^{FL/FL}$;Ksp-Cre* ureters. Most of the remaining attached urothelial cells in *Sec10$^{FL/FL}$;Ksp-Cre* ureters displayed characteristics of cell damage and necrosis, but not apoptosis. Bar = 4 μm. C-D) Serial sections of a representative E17.5 *Sec10$^{FL/FL}$;Ksp-Cre* ureter (dotted line depicts the basement membrane) demonstrated that although the urothelium was a damaged single layer (H&E staining, C), very few cells were positive for activated caspase-3 (red, D). Bar = 20 μm. E) Measurement of cleaved caspase-3 and cleaved PARP protein levels in multiple *Sec10$^{FL/FL}$* and *Sec10$^{FL/FL}$;Ksp-Cre* ureters did not detect any significant increase in these apoptotic markers at E17.5. Columns represent the means of relative fluorescent units (RFU), with error bars representing SEM.

Based on TEM images of the disrupted urothelium at E17.5, we performed fluorescein isothiocyanate dextran (FITC-dextran) injections into the renal pelvis of the kidney to determine if there was any sign of urothelial barrier dysfunction in the ureter. In control E17.5 ureters (the left injected ureter marked by arrow, Fig. 34A), the FITC-dextran was not retained in the ureters and passed through the ureters and into the

bladders, indicating a strong luminal barrier. In contrast, E17.5 *Sec10*$^{FL/FL}$*;Ksp-Cre* ureters retained a very strong green fluorescence in the injected ureters (arrow, Fig. 34B), indicating the retention of the FITC-dextran in the tissue. Thus, the disrupted differentiation of the Sec10-knockout urothelium has a functional consequence of compromising the urothelial barrier by E17.5.

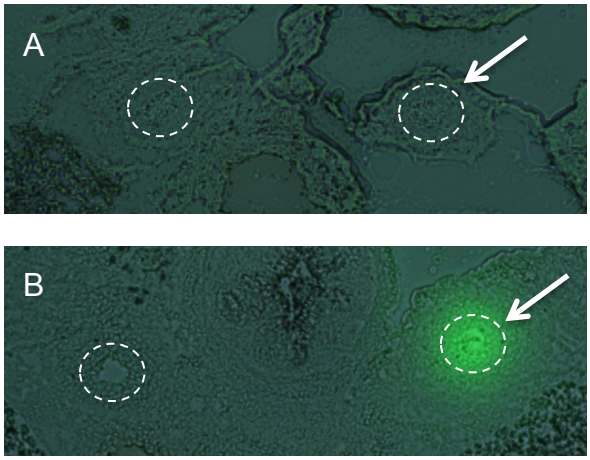

Figure 34: *Sec10* knockout in ureters leads to a disrupted urothelial barrier: E17.5 embryos, the left renal pelvis was injected with FITC-dextran which was allowed to flow to the bladder, then tissue was frozen and cryosectioned (ureters are circled, arrows note left ureter). A) Normal *Sec10*$^{FL/FL}$ controls had very little FITC-dextran retained in the injected ureter (arrow), but B) *Sec10*$^{FL/FL}$*;Ksp-Cre* mice had a much larger retention of the dextran in the injected ureter tissue, indicating leakiness of the urothelial barrier.

4.2.5) Urothelial degeneration in the developing *Sec10*$^{FL/FL}$*;Ksp-Cre* ureter induces a fibroproliferative response that rapidly occludes the lumen

In histological sections of our *Sec10* knockout ureter cross sections, we noted that the tissue in the UPJ obstruction looked similar to granulation tissue, characteristic of wound healing. Granulation tissue includes the presence of myofibroblasts, extracellular matrix (ECM) deposition and remodeling, inflammatory cells, and newly formed capillaries. Although often associated with wound healing of the skin, the fibroproliferative response seen in granulation tissue can also occur in internal epithelial tissues to obliterate lumens, such as in bronchiolitis obliterans[106]. Here, we expanded on our original findings and performed ultrastructure morphological and molecular

analysis at the UPJ obstruction to evaluate the degree of fibrotic response. TEM analysis of control *Sec10*$^{FL/FL}$ ureters at E18.5 confirmed a mature multilayered structure with numerous uroplakin vesicles (Fig. 35A), and a distinct basement membrane (data not shown). However, *Sec10*$^{FL/FL}$*;Ksp-Cre* ureters exhibited a complete loss of the epithelial layer, previously shown by immunostaining for epithelial markers such as E-cadherin[101]. Instead, the lumen was filled with migrating fibroblastic cells and deposits of ECM (Fig. 35B), suggesting the presence of a fibrotic wound healing response at the obstruction. Immunohistochemistry of collagen IV in *Sec10*$^{FL/FL}$ ureters showed a distinct basement membrane attached to the basal layer of the urothelium separating the mucosa from the smooth muscle cells (Fig. 35C). In contrast, *Sec10*$^{FL/FL}$*;Ksp-Cre* ureters had a reorganization of collagen IV throughout the new tissue in the lumen of the ureter, indicating a disrupted and expanded basement membrane that allowed the surrounding mesenchyme to penetrate the lumen (Fig. 36D).

TGF-β1 is a critical mediator of wound healing and fibrosis, and was found in a previous study to be increased in human UPJ samples[107]. We hypothesized that the *TGFβ1* pathway may be activated from urinary leakage into the tissue underlying the disrupted urothelium in *Sec10*$^{FL/FL}$*;Ksp-Cre* ureters. We measured *TGF-β1* mRNA expression using real time qPCR in E16.5-E18.5 *Sec10*$^{FL/FL}$*;Ksp-Cre* ureters and compared to *Sec10*$^{FL/FL}$ controls. *TGF-β1* had a five-fold expression increase in *Sec10*$^{FL/FL}$*;Ksp-Cre* at E17.5 and E18.5 compared to *Sec10*$^{FL/FL}$ ureters (Fig. 35E). At E16.5 however, prior to the observed urothelial degeneration, we measured no change in *TGF-β1* expression.

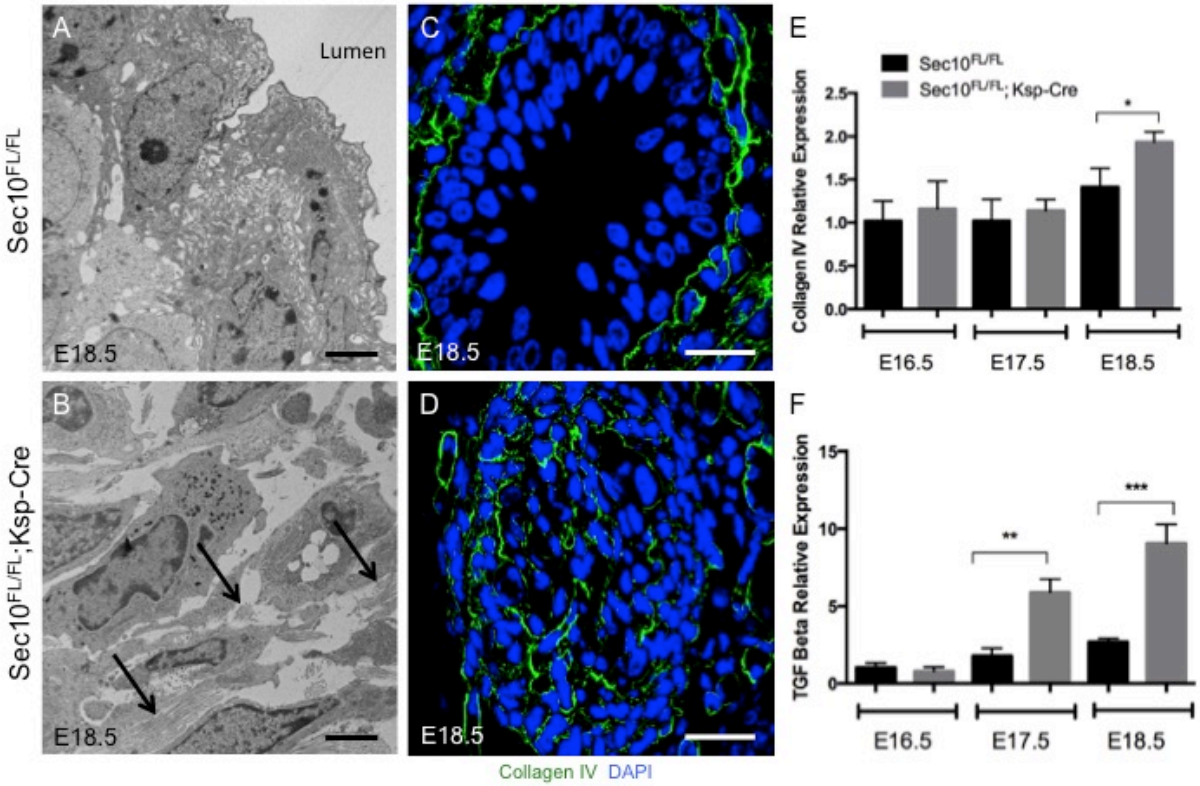

Figure 35: Obstructed *Sec10$^{FL/FL}$;Ksp-Cre* ureters have stromal remodeling and increased expression of *TGFβ1* and other fibroblastic markers. A-B) TEM of ureter cross-sections at E18.5. *Sec10$^{FL/FL}$* sections show mature superficial urothelial cells with uroplakin plaques on the apical membrane. In *Sec10$^{FL/FL}$;Ksp-Cre* ureters, the lumen has been filled with fibroblastic cells and extracellular matrix deposits. Arrows mark collagen fibers in the filled lumen. Scale Bar = 4 μm. C) Immunohistochemistry of collagen IV in a *Sec10$^{FL/FL}$* E18.5 ureter cross-section revealed a distinct basement membrane separating the epithelial and smooth muscle layers. D) Collagen IV immunohistochemistry in *Sec10$^{FL/FL}$;Ksp-Cre* E18.5 ureter cross sections revealed a remodeled basement membrane and no distinction between cell layers. Scale Bar = 20 μm. E-F) Real time qPCR analysis of *TGFβ1 and Col4* relative gene expression in *Sec10$^{FL/FL}$;Ksp-Cre* and *Sec10$^{FL/FL}$* embryonic ureters. * p<0.05, ** p<0.01, *** p<0.001, ****p<0.0001. C_t values for each gene were normalized against *beta actin*.

We had previously reported an over proliferation of cells positive for SMA in the surrounding mesenchyme at E17.5 prior to the onset of the obstruction[101]. However, multiple cell types express SMA, including smooth muscle cells and activated myofibroblasts. The presence of activated fibroblasts (myofibroblasts) is one of the key characteristics of the wound healing response. Quantitative PCR analysis showed a significant increase in expression of S100A4 (*fibroblast specific protein*, FSP) at E17.5 and E18.5 (Fig. 36A). There was also a significantly increased level of *periostin*

expression at E18.5 (Fig. 36B), but decreased *desmin* expression in the ureters at E17.5 and E18.5 (Fig. 36C). Periostin is a matricellular protein that has been shown to promote myofibroblast proliferation and differentiation during wound healing and fibrosis[108–110]. In contrast, desmin is specific to smooth muscle cells and is not expressed in myofibroblasts. This expression data indicated that the cells invading the ureter lumen in *Sec10$^{FL/FL}$;Ksp-Cre* embryos were activated myofibroblasts, rather than an expanded smooth muscle cell population. In summary, the evidence supports our hypothesis that the UPJ obstruction arises in these *Sec10* mutant mice from a fibroproliferative wound healing response after degeneration of the urothelium in the embryonic ureter.

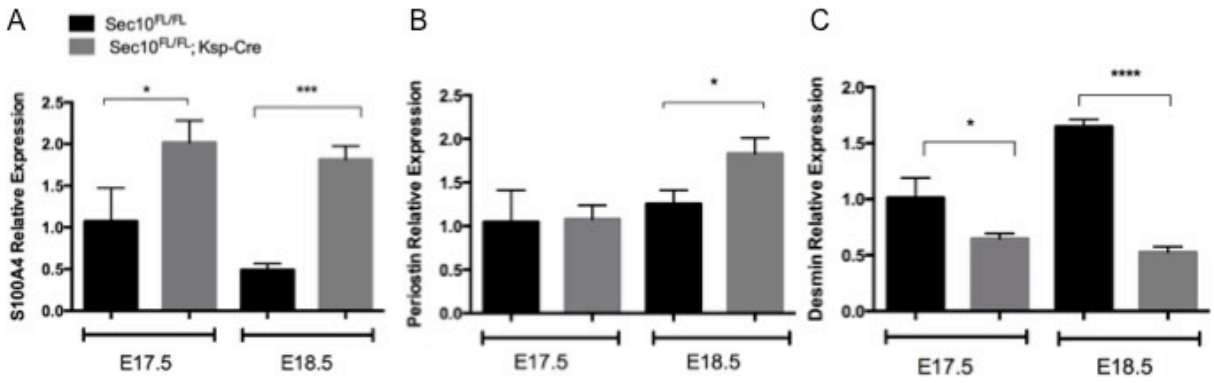

Figure 36: *Sec10$^{FL/FL}$;Ksp-Cre* ureters have increased expression of fibroblastic specific proteins. A-C) Real time qPCR analysis of *S100A4* (*fibroblast specific protein*), *periostin*, and *desmin* relative gene expression in *Sec10$^{FL/FL}$;Ksp-Cre* and *Sec10$^{FL/FL}$* embryonic ureters. * p<0.05, ** p<0.01, *** p<0.001, ****p<0.0001. C_t values for each gene were normalized against *beta actin*.

4.2.6) Generation of an *ex vivo* ureter explant model to better study urothelial differentiation and ureter development

In order to investigate key signaling pathways essential for the regulation of urothelial differentiation, we adapted a protocol for culturing embryonic ureter tissue from Cain et al 2011[111]. In this protocol dissected ureters are seeded on a 1.0μm filter in DMEM/ Hams F12 medium (containing transferrin) at the air liquid interface. Ureter *ex vivo* explant cultures dissected from E15.5 embryos initially have a single urothelial layer at time=0 (Fig.37A), but after 72 hours in culture they have properly established a mature multilayered urothelium (Fig.37B). We used uroplakin 3 protein localization at the apical surface as a marker for urothelial superficial maturation and the presence of peristalsis as an indicator of overall ureter explant viability. Control *ex vivo* ureters at E15.5 begin as a monolayered urothelium indicated by ureter cross-sections immunostained with E-cadherin (green) and smooth muscle actin (red) at 0 hours (Fig. 37C). After 72 hours, control ureter explants develop into a stratified urothelium with multiple urothelial layers (E-cadherin) and the presence of uroplakin 3 at the apical surface (Fig. 37D and E). This urothelial stratification and development after 72 hours in culture shows that we can use this model to study urothelial differentiation.

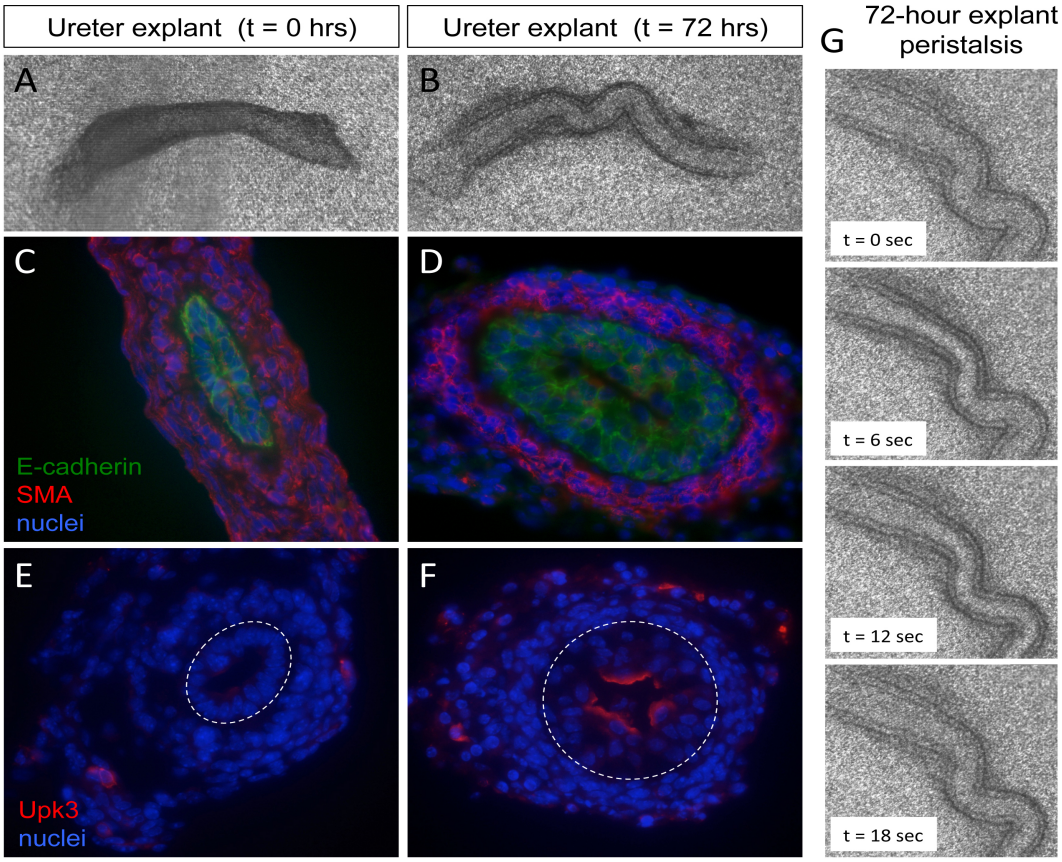

Figure 37: Our E15.5 *ex vivo* ureter explant culture model. Ureters from E15.5 wild type embryos were dissected and plated on 1.0um nucleopore filters at the air liquid interface in a 12-well plate. A) Ureter explant at day 0 (equivalent to E15.5). B) Ureter explant at day 3 (72 hours, equivalent to E18.5) showed a multilayered structure. C,E) Ureter explants at day 0 had a single epithelial layer as shown by E-cadherin immunostaining, and no uroplakin expression on the apical surface. D,F) After 72 hours in culture, ureter explants formed a multilayered epithelium and showed uroplakin protein localization to the luminal surface. G) Peristalsis of ureter explant culture at 72 hours showed the explants remained viable for further analysis.

4.2.7) *Sec10$^{FL/FL}$;Ksp-Cre ex vivo* ureters in the absence of urine have defects in urothelial cell differentiation but not stromal remodeling in the lumen

Previously, we described that *Sec10$^{FL/FL}$;Ksp-Cre* ureters have defects in urothelial cell differentiation. We reported that the defects in differentiation cause a breakdown of the urothelial barrier, which leads to a fibroproliferative response, possibly due to the leakage of urine into the interstitium of the ureter. Here, we asked whether the *Sec10$^{FL/FL}$;Ksp-Cre* ureters still showed these defects, including the fibroproliferative response, even in the absence of urine. Utilizing the *ex vivo* ureter explants described above, we compared the differences in *Sec10$^{FL/FL}$* and *Sec10$^{FL/FL}$;Ksp-Cre* ureter cultures. Following 72 hours in culture, *Sec10$^{FL/FL}$* control explants expressed uroplakin on the apical surface, had multiple layers of E-cadherin-labeled cells, and a distinct basement membrane (Fig. 38 A,C,E). In contrast, *Sec10$^{FL/FL}$;Ksp-Cre* ureter explants had E-cadherin positive cells sloughing off and entering the lumen of the ureter (Fig. 38B). The *Sec10$^{FL/FL}$;Ksp-Cre* ureters also had no detectable uroplakin-3 protein, but the Collagen-IV positive basement membrane remained intact (Fig. 38D and F). This indicated that there are no defects to the smooth muscle layer or activation of myofibroblasts. Also, this suggests that there is no fibroproliferative response without the presence of urine, supporting our hypothesis that the onset of urine contributes to the fibroproliferative response in the mutant ureters *in vivo*. We also confirmed that in the *Sec10$^{FL/FL}$;Ksp-Cre* explant ureters, there are defects in the differentiation of the urothelial layer, since no cells were positive for uroplakins. In future experiments, we can introduce inhibitors and agonists to the explant cultures to interrogate specific pathways involved in urothelial differentiation.

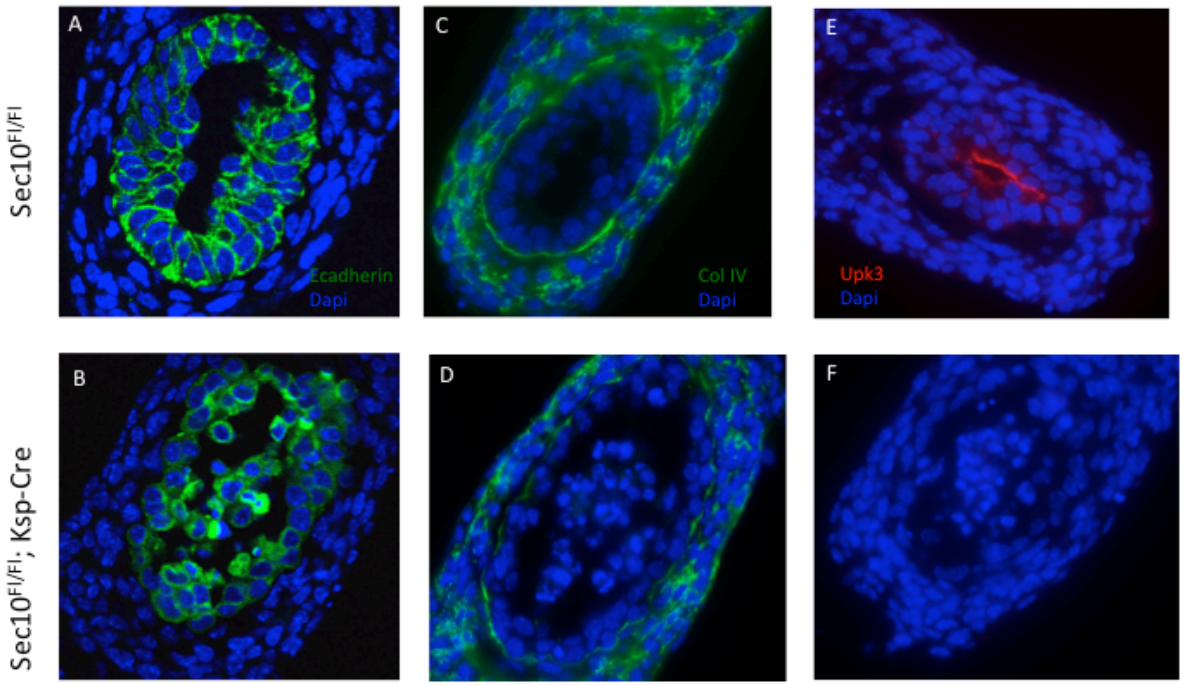

Figure 38: *Sec10$^{FL/FL}$;Ksp-Cre ex vivo* ureter explant cultures at 72 hours show defects in urothelial stratification but not myofibroblast expansion. A) Control *ex vivo* ureter cultures at 72 hours showing a multilayered urothelium indicated by E-cadherin (green), C) the presence of a basement membrane, and E) a stratified urothelial layer indicated by the presence of uroplakin 3 (red). B,D,F) *Sec10$^{FL/FL}$;Ksp-Cre* ureters have a disrupted urothelial layer with cells detaching from the smooth muscle layer, entering the lumen, and no uroplakin expression.

4.3) DISCUSSION

In this study, we identify the underlying cellular basis of the *in utero* UPJ obstruction, and a timeline of ureter maldevelopment, in a *Sec10* conditional knockout mouse. We provide evidence that Sec10 is necessary for proper differentiation of superficial urothelial cells and establishment of the uroplakin barrier. It is not clear what exactly causes the cell death observed in E17.5 *Sec10$^{FL/FL}$;Ksp-Cre* urothelium, but our data shows that it is primarily necrotic in origin. Since the *Sec10* deletion occurs in these cells prior to E13.5[101], we hypothesize that the cell death after E16.5 is either in response to a failure of superficial differentiation or the lack of protection against the growing urine flow, or likely a combination of multiple factors. *We also hypothesized that the leakage of urine through the urothelial barrier induces the observed fibrotic wound healing response from the surrounding mesenchyme.* We measured no change in *TGF-β1* expression at E16.5 in *Sec10$^{FL/FL}$;Ksp-Cre* ureters, prior to the urothelial cell death and barrier degeneration. But beginning at E17.5, we measured an increase in *TGF-β1* expression (Fig. 35F), as well as an increase in the fibroblast specific gene *S100A4* (Fig. 36A). We also measured increased expression of *periostin* at E18.5, which is now recognized to be a critical regulator of the activation of fibroblast during wound healing and fibrosis[108–110]. This correlates with a decrease in the relative expression of *desmin*, by the smooth muscle cells. Although the surrounding mesenchyme includes both fibroblasts and smooth muscle cells, our data suggest the resident fibroblast population becomes activated myofibroblasts that rapidly proliferate and migrate to obstruct the ureter lumen between E17.5 and E18.5.

Clinical cases of UPJ obstructions, often detected as hydronephrosis via prenatal ultrasound, are highly variable in severity and progression[35–37]. In addition, the lack of prognostic indicators or biomarkers requires ongoing surveillance, which is a burden to the patient and costly[95,112]. Typically, cases of UPJ obstructions can be classified as intrinsic or extrinsic, where the more common intrinsic factors involve malformation of the ureter or cellular overgrowth in the ureter lumen, while extrinsic causes include pressure on the ureter from other tissues such as crossing vessels. One histological study demonstrated that surgically removed human samples of intrinsic obstructed UPJ regions had excessive collagen fibers that replaced smooth muscle in the ureter[113].

Another study of congenital UPJ obstructions from 25 patients (versus 15 age-matched control samples) showed an increase in *TGF-β1* mRNA expression and protein levels in the stenotic segments[114]. Taken together, these studies show that at least for a percentage of human UPJ obstructions, there is a significant increase in fibrosis at the stenotic region. Thus, the molecular and histological findings in our *Sec10* mouse model of UPJ obstructions are consistent with the ureter pathology of a significant portion of human clinical cases of UPJ obstructions.

Based on crosses with our *tdTomato* reporter mice, we know Cre-mediated inactivation occurs prior to E13.5 in *Sec10$^{FL/FL}$;Ksp-Cre* embryos[101]. However, the first abnormalities that we have detected did not occur until ~E16.5, which demonstrates that Sec10 knockout in these epithelial cells does not *de facto* cause cell death. At E16.5, there was a significant decrease in *PPARγ* expression (Fig. 32E), which is normally expressed at high levels during urothelial differentiation of the superficial cells and regulates transcription of the uroplakin gene family through FOXA1 and IRF-1 mediators[105,115]. A *PPARγ* conditional knockout mouse, created using the *Hoxb7-Cre* strain that targets the same ureteric bud derived epithelial cells as the *Ksp-Cre* mice, showed that although *PPARγ* is specifically important for differentiation of superficial urothelial cells, but knockout of *PPARγ* did not lead to urothelial cell death or prenatal UPJ obstructions. Both *Upk2* and *Upk3* knockout mice have also been reported, and they had severe defects in uroplakin plaque formation at the apical surface and did not have proper urothelial barrier function[103,116]. However, these knockout mice also did not display the *in utero* urothelial degeneration and fibroproliferative UPJ obstructions seen in our *Sec10* knockout model. This suggests that failure of superficial differentiation, or failure to produce uroplakin plaques, is not sufficient to produce our UPJ obstruction phenotype. Thus, the exocyst likely has additional roles in urothelial cells or their progenitors making this *Sec10* knockout model a unique tool to bridge the gap between urothelial differentiation and the onset of UPJ obstructions.

Significant decrease in mRNA expression of the four members of the uroplakin gene family in the *Sec10$^{FL/FL}$;Ksp-Cre* ureters starting at E16.5 (Fig. 32A-D) indicate that the exocyst regulates superficial cell differentiation. It is also possible that the exocyst plays a direct role in uroplakin vesicle trafficking to the apical membrane. The

decreased microvilli on the apical surface of E16.5 *Sec10$^{FL/FL}$;Ksp-Cre* urothelial cells (Fig. 31E and F) indicates disrupted membrane trafficking toward the apical plasma membrane where *Sec10* and *Sec3* are localized in control ureters (Fig. 31A and C). Although some evidence has suggested the exocyst is primarily a basolateral vesicle regulator in polarized epithelial cells[24,70], other studies have shown apical trafficking in some epithelial cell types can utilize the exocyst[117]. Several previous studies have also firmly established that the exocyst subunit *Sec15* interacts directly with *Rab11* and *Rab8* GTPases to promote exocytosis of vesicles bound to those proteins[54,57-59]. *Rab8* and *Rab11* are both present on uroplakin-containing discoidal/fusiform vesicles in bladder superficial cells, and both have been shown to be critical for the stretch-induced exocytosis of new uroplakin plaques[118,119]. This established connection between two Rab GTPases, which directly regulate uroplakin exocytosis and recycling, and the exocyst complex suggests that the exocyst also has a direct role in uroplakin exocytosis and dynamic recycling. Utilizing inducible Cre mouse strains that avoid urothelial differentiation defects could allow investigations of uroplakin trafficking in mature Sec10-knockout superficial cells.

Our histological analysis of the obstructed ureter at the UPJ region identified pathological changes similar to granulation tissue, with a robust and rapid fibroproliferative response between E17.5 and E18.5. This included invasion of the lumen by cells with a myofibroblastic appearance, deposition of ECM, and disruption of the basement membrane underlying the epithelium. Based on our *tdTomato* labeling of the Sec10-knockout urothelial cells, and the absence of any red-labeled fibroblastic cells in the obstructed lumens, we ruled out EMT as a contributor to the fibrotic response. We hypothesize the pathogenesis in our model of *in utero* UPJ obstructions shares similarities with other diseases of epithelial injury and aberrant stromal remodeling of internal tissues, such as obliterative bronchiolitis. In this pulmonary pathology commonly associated with lung transplants, the epithelial cell layer lining the bronchioles is damaged, triggering a fibroproliferative response of the underlying stroma that obstructs the airway lumen[106]. Our *Sec10$^{FL/FL}$;Ksp-Cre* mouse model shows that this mechanism may also contribute to prenatal UPJ obstructions, which may be triggered by leakage of the urine into the ureter's interstitial tissue. This mechanism for

congenital UPJ obstructions was previously hypothesized based on histological observations of human pyeloplasty samples. Although Bartoli et al. first published this hypothesis 20 years ago[120], our model provides the first experimental evidence that defective urothelial maturation during prenatal development can induce a fibroproliferative response from the underlying mesenchyme.

Future investigations will aim to identify exactly how the exocyst intersects with specific genetic signaling pathways and morphogens known to regulate urothelial differentiation and ureter development. Key to our understanding of the role of the exocyst in these processes will be identifying which proteins are trafficked by the exocyst complex in urothelial cells. We will likely find the exocyst is multifunctional in this cell type, as this complex has already been implicated in extremely diverse cellular processes, depending on the cell type and environment. Additionally, it will be important to investigate how the urine may damage the tissue underlying the leaky *Sec10$^{FL/FL}$;Ksp-Cre* urothelium at E17.5, and test how this damage induces the fibroproliferative response that rapidly occludes the lumen. This has direct implications to clinical cases of both intrinsic and extrinsic UPJ obstructions, and we may be able to use the *Sec10$^{FL/FL}$;Ksp-Cre* mouse model to screen potential therapeutics that ameliorate this type of response, or identify potential diagnostic or predictive biomarkers. Collectively, findings presented in this study demonstrate this *Sec10$^{FL/FL}$;Ksp-Cre* mouse model may be highly valuable for extending our understanding of the etiology of human congenital UPJ obstructions and the associated renal disease, as well as identifying novel approaches for treatments.

4.4) MATERIALS and METHODS

Animals

All animal procedures and protocols were carried out in accordance with IACUC specifications approved by the University of Hawaii Animal and Veterinary Services. Dr. Fogelgren's IACUC approved protocol is #11-1094, and the University of Hawaii has an Animal Welfare Assurance on file with the Office of Laboratory Animal Welfare (OLAW), assurance number is A3423-01. Adult mice were housed under standard conditions with 12-hr light cycle and supplied with water and food *ad libitum*. The floxed *Sec10* mouse strain (*Sec10*$^{FL/FL}$) was generated and used as previously described[18]. The *Ksp-Cre* mouse strain was obtained from Jackson Laboratories[23,24]. The *B6.Cg-Gt(ROSA)26Sor*$^{tm9(CAG-tdTomato)Hze}$*/J* reporter mouse strain (here designated *tdTomato* or *To*) was kindly provided by Dr. Michelle Tallquist at University of Hawaii and was used to detect Cre recombinase activity through Cre-activated expression of the tdTomato red fluorescent protein[63]. All mice were of C57Bl/6J inbred background. For timed matings, females mated with a male overnight were examined for a vaginal plug the following morning and constituted gestational day E0.5 if present. Both male and female embryos were obtained between days E13.5 and E18.5 and were subsequently staged using Theiler staging criteria (TS) to ensure the developmental stage of each embryo was similar to the conception day (E) designation[64]. Only animals of the same E designation and TS were compared.

Electron Microscopy

Dissected kidneys and ureters were fixed with 2.5% glutaraldehyde and in 0.1 M sodium cacodylate buffer, pH 7.2, washed in 0.1 M cacodylate buffer for 3 x 15 min, followed by post fixation with 1% OsO_4 in 0.1 M cacodylate buffer for 1 hour. The tissue was dehydrated in a graded ethanol series (30%, 50%, 70%, 85%, 95%, 100%), substituted with propylene oxide, and either embedded in LX112 epoxy resin for transmission electron microscopy (TEM) or dried in a Tousimis Samdri-795 critical point dryer for scanning electron microscopy (SEM). For TEM, ultrathin sections (60-80 nm) were obtained on a Reichert Ultracut E ultramicrotome, double stained with uranyl acetate and lead citrate, viewed on a Hitachi HT7700 TEM at 100 kV, and photographed with an

AMT XR-41B 2k x 2k CCD camera. For SEM, tissues were mounted on aluminum stubs with double stick tape and ureters were opened using a razor blade, and subsequently coated with gold/palladium in a Hummer 6.2 sputter coater. Tissues were viewed and digital images were obtained with a Hitachi S-4800 Field Emission Scanning Electron Microscope at an accelerating voltage of 5 kV.

Quantitative real time PCR analysis

Gene expression in embryonic tissues using real time quantitative PCR (qPCR) was performed as described previously, using the 2^(-ΔΔCt) method of analysis to calculate fold changes of expression[65]. Briefly, ureter segments from the UPJ region from embryos of various stages were dissected and placed immediately into RNAlater (Sigma) and stored at -20˚C. Ureters from three animals of the same stage and with the same genotype were pooled and extracted using the RNeasy micro kit (Qiagen). cDNA was generated from extracted RNA using the iSCRIPT reverse transcriptase (Bio-Rad) and qPCR was performed using SYBR green (Bio-Rad) with a CFX96 Real Time System (Bio-Rad), as per the manufacturer's recommended instructions. Please refer to Supplementary Information for a complete list of primer sequences used for qPCR. Expression data was analyzed using Graphpad Prism software. Differences between means for any parameter measured in two groups of age-matched mice were evaluated using Student's t-tests.

Primer	Sequence 5' – 3'
Gli3- F	CAC CAA AAC AGA ACA CAT TCC A
Gli3-R	GGG GTC TGT GTA ACG CTT G
Gli1-F	CTG ACT GTG CCC GAG AGT G
Gli1-R	CGC TGC TGC AAG AGG ACT
Upk1a-F	AGG CAA GGA TGA TGT CTT CG
Upk1a-R	ATG AGC ATC AGC AGC AGG TA
Upk1b-F	CTT GGA TAG GCA TGT TCG TG
Upk1b-R	CTG TGA TGC AAG ATG CCA CT
Upk2-F	ATC CTG ATT CTG CTG GCT GT
Upk2-R	GGC ACC ACA AAG TCT GAC TT
Upk3a-F	CGG CCA CTG AGT ACA GAT TC
Upk3a-R	GGA CGT GAT GAC AAT CAT GC
Upk3b-F	ATC AGC TGC CAT GTG AGG AC
Upk3b-R	ACC ACT TCG TCT CAG CCT TG
Krt20-F	TCA CAG TGA ACA CGG AGG AG
Krt20-R	ACG AGC CTT GAC GTC CTC TA
Krt5-F	GCC TAC ATG AAC AAG GTG GA
Krt5-R	GTT GGC AAT GTC CTC GTA CT
Collagen IV-F	TCC AGG CCC TGG AAC TGT
Collagen IV-R	GAG GGC CTG GTT GGC CTG
TGF-beta-F	AGG GCT ACC ATG CCA ACT TC
TGF-beta-R	CCA CGT AGT AGA CGA TGG GC
S100A4-F	CAG GCA AAG GTG ACA AG
S100A4-R	CAA TGC AGG ACA GGA AGA CA
Periostin-F	GAA TGG TGT CAT CCA CCT GA
Periostin-R	GTC CAT GCT CAG AGT GTC AT
B actin-F	CAT CCG TAA AGA CCT CTA TGC CAA C
B actin-R	ATG GAG CCA CCG ATC CAC A
Desmin-F	ACC TTC TCT GCT CTC AAC TTC A
Desmin-R	CGC TGA CAA CCT CTC CAT CC

Table 2: Primer sequences used for qPCR analysis.

Histology and Immunohistochemistry

Caudal torsos of Sec10 knockout and control animals were dissected, the abdominal cavity opened, immediately placed in freshly prepared 4% formaldehyde in PBS, and fixed overnight with rocking at 4˚C. Some samples were embedded in paraffin according to standard methods, and some samples were instead subjected to cryosectioning. The tissues were sectioned into 5 μm sections and staining and immunohistochemistry procedures were performed as previously reported[18]. Primary antibodies used for immunostaining were: anti-cleaved caspase-3 at 1:400 (Cat # 9664, Cell Signaling Tech.); anti-p63 at manufacturer's prepared dilution (Cat # API 3050 G3, Biocare Medical); anti-collagen IV at 1:200 (Cat # ab6586, Abcam); anti-E-cadherin at 1:200 (Cat # 3195, Cell Signaling Tech.); anti-smooth muscle actin at 1:800 (Cat # A2547, Sigma). Stained sections were analyzed using a fluorescent Olympus BX41 microscope or an Olympus Fluoview1000 confocal microscope. Image processing, quantification of cell layer widths, and cell counts were done using Image J software (NIH). For ureter injections, fluorescein isothiocyanate (FITC) labeled dextran (average molecular weight 10,000, Cat # FD10S, Sigma) was dissolved in PBS to make a stock solution of 25 mg/ml. The FITC-dextran solution was injected into the renal pelvis (left kidney only) of genitourinary tracts and allowed to flow to the bladder. Injected tissues were frozen in OCT, cryosectioned, dried, and analyzed with a fluorescent Olympus BX41 microscope.

Protein Analysis

Ureters were dissected from E17.5 and E18.5 embryos and immediately frozen. Proteins were extracted using standard RIPA lysis buffer with phosphatase and protease inhibitors. Protein quantification was performed using the Bradford Assay and 1.0 μg/μl of protein lysate was placed onto each chamber of the PathScan Intracellular signaling array (Cell Signaling Technology #7744). Assay conditions and procedures followed the manufacturer's recommendations. Florescence readout was performed using the Licor Odyssey Imager. PathScan data analysis was quantified using ImageStudio software provided by Licor Biosciences. The relative fluorescence unit (RFU) of each antibody spot was quantified according to the Cell Signaling protocol and

normalized to the positive control antibody spots (also provided on the Cell Signaling array). Student t-test comparisons were performed using Prism GraphPad software.

Ex vivo ureter explants

Ureters at E15.5 were dissected and placed on 1.0μm filters and placed into a 12-well plate with DMEM/Hams F12 containing 5μg/ml transferrin, 100μg/ml penicillin, and 100U/ml streptomycin. *Ex vivo* ureters were incubated at 37°C for 72 hours. Gross images and peristalsis videos were taken using an Olympus CKX41 microscope. After 72 hours in culture, the ureter explants were fixed with 4% paraformaldehyde overnight and subsequently placed in sucrose for cryo sectioning and histological analysis.

CHAPTER 5: Conclusions and Future Directions

5.1) Conclusions from these studies:

In this dissertation we investigated the importance of *Sec10* and the exocyst complex in the regulation of epithelial differentiation, morphology, and homeostasis. This includes epithelial characteristics such as barrier formation, apical basal polarity, primary ciliogenesis, and planar cell polarity.

In Chapter 2, we described findings from using an *in vitro* model of MDCK epithelial cystogenesis that showed the exocyst is not necessary for lumen formation through the cavitation process. However, *Sec10* is required for the formation of the primary cilium and maintenance of planar cell polarity in these MDCK cysts. Also, we showed that loss of *Sec10* led to high rates of basal cell extrusion, likely due to increased apoptotic sensitivity. This was the first time that the exocyst complex has been identified as regulating epithelial cell extrusion, planar cell polarity, and apoptotic sensitivity in epithelial cells.

In Chapter 3, we described the generation of a novel and unique *Sec10* conditional knockout mouse strain, which should be useful in studying the exocyst function in a large variety of tissues and diseases. With this mouse, we deleted the *Sec10* gene specifically in the epithelium of the kidney collecting system and the ureter. We found that this *Sec10* knockout leads to severe hydronephrosis, anuria, and neonatal death due to a physical obstruction in the ureteric pelvic junction.

In Chapter 4, we performed extensive embryonic analysis of $Sec10^{FL/FL}$*;Ksp-Cre* mutant ureters compared to controls. We showed that $Sec10^{FL/FL}$*;Ksp-Cre* ureters develop similarly to controls until E16.5. However, beginning at E17.5, $Sec10^{FL/FL}$*;Ksp-Cre* ureters are unable to differentiate a stratified urothelium and then urothelial cells begin to undergo necrosis. At E18.5, there is a complete overgrowth of mesenchymal cells to obliterate the ureter lumen, and an increase in TGFβ1 gene expression, a gene associated with fibrosis and wound healing. Loss of *Sec10* results in decreased *PPARγ, uroplakin, and cytokeratin* gene expression, which are crucial markers of a mature urothelium. *Our overall conclusion is that Sec10 knockout leads to defects in urothelial stratification causing a dysfuncational barrier, allowing urine to escape into the*

interstitial spaces. This leakage leads to a fibroproliferative response causing occlusion of the ureter (Fig. 39).

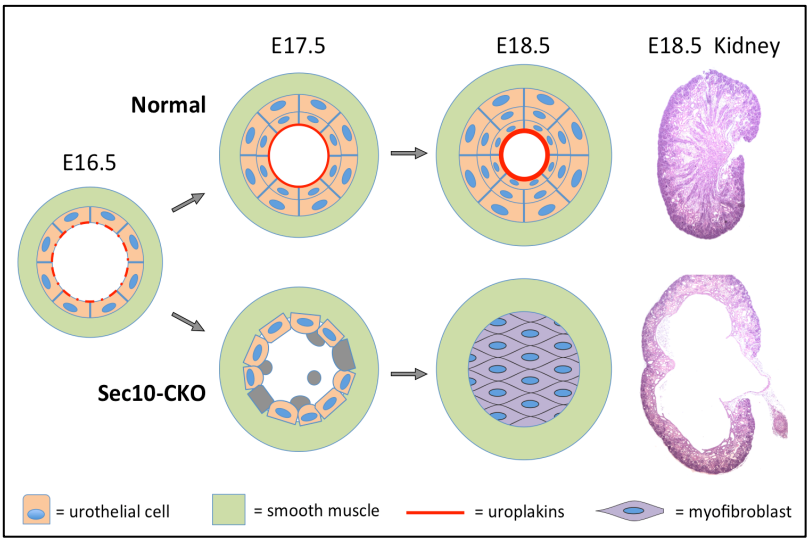

Figure 39: Summary for the development of hydronephrosis in *Sec10$^{Fl/Fl}$; Ksp-Cre.* Control and *Sec10$^{Fl/Fl}$; Ksp-Cre* (Sec10-CKO) ureters develop a monolayer of urothelial cells with some uroplakin expression at E16.5. At E17.5 control and Sec10-CKO ureters begin to have different phenotypes. Normal ureters develop multiple urothelial layers with increasing uroplakin expression, while Sec10-CKO ureters lose uroplakin and the cells begin to die and slough off. The cell death causes a leaky barrier and mesenchymal cells occlude the lumen.

5.2) Significance of this research to human disease, and potential clinical applications:

Our *Sec10$^{FL/FL}$;Ksp-Cre* mouse model is a unique model of CON that will increase our understanding and knowledge of ureter development and the mechanisms behind injury to the urothelium that may lead to UPJ obstructions in human cases. CON has been an understudied disease due to the lack of non-surgical genetic models. **Here, we provide both a novel and unique model, and a potential mechanism for the onset of CON during development**. To our knowledge, this is the first time CON has been linked to defects in urothelial stratification *in utero* during embryonic development. Previous studies have been focused on defects in differentiation of smooth muscle that could potentially lead to functional obstructions and hydronephrosis[38], or they have been limited to post-natal analysis of the obstruction region in human samples. We

hope that this model of *Sec10* knockout in urothelial cells will provide further insight into the development of UPJ obstructions prior to birth. Understanding the timing of ureter development and the onset of UPJ obstructions is crucial for diagnosing patients with CON. If we can identify biomarkers prior to the development of the obstruction, we can perhaps design early treatments, or develop a novel indicator to predict patient prognosis. One possible biomarker is *Upk3,* because in humans, mutations in *Upk3* have been described in patients with vesicoureteral reflux, hydronephrosis and multicystic dysplastic kidneys[121–123].

Another possible clinical application would to determine potential therapeutic targets based on the understanding of cell populations and signaling pathways that lead to UPJ obstructions. In 2003, Yang et al performed studies on stenotic regions of children with UPJ obstructions[107]. They discovered increased TGFβ1 mRNA expression, which influences mesenchymal differentiation, and can be an important therapeutic target. *TGFβ1* inhibitors could be potentially used to inhibit the fibroproliferation we observed in our *Sec10$^{FL/FL}$;Ksp-Cre* ureters with damaged urothelium.

In 1996, Bartoli et al presented a new hypothesis where they studied the stenotic segments of 10 children with UPJ obstructions[120]. Their histological studies showed that children with UPJ obstructions could have a damaged urothelium[120]. They showed that some regions of the stenotic ureters lacked an epithelium and they hypothesized that the lack of urothelium could lead to urine diffusion and cause massive immunological and fibrotic responses. This was the first time that urothelial defects were mentioned as a potential mechanism for the development of UPJ obstructions. The phenotype and molecular mechanism that we have reported in our *Sec10$^{FL/FL}$;Ksp-Cre* mice coincide with reports of clinical human cases and we can conclude that this model of UPJ obstructions may be useful for determining clinical treatments.

5.3) Current working hypothesis:

Our current working hypothesis is that the exocyst complex is responsible for trafficking key proteins to the apical surface of the urothelial progenitor cells. We predict that these key proteins play an essential role in the development of the ureter and improper trafficking could lead to detrimental defects, such as a UPJ obstruction. Based

on previous studies of exocyst regulation of EGFR[124], we hypothesize that EGFR interaction with *Sec10* could be one of the key trafficking events that occur in these urothelial progenitors. EGFR is a member of the Erb1 receptor tyrosine kinases that when phosphorylated, it gets internalized and activates a number of different intracellular signaling pathways[124,125]. Some of these pathways include the MAPK, JAK/STAT, and ERK pathways responsible for cell survival, proliferation, and differentiation[125]. EGFR has been associated with acute kidney injury, chronic kidney injury, and renal fibrosis. In all of these cases, there was an increase in phosphorylated EGFR, and EGFR has become a therapeutic target[126–128]. *We hypothesize that since Sec10 and EGFR directly interact with each other[124], Sec10 knockout leads to improper trafficking of EGFR to the membrane.*

There are several other potential candidates for exocyst trafficking in the urothelial progenitor cells. With a well-accepted association between the exocyst and cell-cell adhesion molecules, it could be that these cells are unable to make the specific cell-cell contacts needed for epithelial stratification. The exocyst complex may also traffic the uroplakin proteins to the apical membrane. Dr. Gerard Apodaca showed that Rab8, Rabin8, and Rab11 are all important for uroplakin trafficking to the luminal membrane[118,119]. Exocyst components have also been shown to interact with these same Rab proteins in order to direct exocytosis to particular locales[58,129]. We showed that both the exocyst complex and Rab proteins co-localize to the apical membrane in these urothelial progenitor cells, which suggest they may work together to traffic uroplakins to the apical surface for the formation of a mature barrier against urine.

5.4) Future Directions

As with many scientific studies, successful experiments and novel findings lead to new questions to be explored. Even with these data presented in this dissertation, some major questions remain, which hopefully we can address in the future.

1. What proteins are being trafficked to the apical surface of the urothelium by the exocyst complex?

Due to the observation that *Sec10$^{FL/FL}$;Ksp-Cre* ureters are unable to differentiate into stratified urothelium and the urothelial cells begin to undergo necrosis at E17.5. We wanted to determine which signaling pathways at E16.5 are misregulated and lead to the phenotype we observe. We extracted RNA from E16.5 ureters, pooled RNA samples together (n=3 ureters), and analyzed gene expression using both Affymetrix Clariom D mouse arrays and RNAseq (next generation sequencing). These analyses allowed us to map the transcriptome including non-coding RNA and microRNAs, comparing mutant ureters with control littermates. Our samples were analyzed for quality and adequate concentration (data not shown). The quality of the RNA samples was determined based on the A260/280 ratio and the RIN value. Once we were confident in our samples, we utilized the University of Hawaii Cancer Center Genomics Core Facility for the Affymetrix Claroim D microassays, and we sent a larger aliquot of the exact same samples to Genewiz for RNAseq.

In the preliminary analysis of these data sets using the Transcriptome Analysis Console provided by Affymetrix, we looked at genes we previously confirmed to be decreased in *Sec10$^{FL/FL}$;Ksp-Cre* ureters compared to controls. Unlike our qPCR on both pooled and individual ureter samples (Chap 4), we failed to see a significant decrease in expression of *Sec10*, uroplakins, cytokeratins, and *PPARγ* in our mutant samples. We saw similar negative findings with the RNAseq data, where we didn't measure a significant decrease in expression of these genes we previously reported. We also saw large variation among the samples, and concluded that further bioinformatics and analysis is warranted.

One of the potential pitfalls of working with whole ureters in RNA and protein analysis is the abundance of non-urothelial cells in the ureter. The ureter consists of smooth muscle cells, fibroblasts, and urothelial cells. These non-urothelial cells can provide altered expression profiles and can conceal what is occurring in the urothelial cells. We have begun to optimize a epithelial cell separation kit from Stem Cell Technologies that specifically enriches epithelial cells. In this experiment, *Sec10$^{FL/FL}$;Ksp-Cre* ureters and control ureters will be digested using a cocktail of

collagenase and hyaluronidase at 37°C following by cell separation using trypsin. The cells are then placed into the Selection cocktail that utilizes biotinylated antibodies and magnetic particles to select against non-epithelial cells. Once the ureter cell solution has been incubated with the selection cocktail, it is placed in a tube on an EasyEights EasySep magnet that binds all the non-epithelial cells that have been labeled with a magnetic particle. The remaining cells should consist of only epithelial cells, and then RNA analysis can be performed without any background cell interference.

As mentioned previously, EGFR was biochemically shown to interact with *Sec10* in MDCK cells, and we would like to follow up on the relationship and potential interaction of *Sec10* and EGFR. Using our *in vivo* model we can perform immunohistochemistry and FITC-EGF injections into ureters at various embryonic stages. In Figure 40, we show EGFR immunostaining of control ureters localizing to the basolateral surface. Comparison of EGFR localization in control versus *Sec10*$^{FL/FL}$*;Ksp-Cre* ureters will provide insight into the relationship between *Sec10* and EGFR. We also have a FITC-labeled EGF reagent, which we can inject into the pelvis of the kidney and analyze for EGF binding to EGFR by quantifying the amount of retained fluorescence.

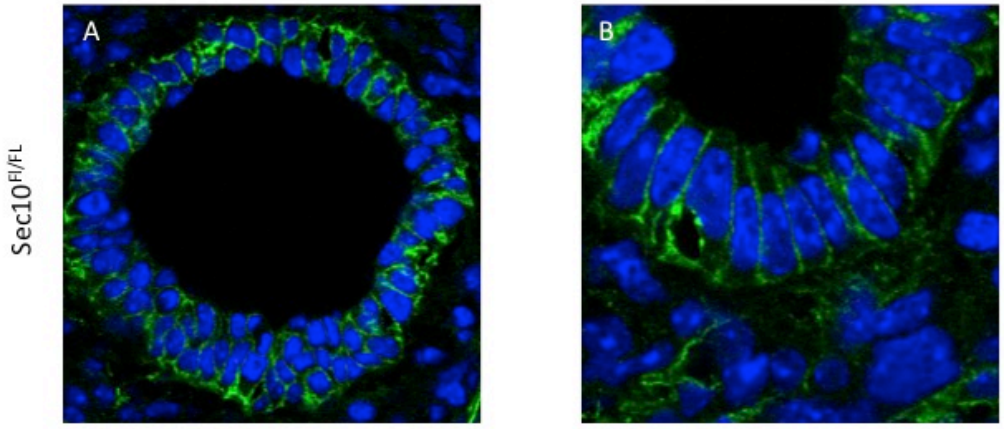

Figure 40: Confocal microscopy of EGFR in E16.5 ureter cross sections. A-B *Sec10*$^{FL/FL}$ ureters immunostained with EGFR (green) and Dapi (blue). EGFR appears to be localized to the basolateral surface of the urothelium.

We have an *Upk3a-GFPCre*^{Ert2} mouse strain that when crossed with our floxed Sec10 mouse strain, *Sec10* knockout will occur in uroplakin 3 expressing cells (superficial urothelial cells). Using tdTomato reporter expression, we have confirmed Cre recombination specifically in the superficial cells of the urothelium of *Upk3a-GFPCre*^{Ert2} mice (Fig. 43). This mouse strain allows us to activate *Sec10* deletion in adults upon tamoxifen treatment. *We hypothesize that if knocked out prior to urothelial stratification, a UPJ obstruction phenotype will occur. If knocked out after stratification, we will observe a similar phenotype to the Upk2 and Upk3 knockout mice.* We will also perform TEM and SEM of *Sec10*$^{FL/FL}$*;Upk3a-GFPCre*^{Ert2} mice to determine if there are any defects in uroplakin plaque trafficking to the apical surface. If there are no uroplakin plaques similar to what was observed in the Sec10$^{FL/FL}$ control mice, we can conclude that *Sec10* plays an important role in the trafficking of uroplakins to the apical membrane of mature superficial cells.

Figure 41: *Upk3a-GFPCre*^{Ert2}*;To/+* adult bladder. Tomato expression (red) indicates the presence of recombination in Upk3 expressing cells on the luminal surface of the bladder.

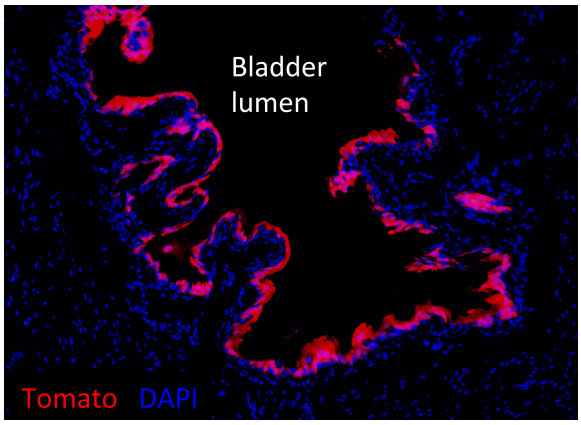

Finally, we can use immunohistochemistry and biotinylation of apical surface proteins to determine differences in the luminal membrane proteins of *Sec10*$^{FL/FL}$*;Upk3a-GFPCre*^{Ert2} mice compared to controls. Biotinylation is a technique where an EZ-Link Sulfo-NHS-Biotin (Thermo Scientific) can be injected into the pelvis of the kidney until it travels down the ureter. The biotin is incubated in the ureter for 15 minutes to allow for the biotin to bind to all the apical surface proteins[1]. After incubation, an avidin column will pull out all the proteins that bound to biotin. We can perform

subsequent proteomic analysis of the captured membrane proteins. Without *Sec10* in the *Upk3* expressing cells, we hypothesize that key proteins involved in superficial cell maturation, such as uroplakins and cytokeratins will be decreased on the plasma membrane or be absent all together.

2. Does the exocsyt complex regulate key developmental signaling pathways in the maturation of the urothelium?

In this approach we will utilize our *ex vivo* ureter explant model to determine key signaling pathways essential for the regulation of urothelial differentiation. We can interrogate paracrine-signaling pathways identified in ureter development on wild type ureter explants. Some of these pathways include retinoic acid (RA), sonic hedgehog (shh), BMP4, and EGFR. We have performed preliminary inhibitor treatments (Fig. 44) and will follow this up with further analysis.

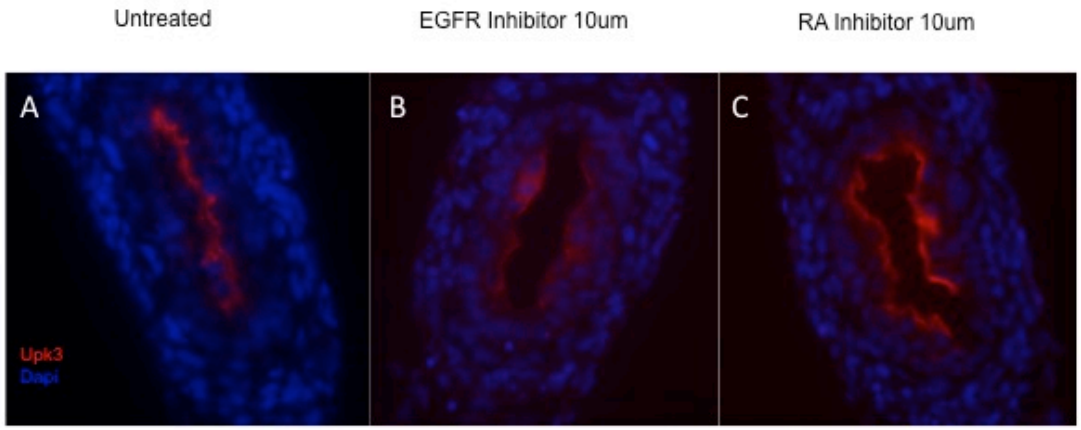

Figure 42: Preliminary inhibitor treatment of ureter explants with retinoic acid (RA) and EGFR inhibitors. Ureter explants were dissected and treated for 72 hours with respective inhibitors. A) untreated ureter explant immunostained with Upk3 (red) to mark a stratified urothelium. B) Ureter explant treated with EGFR inhibitor (IRESSA) for 72 hours and immunostained with Upk3. C) Ureter explant treated with retinoic acid inhibitor BMS453 and immunostained with Upk3.

In conclusion, the conditional *Sec10* knockout mouse model we have presented in this dissertation is a useful animal model of congenital obstructive nephropathy and ureter development. It has a similar phenotype to what has been observed in human cases and we can use it to find potential biomarkers and therapeutic targets. This mouse model also allows us to study ureter development and we have shown for the first time a role for the exocyst in urothelial biology.

REFERENCES

1. Davidson, A. Mouse kidney development. *StemBook* 1–30 (2008). doi:10.3824/stembook.1.34.1
2. Dressler, G. R. Advances in early kidney specification, development and patterning. *Development* **136,** 3863–74 (2009).
3. Reidy, K. J. & Rosenblum, N. D. Cell and Molecular Biology of Kidney Development. *Semin. Nephrol.* **29,** 321–337 (2009).
4. Little, M. H. & McMahon, A. P. Mammalian kidney development: Principles, progress, and projections. *Cold Spring Harb. Perspect. Biol.* **4,** 3 (2012).
5. Costantini, F. GDNF/Ret signaling and renal branching morphogenesis: From mesenchymal signals to epithelial cell behaviors. *Organogenesis* **6,** 252–262 (2010).
6. Pepicelli, C. V., Kispert, A., Rowitch, D. H. & McMahon, A. P. GDNF induces branching and increased cell proliferation in the ureter of the mouse. *Dev. Biol.* **192,** 193–8 (1997).
7. Sariola, H. & Saarma, M. GDNF and its receptors in the regulation of the ureteric branching. *International Journal of Developmental Biology* **43,** 413–418 (1999).
8. Woolf, A. S. & Davies, J. A. Cell biology of ureter development. *J. Am. Soc. Nephrol.* **24,** 19–25 (2013).
9. Uhlenhaut, N. H. & Treier, M. Transcriptional regulators in kidney disease: gatekeepers of renal homeostasis. *Trends in Genetics* **24,** 361–371 (2008).
10. Guo, W., Roth, D., Gatti, E., De Camilli, P. & Novick, P. Identification and characterization of homologues of the Exocyst component Sec10p. *FEBS Lett.* **404,** 135–139 (1997).
11. Novick, P., Ferro, S. & Schekman, R. Order of events in the yeast secretory pathway. *Cell* **25,** 461–469 (1981).
12. Novick, P. & Schekman, R. Secretion and cell-surface growth are blocked in a temperature-sensitive mutant of Saccharomyces cerevisiae. *Proc. Natl. Acad. Sci. U. S. A.* **76,** 1858–1862 (1979).
13. Inoue, M., Akama, T., Jiang, Y. & Chun, T.-H. The exocyst complex regulates free Fatty Acid uptake by adipocytes. *PLoS One* **10,** e0120289 (2015).
14. Nichols, C. D. & Casanova, J. E. Salmonella-directed recruitment of new membrane to invasion foci via the host exocyst complex. *Curr. Biol.* **20,** 1316–1320 (2010).
15. Guichard, A. *et al.* Cholera toxin disrupts barrier function by inhibiting exocyst-mediated trafficking of host proteins to intestinal cell junctions. *Cell Host Microbe* **14,** 294–305 (2013).
16. Lu, H. *et al.* Exo70 isoform switching upon epithelial-mesenchymal transition mediates cancer cell invasion. *Dev. Cell* **27,** 560–573 (2013).
17. Bodemann, B. O. *et al.* NIH Public Access. **144,** 253–267 (2012).
18. Letinic, K., Sebastian, R., Toomre, D. & Rakic, P. Exocyst is involved in polarized cell migration and cerebral cortical development. *Proc. Natl. Acad. Sci. U. S. A.* **106,** 11342–11347 (2009).
19. Heider, M. R. & Munson, M. Exorcising the Exocyst Complex. *Traffic* **13,** 898–907 (2012).

20. Zuo, X., Fogelgren, B. & Lipschutz, J. H. The small GTPase Cdc42 is necessary for primary ciliogenesis in renal tubular epithelial cells. *J. Biol. Chem.* **286,** 22469–22477 (2011).
21. Fogelgren, B. *et al.* The exocyst protein sec10 interacts with polycystin-2 and knockdown causes PKD-phenotypes. *PLoS Genet.* **7,** (2011).
22. Friedrich, G. a, Hildebrand, J. D. & Soriano, P. The secretory protein Sec8 is required for paraxial mesoderm formation in the mouse. *Dev. Biol.* **192,** 364–74 (1997).
23. Roth, D., Guo, W. & Novick, P. Dominant negative alleles of SEC10 reveal distinct domains involved in secretion and morphogenesis in yeast. *Mol. Biol. Cell* **9,** 1725–1739 (1998).
24. Choi, S. Y. *et al.* Exocyst Sec10 is involved in basolateral protein translation and translocation in the endoplasmic reticulum. *Nephron - Exp. Nephrol.* **120,** (2012).
25. Mochizuki, T., Tsuchiya, K. & Nitta, K. Autosomal dominant polycystic kidney disease: Recent advances in pathogenesis and potential therapies. *Clin. Exp. Nephrol.* **17,** 317–326 (2013).
26. Satir, P., Pedersen, L. B. & Christensen, S. T. The primary cilium at a glance. *J Cell Sci* **123,** 499–503 (2010).
27. Delling, M., DeCaen, P. G., Doerner, J. F., Febvay, S. & Clapham, D. E. Primary cilia are specialized calcium signalling organelles. *Nature* **504,** 311–314 (2013).
28. Pedersen, L. B., Veland, I. R., Schrøder, J. M. & Christensen, S. T. Assembly of primary cilia. *Developmental Dynamics* **237,** 1993–2006 (2008).
29. Veland, I. R., Awan, A., Pedersen, L. B., Yoder, B. K. & Christensen, S. T. Primary cilia and signaling pathways in mammalian development, health and disease. *Nephron - Physiol.* **111,** (2009).
30. Choi, S. Y. *et al.* Cdc42 deficiency causes ciliary abnormalities and cystic kidneys. *J. Am. Soc. Nephrol.* **24,** 1435–50 (2013).
31. Wang, S. & Dong, Z. Primary cilia and kidney injury: current research status and future perspectives. *Am. J. Physiol. Renal Physiol.* **305,** F1085-98 (2013).
32. Benfield, M. R., McDonald, R. a, Bartosh, S., Ho, P. L. & Harmon, W. Changing trends in pediatric transplantation: 2001 Annual Report of the North American Pediatric Renal Transplant Cooperative Study. *Pediatr. Transplant.* **7,** 321–335 (2003).
33. Woolf, A. S. & Thiruchelvam, N. Congenital obstructive uropathy: its origin and contribution to end-stage renal disease in children. *Adv Ren Replace Ther* **8,** 157–163 (2001).
34. Foley, R. N. & Collins, A. J. End-stage renal disease in the United States: an update from the United States Renal Data System. *J. Am. Soc. Nephrol.* **18,** 2644–8 (2007).
35. Roth, K. S., Koo, H. P., Spottswood, S. E. & Chan, J. C. M. Obstructive uropathy: an important cause of chronic renal failure in children. *Clin. Pediatr. (Phila).* **41,** 309–314 (2002).
36. Woodward, M. & Frank, D. Postnatal management of antenatal hydronephrosis. *BJU Int.* **89,** 149–156 (2002).
37. Mesrobian, H. G. O. & Mirza, S. P. Hydronephrosis. A View from the Inside. *Pediatr. Clin. North Am.* **59,** 840–851 (2012).

38. Klein, J. *et al.* Congenital ureteropelvic junction obstruction: Human disease and animal models. *Int. J. Exp. Pathol.* **92,** 168–192 (2011).
39. Ingraham, S. E. & McHugh, K. M. Current perspectives on congenital obstructive nephropathy. in *Pediatric Nephrology* **26,** 1453–1461 (2011).
40. Bascands, J. L. & Schanstra, J. P. Obstructive nephropathy: Insights from genetically engineered animals. *Kidney International* **68,** 925–937 (2005).
41. Bohnenpoll, T. & Kispert, A. Ureter growth and differentiation. *Semin. Cell Dev. Biol.* **36,** 21–30 (2014).
42. Yamany, T., Van Batavia, J. & Mendelsohn, C. Formation and regeneration of the urothelium. *Curr. Opin. Organ Transplant.* **19,** 323–30 (2014).
43. Gandhi, D. *et al.* Retinoid signaling in progenitors controls specification and regeneration of the urothelium. *Dev. Cell* **26,** 469–482 (2013).
44. Papafotiou, G. *et al.* ARTICLE KRT14 marks a subpopulation of bladder basal cells with pivotal role in regeneration and tumorigenesis. *Nat. Commun.* **7,** 1–11 (2016).
45. Wu, X.-R., Kong, X.-P., Pellicer, A., Kreibich, G. & Sun, T.-T. Uroplakins in urothelial biology, function, and disease. *Kidney Int.* **75,** 1153–65 (2009).
46. Truschel, S. T. *et al.* Stretch-regulated exocytosis/endocytosis in bladder umbrella cells. *Mol. Biol. Cell* **13,** 830–46 (2002).
47. Roignot, J., Peng, X. & Mostov, K. Polarity in mammalian epithelial morphogenesis. *Cold Spring Harb. Perspect. Biol.* **5,** (2013).
48. Martín-Belmonte, F. *et al.* Cell-Polarity Dynamics Controls the Mechanism of Lumen Formation in Epithelial Morphogenesis. *Curr. Biol.* **18,** 507–513 (2008).
49. Overeem, A. W., Bryant, D. M. & van IJzendoorn, S. C. D. Mechanisms of apical-basal axis orientation and epithelial lumen positioning. *Trends Cell Biol.* **25,** 476–485 (2015).
50. Pieczynski, J. & Margolis, B. Protein complexes that control renal epithelial polarity. *Am J Physiol-Renal* **300,** 589–601 (2011).
51. Lee, J. L. & Streuli, C. H. Integrins and epithelial cell polarity. *J. Cell Sci.* **127,** 3217–3225 (2014).
52. Schnell, U. & Carroll, T. J. Planar cell polarity of the kidney. *Exp. Cell Res.* **343,** 258–266 (2016).
53. Lawrence, P., Struhl, G. & Casal, J. Planar cell polarity: one or two pathways? *Nat. Rev. Genet.* **8,** 555–563 (2007).
54. Wallingford, J. B. Planar cell polarity, ciliogenesis and neural tube defects. *Hum. Mol. Genet.* **15,** (2006).
55. Yeaman, C. *et al.* Exocyst is involved in cystogenesis and tubulogenesis and acts by modulating synthesis and delivery of basolateral plasma membrane and secretory proteins. *Mol. Biol. Cell* **11,** 308–317 (2000).
56. Martin-Belmonte, F. & Mostov, K. Regulation of cell polarity during epithelial morphogenesis. *Current Opinion in Cell Biology* **20,** 227–234 (2008).
57. Polgar, N., Lee, A. J., Lui, V. H., Napoli, J. A. & Fogelgren, B. The exocyst gene Sec10 regulates renal epithelial monolayer homeostasis and apoptotic sensitivity. *Am. J. Physiol. Cell Physiol.* **309,** C190-201 (2015).
58. Bryant, D. M. *et al.* A molecular network for de novo generation of the apical surface and lumen. *Nat. Cell Biol.* **12,** 1035–1045 (2010).

59. Zuo, X., Guo, W. & Lipschutz, J. H. The Exocyst Protein Sec10 Is Necessary for Primary Ciliogenesis and Cystogenesis In Vitro. *Mol. Bilogy Cell* **20,** 2522–2529 (2009).
60. Pazour, G. J. & Witman, G. B. The vertebrate primary cilium is a sensory organelle. *Current Opinion in Cell Biology* **15,** 105–110 (2002).
61. Gu, Y., Forostyan, T., Sabbadini, R. & Rosenblatt, J. Epithelial cell extrusion requires the sphingosine-1-phosphate receptor 2 pathway. *J. Cell Biol.* **193,** 667–676 (2011).
62. Eisenhoffer, G. T. *et al.* Crowding induces live cell extrusion to maintain homeostatic cell numbers in epithelia. *Nature* **484,** 546–549 (2013).
63. Gu, Y. & Rosenblatt, J. New emerging roles for epithelial cell extrusion. *Curr. Opin. Cell Biol.* **24,** 865–870 (2012).
64. Rosenblatt, J., Raff, M. C. & Cramer, L. P. An epithelial cell destined for apoptosis signals its neighbors to extrude it by an actin- and myosin-dependent mechanism. *Curr. Biol.* **11,** 1847–1857 (2001).
65. Otto, E. a *et al.* Mutations in INVS encoding inversin cause nephronophthisis type 2, linking renal cystic disease to the function of primary cilia and left-right axis determination. *Nat. Genet.* **34,** 413–420 (2003).
66. Fedeles, S. & Gallagher, A. R. Cell polarity and cystic kidney disease. *Pediatr. Nephrol.* **28,** 1161–1172 (2013).
67. Lin, F. *et al.* Kidney-specific inactivation of the KIF3A subunit of kinesin-II inhibits renal ciliogenesis and produces polycystic kidney disease. *Proc. Natl. Acad. Sci. U. S. A.* **100,** 5286–91 (2003).
68. Mao, Z., Streets, A. J. & Ong, A. C. M. Thiazolidinediones inhibit MDCK cyst growth through disrupting oriented cell division and apicobasal polarity. *Am. J. Physiol. Renal Physiol.* **300,** F1375-84 (2011).
69. Wang, S., Wei, Q., Dong, G. & Dong, Z. ERK-mediated suppression of cilia in cisplatin-induced tubular cell apoptosis and acute kidney injury. *Biochim. Biophys. Acta* **1832,** 1582–90 (2013).
70. Lipschutz, J. H. *et al.* Exocyst is involved in cystogenesis and tubulogenesis and acts by modulating synthesis and delivery of basolateral plasma membrane and secretory proteins. *Mol. Biol. Cell* **11,** 4259–75 (2000).
71. O'Brien, L. E. *et al.* Rac1 orientates epithelial apical polarity through effects on basolateral laminin assembly. *Nat. Cell Biol.* **3,** 831–838 (2001).
72. Schneider, C. a, Rasband, W. S. & Eliceiri, K. W. NIH Image to ImageJ: 25 years of image analysis. *Nat. Methods* **9,** 671–675 (2012).
73. Shao, X. A Minimal Ksp-Cadherin Promoter Linked to a Green Fluorescent Protein Reporter Gene Exhibits Tissue-Specific Expression in the Developing Kidney and Genitourinary Tract. *J. Am. Soc. Nephrol.* **13,** 1824–1836 (2002).
74. Shao, X., Johnson, J. E., Richardson, J. a, Hiesberger, T. & Igarashi, P. A minimal Ksp-cadherin promoter linked to a green fluorescent protein reporter gene exhibits tissue-specific expression in the developing kidney and genitourinary tract. *J. Am. Soc. Nephrol.* **13,** 1824–1836 (2002).
75. Shao, X., Somlo, S. & Igarashi, P. Epithelial-specific Cre/lox recombination in the developing kidney and genitourinary tract. *J. Am. Soc. Nephrol.* **13,** 1837–46 (2002).

76. Rubera, I., Hummler, E. & Beermann, F. Transgenic mice and their impact on kidney research. *Pflugers Arch. Eur. J. Physiol.* **458,** 211–222 (2009).
77. Whyte, D. A. *et al.* Ksp-cadherin gene promoter. I. Characterization and renal epithelial cell-specific activity. *Am. J. Physiol.* **277,** F587-98 (1999).
78. Igarashi, P. *et al.* Ksp-cadherin gene promoter. II. Kidney-specific activity in transgenic mice. *Am. J. Physiol.* **277,** F599-610 (1999).
79. Shao, X. Epithelial-Specific Cre/lox Recombination in the Developing Kidney and Genitourinary Tract. *J. Am. Soc. Nephrol.* **13,** 1837–1846 (2002).
80. Igarashi, P. Following the expression of a kidney-specific gene from early development to adulthood. *Nephron. Exp. Nephrol.* **94,** e1–e6 (2003).
81. Aziz, F., Tk, L.-A., Enweluzo, C., Dutta, S. & Zaeem, M. Diastolic heart failure: a concise review. *J. Clin. Med. Res.* **5,** 327–34 (2013).
82. Henein, M. Y. & Gibson, D. G. Suppression of left ventricular early diastolic filling by long axis asynchrony. *Br. Heart J.* **73,** 151–157 (1995).
83. van Dierendonck, J. H., Keijzer, R., van de Velde, C. J. H. & Cornelisse, C. J. Nuclear Distribution of the Ki-67 Antigen during the Cell Cycle: Comparison with Growth Fraction in Human Breast Cancer Cells. *Cancer Res.* **49,** 2999–3006 (1989).
84. Chevalier, R. L., Thornhill, B. A., Forbes, M. S. & Kiley, S. C. Mechanisms of renal injury and progression of renal disease in congenital obstructive nephropathy. *Pediatr. Nephrol.* **25,** 687–697 (2010).
85. Bascands, J. L. & Schanstra, J. P. Obstructive nephropathy: Insights from genetically engineered animals. *Kidney Int.* **68,** 925–937 (2005).
86. Ingraham, S. E. *et al.* Pathogenesis of renal injury in the megabladder mouse: A genetic model of congenital obstructive nephropathy. *Pediatr. Res.* **68,** 500–507 (2010).
87. Singh, S. *et al.* Identification of a unique transgenic mouse line that develops megabladder, obstructive uropathy, and renal dysfunction. *J. Am. Soc. Nephrol.* **18,** 461–471 (2007).
88. Singh, S. *et al.* Transcriptional profiling of the megabladder mouse: A unique model of bladder dysmorphogenesis. *Dev. Dyn.* **237,** 170–186 (2008).
89. Li, Y. *et al.* Sonic hedgehog signaling regulates Gli3 processing, mesenchymal proliferation, and differentiation during mouse lung organogenesis. *Dev. Biol.* **270,** 214–31 (2004).
90. Haraguchi, R. *et al.* The hedgehog signal induced modulation of bone morphogenetic protein signaling: An essential signaling relay for urinary tract morphogenesis. *PLoS One* **7,** (2012).
91. Aoki, Y. *et al.* Id2 haploinsufficiency in mice leads to congenital hydronephrosis resembling that in humans. *Genes to Cells* **9,** 1287–1296 (2004).
92. Tripathi, P., Wang, Y., Casey, a. M. & Chen, F. Absence of Canonical Smad Signaling in Ureteral and Bladder Mesenchyme Causes Ureteropelvic Junction Obstruction. *J. Am. Soc. Nephrol.* **23,** 618–628 (2012).
93. Erman, a, Veranic, P., Psenicnik, M. & Jezernik, K. Superficial cell differentiation during embryonic and postnatal development of mouse urothelium. *Tissue Cell* **38,** 293–301 (2006).
94. Kong, X. T. *et al.* Roles of uroplakins in plaque formation, umbrella cell

enlargement, and urinary tract diseases. *J. Cell Biol.* **167,** 1195–1204 (2004).
95. Decramer, S. *et al.* Predicting the clinical outcome of congenital unilateral ureteropelvic junction obstruction in newborn by urinary proteome analysis. *Nat. Med.* **12,** 398–400 (2006).
96. Lloyd, K. C. K. A knockout mouse resource for the biomedical research community. *Ann. N. Y. Acad. Sci.* **1245,** 24–26 (2011).
97. Henrich, V. C. *et al.* Widespread recombinase expression using FLPeR (flipper) mice. *Genesis* **28,** 106–110 (2000).
98. Bergqvist, I., Eriksson, B., Eriksson, M. & Holmberg, D. Transgenic Cre recombinase expression in germ cells and early embryogenesis directs homogeneous and ubiquitous deletion of loxP-flanked gene segments. *FEBS Lett.* **438,** 76–80 (1998).
99. Fogelgren, B. *et al.* Deficiency in Six2 during prenatal development is associated with reduced nephron number, chronic renal failure, and hypertension in Br/+ adult mice. *Am. J. Physiol. Renal Physiol.* **296,** F1166-78 (2009).
100. Walker, K. A. *et al.* Fgfr2 is integral for bladder mesenchyme patterning and function. *Am. J. Physiol. Renal Physiol.* **308,** F888-98 (2015).
101. Fogelgren, B. *et al.* Urothelial defects from targeted inactivation of exocyst Sec10 in mice cause ureteropelvic junction obstructions. *PLoS One* **10,** (2015).
102. Mills, A. A. *et al.* P63 Is a P53 Homologue Required for Limb and Epidermal Morphogenesis. *Nature* **398,** 708–713 (1999).
103. Aboushwareb, T. *et al.* Alterations in bladder function associated with urothelial defects in uroplakin II and IIIa knockout mice. *Neurourol. Urodyn.* **28,** 1028–1033 (2009).
104. Varley, C. L. *et al.* PPAR??-regulated tight junction development during human urothelial cytodifferentiation. *J. Cell. Physiol.* **208,** 407–417 (2006).
105. Weiss, R. M. *et al.* Brg1 determines urothelial cell fate during ureter development. *J Am Soc Nephrol* **24,** 618–626 (2013).
106. Lynch, J. *et al.* Obliterative (constrictive) bronchiolitis. *Semin. Respir. Crit. Care Med.* **33,** 509–532 (2012).
107. Yang, Y., Zhou, X., Gao, H., Ji, S. J. & Wang, C. The Expression of Epidermal Growth Factor and Transforming Growth Factor-Beta1 in the Stenotic Tissue of Congenital Pelvi-Ureteric Junction Obstruction in Children. *J. Pediatr. Surg.* **38,** 1656–1660 (2003).
108. Huang, Y. *et al.* Matricellular protein periostin contributes to hepatic inflammation and fibrosis. *Am. J. Pathol.* **185,** 786–797 (2015).
109. Crawford, J., Nygard, K., Gan, B. S. & O'Gorman, D. B. Periostin induces fibroblast proliferation and myofibroblast persistence in hypertrophic scarring. *Exp. Dermatol.* **24,** 120–126 (2015).
110. Chevalier, R. L., Forbes, M. S. & Thornhill, B. A. Ureteral obstruction as a model of renal interstitial fibrosis and obstructive nephropathy. *Kidney Int* **75,** 1145–1152 (2009).
111. Cain, J. E., Islam, E., Haxho, F., Blake, J. & Rosenblum, N. D. GLI3 repressor controls functional development of the mouse ureter. *J. Clin. Invest.* **121,** 1199–1206 (2011).
112. Mesrobian, H. G. O. *et al.* Candidate urinary biomarker discovery in ureteropelvic

junction obstruction: A proteomic approach. *J. Urol.* **184,** 709–714 (2010).
113. Yurtçu, M. & Gürbüzer, N. Investigation of Histopathologic Changes in Pelviureteral Junction Obstruction. 162–166 (2010). doi:10.3109/08860220903541101
114. Elliott, C. G. *et al.* Periostin modulates myofibroblast differentiation during full-thickness cutaneous wound repair. *J. Cell Sci.* **125,** 121–32 (2012).
115. Varley, C. L., Bacon, E. J., Holder, J. C. & Southgate, J. FOXA1 and IRF-1 intermediary transcriptional regulators of PPARgamma-induced urothelial cytodifferentiation. *Cell Death Differ.* **16,** 103–114 (2009).
116. Hu, P. *et al.* Ablation of uroplakin III gene results in small urothelial plaques, urothelial leakage, and vesicoureteral reflux. *J. Cell Biol.* **151,** 961–971 (2000).
117. Chen, D. *et al.* Exocyst Requirement for Endocytic Traffic Directed Toward the Apical and Basolateral Poles of Polarized MDCK Cells. *Mol. Biol. Cell* **19,** 308–317 (2008).
118. Khandelwal, P. *et al.* Rab11a-dependent exocytosis of discoidal/fusiform vesicles in bladder umbrella cells. *Proc. Natl. Acad. Sci. U. S. A.* **105,** 15773–15778 (2008).
119. Khandelwal, P. *et al.* A Rab11a-Rab8a-Myo5B network promotes stretch-regulated exocytosis in bladder umbrella cells. *Mol. Biol. Cell* **24,** 1007–19 (2013).
120. Bartoli, F. A. *et al.* Urothelium damage as the primary cause of ureteropelvic junction obstruction: A new hypothesis. *Urol. Res.* **24,** 9–13 (1996).
121. Lye, C. M., Fasano, L. & Woolf, A. S. Ureter myogenesis: putting Teashirt into context. *J. Am. Soc. Nephrol.* **21,** 24–30 (2010).
122. Jenkins, D. *et al.* De novo Uroplakin IIIa heterozygous mutations cause human renal adysplasia leading to severe kidney failure. *J. Am. Soc. Nephrol.* **16,** 2141–9 (2005).
123. Schönfelder, E. M. *et al.* Mutations in Uroplakin IIIA Are a Rare Cause of Renal Hypodysplasia in Humans. *Am. J. Kidney Dis.* **47,** 1004–1012 (2006).
124. Fogelgren, B. *et al.* Exocyst Sec10 protects renal tubule cells from injury by EGFR/MAPK activation and effects on endocytosis. *Am J Physiol Ren. Physiol* **307,** F1334-41 (2014).
125. Lemmon, M. A. & Schlessinger, J. Cell signaling by receptor tyrosine kinases. *Cell* **141,** 1117–1134 (2010).
126. Tang, J., Liu, N. & Zhuang, S. Role of epidermal growth factor receptor in acute and chronic kidney injury. *Kidney Int.* **83,** 804–10 (2013).
127. Homma, T. *et al.* Induction of heparin-binding epidermal growth factor-like growth factor mRNA in rat kidney after acute injury. *J. Clin. Invest.* **96,** 1018–25 (1995).
128. Lin, J. J., Cybulsky, A. V, Goodyer, P. R., Fine, R. N. & Kaskel, F. J. Insulin-like growth factor-1 enhances epidermal growth factor receptor activation and renal tubular cell regeneration in postischemic acute renal failure. *J. Lab. Clin. Med.* **125,** 724–733 (1995).
129. Novick, P. & Guo, W. Ras family therapy: Rab, Rho and Ral talk to the exocyst. *Trends Cell Biol.* **12,** 247–249 (2002).